THE
PHYSICAL REVIEW
A Journal of Experimental and Theoretical Physics
VOL. 44, No. 2 JULY 15, 1933 SECOND SERIES

The Natural Widths of the $K\alpha$ X-Ray Doublet from 26FE to 47AG

SAMUEL K. ALLISON, *University of Chicago*
(Received May 31, 1933)

The full widths at half maximum of the $K\alpha_1$ and $K\alpha_2$ lines of 14 elements from 26Fe to 47Ag have been investigated with the double spectrometer in the (1, 1) position. The calcite crystals used had been previously studied in the (1, −1) position and shown to give results agreeing well with those to be expected from a perfect calcite crystal. The reported widths are uncorrected for the effects of overlapping of the lines, vertical divergence of the x-ray beam, or diffraction pattern widths of the crystals. They are, in X—units

	26Fe	27Co	28Ni	29Cu	30Zn	32Ge	38Sr	40Zr	41Cb	42Mo	44Ru	45Rh	46Pd	47Ag
$K\alpha_2$	1.06	0.95	0.82	0.77	0.58	0.46	0.36	0.35	0.31	0.32	0.29	0.29	0.29	0.29
$K\alpha_1$	1.00	0.81	0.64	0.58	0.51	0.43	0.35	0.33	0.33	0.29	0.29	0.29	0.28	0.28

The $K\alpha_1$ lines of Fe, Co, Ni, Cu, Zn and Ge are definitely asymmetrical, the center lying to the long wave-length side of the maximum ordinate. Pronounced difference in width of $K\alpha_1$ and $K\alpha_2$ and asymmetrical lines are found in and near the region of the periodic table where the $M_{IV}M_V$ shells are filling with electrons.

INTRODUCTION

THE experiments reported here were performed with the double crystal x-ray spectrometer, which was first applied to experiments of this type by Ehrenberg and Mark and Davis and Purks in 1927. Since that time the study of line breadths and shapes in the x-ray region by this method has been taken up by many investigators.[1] For these measurements the crystals must be placed in a position of finite dispersion, which is the case in which the reflecting surfaces are not parallel. The horizontal divergence of monochromatic radiation reflected from crystal A is then greatly reduced by the selectivity of the Bragg law, and to a first approximation we may consider the radiation incident on B as having been collimated for each wave-length by the action of A. The monochromatic rocking curves would thus have widths close to those given by the diffraction pattern and perfection of the crystal grating, and since the actual widths observed are much greater than this, they must be interpreted as natural widths of the lines. All the results reported here have been obtained with the crystals in the (1, 1) position according to the notation of Allison and Williams.[2] The crystals used were the

[1] Ehrenberg and Mark, Zeits. f. Physik **42**, 807 (1927). Ehrenberg and von Susich, Zeits. f. Physik **42**, 823 (1927). Davis and Purks, Proc. Nat. Acad. Sci. **13**, 419 (1927). Davis and Purks, Proc. Nat. Acad. Sci. **14**, 172 (1928). Purks, Phys. Rev. **31**, 931 (1928). S. K. Allison, Phys. Rev. **34**, 176 (1929). Allison and Williams, Phys. Rev. **35**, 149 (1930). Allison and Williams, Phys. Rev. **35**, 1476 (1930). Mark and von Susich, Zeits. f. Physik **65**, 253 (1930). Spencer, Phys. Rev. **38**, 618 (1931). Richtmyer and Barnes, Phys. Rev. **43**, 1049A (1933). Bearden and Shaw, Phys. Rev. **43**, 1050A (1933).

[2] Allison and Williams, Phys. Rev. **35**, 149 (1930).

calcites IIIA, IIIB, whose rocking curves in the (1, −1) position have been studied for a wide range of wave-lengths[3] and found to agree well with the theory of reflection by a perfect calcite crystal.

Preliminary Adjustments and Tests

The narrow rocking curves in the (1, −1) position which agree with the calculations for diffraction from a perfect calcite crystal have always been obtained from freshly cleaved surfaces. It is therefore of interest to inquire whether or not the reflecting power of these surfaces changes with time. Before beginning, and after completion of the experiments reported here, the (1, −1) curves for Cu $K\alpha_1$ were taken on the crystals. Thus the half width at half maximum of the rocking curve from crystals III has been under observation from November 19, 1931, to March 4, 1933. The data are given in Table I.

Table I. *Widths in (1, −1) position; crystals III.*

Date	Line	Half width at half maximum
Nov. 19, 1931	Mo $K\alpha_1$	2.6 sec.
Nov. 25, 1931	Cu $K\alpha_1$	4.9
Jan. 2, 1932	Mo $K\alpha_1$	2.6
Aug. 24, 1932	Cu $K\alpha_1$	4.9
Mar. 4, 1933	Cu $K\alpha_1$	5.1

From Table I it is concluded that no significant change in the surfaces of these crystals has taken place over this period. They have been kept in a desiccator except at times when runs were in process, and great care has been taken not to touch the reflecting surfaces.

In the parallel positions, if the crystal faces lie in the axes of rotation, and if these axes are parallel, the slit height does not add to the breadth of the rocking curve. This is not the case in positions of finite dispersion such as (1, 1), and the dimensions of the apparatus and height of the slits must be considered. Fig. 1

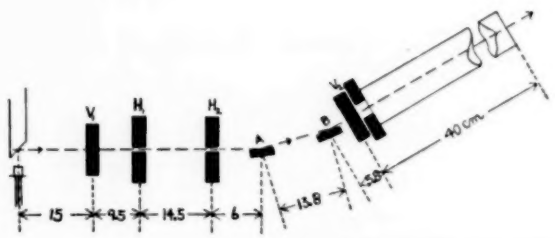

Fig. 1. Important dimensions in the double spectrometer. The axes of rotation of crystals A and B are perpendicular to the plane of the figure. V_1 and V_2 are slits limiting the vertical divergence of the x-ray beam, H_1 and H_2 are corresponding slits for the horizontal divergence.

shows important distances in the spectrometer, which was shown as Fig. 1 in a previous publication of the author.[3] It is seen that the slits limiting the vertical divergence were 49.6 cm apart, whereas the slits limiting the horizontal divergence were separated by 14.5 cm. If strictly monochromatic radiation were available for double spectrometer experiments, the rocking curves in the (1, 1) position would be given by

$$\Phi(\xi_B)=\int_{-\phi_m}^{\phi_m}\int_{-\alpha_m}^{\alpha_m}\left(1-\left|\frac{\phi}{\phi_m}\right|\right)\left(1-\left|\frac{\alpha}{\alpha_m}\right|\right)F\left(\alpha-\frac{\phi^2}{2}\tan\theta\right)F\left(\xi_B-\alpha-\frac{\phi^2}{2}\tan\theta\right)d\alpha d\phi. \qquad (1)$$

The above equation applies to the case in which the slits limiting the vertical and horizontal divergence of the beam consist of rectangular apertures. α_m and ϕ_m are the maximum horizontal and vertical divergences, respectively. If L_H is the distance between the slits limiting the horizontal divergence, each of equal width a, then $\alpha_m=a/L_H$, and an analogous definition holds for ϕ_m. ϕ and α represent the vertical and horizontal divergence of any ray in the bundle passing through all the slits, and can have values from $-\phi_m$ to ϕ_m, or $-\alpha_m$ to α_m, respectively. The function F is the diffraction pattern function from a single crystal, which, if perfect crystals are used, would be Darwin's formula as modified by Prins, which appears as Eq. (13) in a previous publication of the author.[3] θ is the Bragg angle, and ξ_B represents the deviation of crystal B from some reference angle in the vicinity of the rocking curve. The equation in the form (1) applies to an experiment in which crystal A is left stationary and B is turned.

[3] S. K. Allison, Phys. Rev. **41**, 1 (1932).

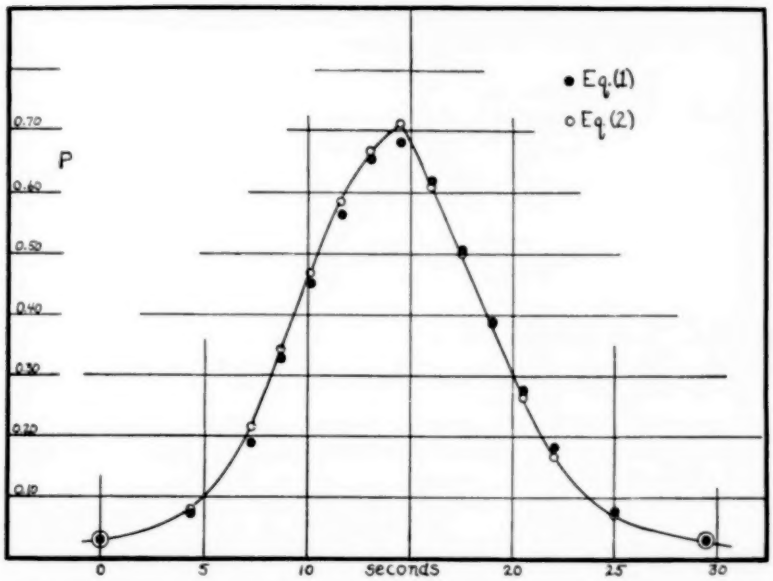

FIG. 2. The calculated effect of a vertical and horizontal divergence of maximum angle 4×10^{-3} on the shape of a (1, 1) monochromatic rocking curve of wave-length 1.537A. Prins' form of the single perfect crystal diffraction pattern is used, and the calculations apply only to the σ-polarized component of the beam. The ordinates are ratios of the power reflected from B to that incident upon it from A. The zero of abscissae represents a setting of the spectrometer in which the central ray makes an angle arc sin $\lambda/2d$ on both crystals. The curve is drawn through points calculated without taking account of divergence of the beam. The solid circles show the corrected curve, which has its center of gravity slightly displaced to larger glancing angles.

If we neglect the effect of vertical divergence, Eq. (1) becomes

$$\Phi(\xi_B)=\int_{-\infty}^{\infty}F(\alpha)F(\xi_B-\alpha)d\alpha. \qquad (2)$$

In passing from Eq. (1) to Eq. (2) the limits of integration of α have been extended to $\pm\infty$, and the variation in the intensity of the incident beam with horizontal divergence is neglected. This is justified by the fact that these unobservable monochromatic curves would extend over a very small angular range. The functions $(1-|\alpha/\alpha_m|)$ and $(1-|\phi/\phi_m|)$ which appear in Eq. (1) represent the intensity of the incident beam as a function of horizontal and vertical divergence, respectively, assuming a uniform distribution on the focal spot and that both slits have the same widths or heights.

With the cooperation of Mrs. G. S. Monk of Ryerson Laboratory, calculations of the shape of the (1, 1) rocking curves at the wave-length of Cu $K\alpha_1$ have been carried out. The calculations were made for a value of ϕ_m of 4×10^{-3}, which corresponds to two slits limiting the vertical divergence 50 cm apart, and each slit 2 mm high. A like value was assumed for α_m, although this has a negligible influence on the shape of the curve. The F functions were those of Prins, using the constants given for this wave-length in a recent paper by Parratt.[4] The F functions depend upon the polarization of the beam, and the present calculations have only been carried out for the σ-component, that is, the component polarized so that its electric vector lies in a plane perpendicular to the plane of incidence. The resultant rocking curves are shown in Fig. 2. It is interesting to note[5] that if the F functions are not symmetrical, the (1, 1) rocking curve also lacks symmetry, in contrast to the (1, −1) curves which are symmetrical irrespective of the nature of the diffraction patterns, so long as these are the same for the two crystals.

[4] Parratt, Phys. Rev. **41**, 561 (1932).

[5] I have received many ideas about these curves from conversations with Professor Carl Eckart of this laboratory, also from the paper of Laue, Zeits. f. Physik **72**, 472 (1932).

TABLE II. *Cu Kα doublet curves at various slit widths.*

Line	Voltage	Location of crystal A	α_m	ϕ_m	Observed full width at half maximum
Cu $K\alpha_1(1, 1)$	46 kv	on α_1	2.2×10^{-3}	$>10^{-2}$	43 sec.
"	46	"	2.2	$>10^{-2}$	42
"	31	"	6.2	4.0×10^{-3}	41
"	31	"	6.2	1.0×10^{-2}	41
"	43	"	6.2	1.0×10^{-2}	39
Cu $K\alpha_2(1, 1)$	46	on α_2	2.2×10^{-3}	$>10^{-2}$	54 sec.
"	46	"	2.2	$>10^{-2}$	55
"	43	"	6.2	1.0×10^{-2}	52

Average angular width of α_1 41 sec. or 0.58 X.U.
Average angular width of α_2 54 sec. or 0.77 X.U.

TABLE III. *Widths of the Cu Kα doublet.*

Author	Orders	Cu $K\alpha_1$ Full width at half maximum	Remarks
Ehrenberg and von Susich (1927)	(1, 1)	0.70 X.U.	Corrected for (1, −1) width
Purks (1928)	(1, 1)	0.63	Crystals probably unreliable; uncorrected
Valasek (1930)	(1), (2)	0.38	Photographic spectrometer; corrected, but method doubtful. Cf. Table IV
Spencer (1931)	(2, 2)	0.60	uncorrected; "universal" spectrometer
Spencer (1931)	(1, 1)	0.61	" " "
Spencer (1931)	(1, 1)	0.69	uncorrected; old type spectrometer
Allison (1933)	(1, 1)	0.58	uncorrected
		Cu $K\alpha_2$	
Purks (1928)	(1, 1)	0.63 X.U.	as above
Spencer (1931)	(2, 2)	0.75	uncorrected; universal
Allison (1933)	(1, 1)	0.77	uncorrected

It is seen that the corrections for slit height and width produce a very minor change in the curve calculated by Eq. (2), which neglects these effects. Of course, in the actual experimental curves obtained in the (1, 1) position, the monochromatic curves of these calculations are entirely covered by the large wave-length spread in a so-called monochromatic x-ray line, but it seems safe to say that if the effect of divergence of the beam on the calculated, truly monochromatic, rocking curve is negligible, it will also be negligible in the observed curve.[6] The conclusions thus arrived at from calculation were given an experimental test by running several curves on the Cu $K\alpha$ doublet with various slit heights and slit widths. The adjustments of the double spectrometer used in these experiments have been described in a previous paper.[3] Before the experiments were begun, crystal B was removed, and the slits limiting the horizontal divergence were made so narrow that α_m was 8.3×10^{-4}; about 2.9 minutes of arc. Using the instrument as a single crystal spectrometer, the setting of crystal A for the peak of Cu $K\alpha_1$ could be readily located, and its setting for any other wave-length calculated. Table II shows the result of the experiments. In this table the values of ϕ_m marked $>10^{-2}$ represent experiments performed before a slit limiting the vertical divergence was placed near the x-ray tube, so that the limiting value was governed by the size of the focal spot. These are the only experiments performed in connection with the work reported in this paper where such an uncertainty as to the limit of the vertical divergence existed, all the other runs being made with both vertical slits in place. The experiments on Cu $K\alpha_1$ show that a sixfold variation in the value of ϕ_m[?] produced no sig-

[6] However, if the spectral range covered is very wide, appreciable intensity may be reflected at some position from parts of the beam having horizontal divergences large enough to be affected by the function $(1-|\alpha/\alpha_m|)$. A method of correcting for this is discussed later in this paper.

TABLE IV. *Full width of Mo $K\alpha_1$ at half maximum, $\Delta\lambda$.*

Authors	Crystal	Orders	$\Delta\lambda$	Remarks
Ehrenberg and Mark (1927)	Diamond (111)	(1, 1)	0.41 X.U.	corr. for (1, −1) width
Ehrenberg and von Susich (1927)	Calcite (100)	(1, 1)	0.38	corrected
Mark and von Susich (1930)	Calcite (100)	(2, 2)	0.326	corrected
Mark and von Susich (1930)	Topaz (001)	(6, 6)	0.288	corrected
Allison and Williams (1930)	Calcite (100)	many	0.294	corrected
Valasek (1930)	Calcite (100)	(1)	0.26	photographic*
Spencer (1931)	Calcite (100)	(2, 2)	0.281	uncorrected
Allison (1933)	Calcite (100)	(1, 1)	0.29	uncorrected

* The correction to be applied to the photographic measurements of Valasek (Phys. Rev. **36**, 1523 (1930)) has been discussed by the author (Phys. Rev. **38**, 203 (1931). According to the method of correction advocated, Valasek's results for Mo $K\alpha_1$ should be nearer 0.38 X.U.

nificant effect on the full width at half maximum of the rocking curve. The widths observed for the copper lines may be compared with those of other observers, as in Table III. From this table it is seen that the widths obtained with this instrument agree with those obtained by Spencer on his "universal" double spectrometer to within about 3 percent.

A further check on the performance of the instrument and crystals was to compare the results on Mo $K\alpha_1$ with the many experiments performed on this line by other observers. The value found in the present experiments was obtained at 43 kv, in the (1, 1) position, with $\alpha_m = 4.8\times10^{-3}$ and $\phi_m = 1.0\times10^{-2}$. The uncorrected full width at half maximum was 20 seconds, corresponding to 0.29 X.U. Table IV shows a comparison of this value with other results.

In Table IV it is seen that the results of Mark and von Susich, Allison and Williams, and Spencer for Mo $K\alpha_1$ are in good agreement with themselves and with the present results. This gives confidence that the apparatus was in proper adjustment and operating in a satisfactory manner. In Table V is shown information concerning operating conditions on the lines studied in the present research.

TABLE V. *Experimental conditions.*

Element	Voltage	Current	α_m	ϕ_m
26Fe	36.5 kv	10 m.a.	4.8×10^{-3}	1.0×10^{-2}
27Co	35.2	10	"	"
28Ni	39.5	6.6	"	"
29Cu		see Table II		
30Zn	39.5	7.4	"	4.0×10^{-3}
32Ge	39.5	4.6	"	1.0×10^{-2}
38Sr	36.5	5.0	"	"
40Zr	39.5	7.0	"	"
41Cb	39.7	6.0	"	"
42Mo	42.6	4.0	"	"
44Ru	39.5	6.0	"	"
45Rh	45.2	6.0	3.4×10^{-3}	"
46Pd	45.2	6.9	"	"
47Ag	45.2	8.5	"	"

PREPARATION OF TARGETS

The x-ray tube used in these experiments was of a design previously described by the author.[7] All the targets were made of the same size, so that they could be interchanged. All the various substances used were attached to a copper base by one method or another. These bases were made from $\frac{3}{4}$ inch solid copper rod, on which a face was cut at 45° to the long axis. In most cases, a circular depression, $\frac{5}{16}$ inch in diameter and $\frac{1}{8}$ inch deep was cut in this face, and the element placed in this cavity. The rod was then bored out for water-cooling, and a sleeve turned down on it so that it fit snugly into a standard brass jacket, carrying the water cooling pipes. It is essential to obtain good thermal junction between the target substance and the copper, especially if the melting point is low, or the substance readily gives off gas when warmed. In the case of Fe, Co, Ni, Ru, Rh, Pd, Ag, disks were prepared of the correct dimensions and silver soldered into the depression in the copper. Zn was melted and poured into such a depression with a little acid flux so that it wet and adhered to the copper. Ge was melted in a hollow copper cylinder whose inside diameter was $\frac{5}{16}$ inch, and which was closed to the air. The Ge adhered to the copper, and a section was sawed out and soft soldered onto a standard diameter copper

[7] S. K. Allison, Phys. Rev. **30**, 245 (1927).

shank. In the case of Sr, a nickel cup whose outside diameter was $\frac{5}{16}$ inch was stamped out of sheet and small pieces of metallic strontium inserted. The cup was provided with a lid which could be spot-welded so that it was nearly air-tight. This arrangement was at once placed in a glass tube, which was then evacuated, and the Sr melted with an induction furnace. The molten strontium made good thermal contact with the nickel, and after cooling, the nickel cup was quickly soldered into the standard copper target. Zr and Cb were obtained in sheets which were spot-welded to nickel sheets, and then the nickel soldered with silver solder to the copper face, no depression having been made. Copper was arc welded onto a molybdenum button by performing the operation in the reducing part of a Bunsen flame. The coppered portion was then silver soldered to the standard target.

Methods of Taking Data

Most of the curves were taken with crystal A stationary, while crystal B was rotated in small steps through the region under investigation. If the angular range moved through by B is large, errors may be introduced due to the fact that as B is turned the region on the crystal faces from which the maximum intensity is reflected changes. Also the region on the focal spot which gives the principal part of the observed intensity changes. These disadvantages have been previously discussed by DuMond and Hoyt.[8] The double spectrometer designed by the author is however of such general construction that it can be used in a way which avoids these difficulties. This will be referred to as the method of double rotation, as contrasted with the method of single rotation, in which B only is moved. Let us suppose that crystal A is rotated through an angle $\delta\theta$ measured from some angle θ_0 at which λ_0 is reflected. Then a wave-length $\lambda_0+(d\lambda/d\theta)\delta\theta$ is reflected from the same portion of crystal A and comes from the same part of the target as did λ_0 at the original position. If furthermore axis B is rotated through an angle $2\delta\theta$ around axis A, it is now in the same position relative to the reflected beam from A as it was in the previous setting. And finally, if crystal B is rotated through $\delta\theta$, the new wave-length strikes the same part of its surface as did the wave-length λ_0 in the original setting. These motions can be carried out without any change in the design of the instrument, since the worm gears driving axis A and axis B are linked together in a two to one ratio, and a slow motion wheel for revolving A in steps of seconds of arc can be locked into the driving mechanism. The double rotation method, then, consists in rotating A about its axis through the same angular range as B is rotated between readings about its own axis. Axis B then follows the beam reflected from crystal A automatically due to the previously mentioned gear ratio.

In the method of double rotation in the (1, 1) position, the dispersion, measured in terms of the angle through which B is rotated about its own axis, is one-half that in the method of single rotation. The resolving power, however, is the same for the two methods, since the monochromatic rocking curves would be half as wide with double as with single rotation.

The following Table VI shows the data taken on cobalt, in which both methods were used. The experiment in the first row was performed with crystal A stationary, and so placed that the central ray through the slits made a glancing

Table VI. *Single and double rotation of the Co Kα doublet.*

Method	Crystal A	α_1		α_2	
		$\Delta\theta$	$\Delta\lambda$	$\Delta\theta$	$\Delta\lambda$
Single rotation	$(\alpha_1+\alpha_2)/2$	59 sec.	0.83 X.U.	66 sec.	0.93 X.U.
Single rotation	α_1	56	0.79		
Single rotation	α_2			66	0.93
Double rotation	varied	29.5	0.83	34	0.95
		Average full width α_1=0.82 X.U.;			α_2=0.94 X.U.

[8] DuMond and Hoyt, Phys. Rev. **36**, 1702 (1930).

angle of 17° 09′ 31″, which is half way between the Bragg angles for Co $K\alpha_1$ and Co $K\alpha_2$. Crystal B was then rotated through the entire range necessary to reflect α_1 and α_2. The experiments in the second and third rows were performed in the usual manner, setting crystal A in a position to reflect the line in question, and then moving B over the range required to cover the line. The data in the fourth row were taken over both α_1 and α_2 by moving the entire spectrometer in the way described above. The results show that curves taken by the single rotation method were not seriously affected by the possibility of running off the focal spot, or changing the reflecting area of the crystal faces.

The Overlapping Factor

The two lines $K\alpha_1$ and $K\alpha_2$ were not completely separated in the elements Fe, Co, Ni, Cu, Zn. This cannot be attributed to an insufficient resolving power of the spectrometer, for the resolving power of the crystals used in this work has been shown to be about 11,000 in this region,[3] whereas the ratio $\lambda/d\lambda$ for the $K\alpha$ doublet of Ni, for instance, is about 430. This overlapping makes corrections to the observed ordinates (other than that due to the base-line of the general and scattered radiation) necessary if the complex is to be completely separated out into two lines. Special assumptions are necessary if the component lines are asymmetrical about their maximum ordinate, as is the case with many of these lines.

In order to obtain some semiquantitative measure of the separation of the two peaks, a number called the "overlapping factor" has been introduced. Let I_1 be the ordinate representing the maximum intensity observed on the α_1 peak, and $I_{\min}$ the minimum ordinate between α_1 and α_2. Then the overlapping factor f is

$$f=(I_{\min}/I_1)R_{1,2} \qquad (3)$$

where $R_{1,2}$ is the ratio of the intensity of α_1 to α_2 which has been taken simply as 2, disregarding the question as to whether this represents the ratio of the areas or maximum ordinates of the two lines.[9] In this form the expression is readily extended other resolutions, for instance $L\alpha_1$ and $L\alpha_2$ where $R_{1,2}$ is 10. According to the definition of f, an overlapping factor of unity means no minimum between the two lines, a factor of zero meaning complete separation.

Corrections to the Observed Widths

The largest overlapping factor observed in these experiments was 0.15 in the Fe $K\alpha$ doublet. In this case the α_1-line is certainly asymmetrical, being steeper on the short than on the long wave-length side. This asymmetry makes corrections for overlapping difficult, but any reasonable method seems to lead to corrections which are less than the experimental variations between different runs on the widths. The full widths at half maximum listed in Table VII are uncorrected for overlapping. Other overlapping factors were 27Co, 0.12; 28Ni, 0.10; 29Cu, 0.08; 30Zn, 0.02. At germanium and for the higher elements, no overlapping could be detected.

The effect of the finite resolving power of the crystals, or, in other words, the width of the (1, 1) rocking curve which would be obtained with truly monochromatic radiation must also be considered. The width of this (1, 1) curve depends, as has been shown, on that of the (1, −1) curve and the vertical divergence of the beam, which enters to the second power only. In Table II it has been shown that a sixfold variation in ϕ_m^2 made no significant difference in the observed width of Cu $K\alpha_1$. It has therefore been assumed in all the experiments that the geometric contribution to the observed widths was negligible. In the curve of Co $K\alpha_1\alpha_2$ shown as Fig. 3, the width of the (1, −1) curve which would have been observed by the method of double rotation is indicated. This was taken from the data of Allison[3] taken previously on this same set of crystals. The ratio of the (1, −1) width to the angular width of Co $K\alpha_1$ observed is 19 percent. This ratio ranged from 17 percent in 26Fe to 23 percent for 47Ag. In some previous work on line widths by this method, the (1, 1) observed line widths have been corrected for the (1, −1) widths by assuming that

[9] Spencer, Phys. Rev. **38**, 630 (1931) has expressed the separation of Mo $K\beta_1$ and Mo $K\beta_3$ by giving the ratio of the minimum ordinate to the maximum of β_1.

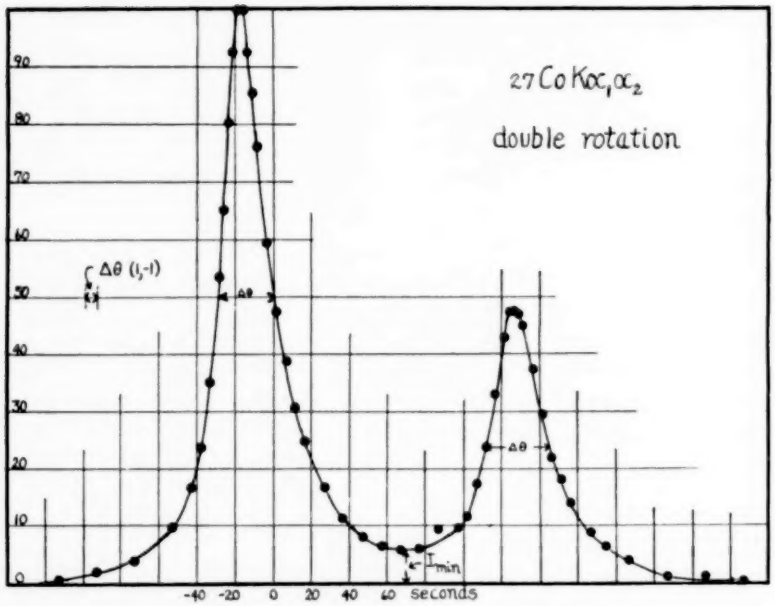

FIG. 3. The curve shown in this figure was obtained in the run mentioned in row 4 of Table VI. The full width at half maximum would be 5.7″ in the (1, −1) position with double rotation, which is 19 percent of the observed width of Co $K\alpha_1$.

the shapes of single crystal diffraction patterns and of spectral lines are given by the Gaussian error curve function. If these assumptions were correct, it can be shown that the observed curves, both in the (1, −1) and (1, 1) positions should also have the Gaussian error curve shape. The work of Williams[10] and of Hoyt[11] has shown that this is not the case for the observed line shapes, or for the (1, −1) curves either, the curves falling off more gradually than does this function. Furthermore Laue[5] has shown that it is impossible to obtain a unique solution for the shape of the single crystal diffraction pattern from the rocking curve in the (1, −1) position. These considerations make the status of the correction doubtful at the present time. Recently Barnes and Palmer[12] have suggested that the observed widths of W $K\alpha_1$ in various orders may be best reduced to the true wave-length width by direct subtraction of the observed widths in the $(n, -n)$ position from those in the (n, n). Such a procedure does not, however, improve the data observed on the line width observed for Mo $K\alpha_1$ in many orders by Allison and Williams,[2] and there seems no good reason for applying it to the softer wave-lengths reported on here. The widths recorded in Table VII are those obtained directly from the experimental data, uncorrected for any of the effects mentioned above. They are in each case the full width at half maximum.

[10] J. H. Williams, Phys. Rev. **37**, 1431 (1931).
[11] A. Hoyt, Phys. Rev. **40**, 477 (1932).
[12] Barnes and Palmer, Bull. Am. Phys. Soc. **8**, 15 (1933).

RESULTS

In Table VII the wave-length, frequency, and voltage widths are calculated from the observed angular widths by the following relations:

$$\Delta\lambda = \lambda^{-1} \tan\theta \Delta\theta \tag{4}$$

$$\Delta\nu/R = 9.1126\times10^{5}\lambda^{-2}\Delta\lambda \tag{5}$$

$$\Delta V = 1.2336\times10^{7}\lambda^{-2}\Delta\lambda. \tag{6}$$

In the above expressions, V is in volts and λ in X-units. The results are shown graphically in Figs. 4 and 5. Perhaps the most striking feature of the results is the large difference in width between α_1 and α_2 for the elements 26Fe to 32Ge inclusive. With the possible exception of Ge, this difference is well beyond the experimental error, and, as has previously been pointed out, has been found in 29Cu by Spencer. The present experiments show that this behavior

TABLE VII. *Results. Full widths at half maximum.*

Line	λ (Siegbahn)	$\Delta\theta$	$\Delta\lambda$	$\Delta\nu/R$	ΔV
26Fe $K\alpha_2$	1936.012 X.U.	76 sec.	1.06 X.U.	0.26	3.5 volts
26Fe $K\alpha_1$	1932.076	72	1.00	0.24	3.3
27Co $K\alpha_2$	1789.19	67	0.95	0.27	3.7
27Co $K\alpha_1$	1785.29	58	0.81	0.23	3.1
28Ni $K\alpha_2$	1685.35	58	0.82	0.26	3.6
28Ni $K\alpha_1$	1654.50	45	0.64	0.21	2.9
29Cu $K\alpha_2$	1541.232	54	0.77	0.30	4.0
29Cu $K\alpha_1$	1537.395	41	0.58	0.22	3.0
30Zn $K\alpha_2$	1436.03	41	0.58	0.26	3.5
30Zn $K\alpha_1$	1432.17	36	0.51	0.23	3.1
32Ge $K\alpha_2$	1255.21	32	0.46	0.27	3.7
32Ge $K\alpha_1$	1251.30	30	0.43	0.25	3.4
38Sr $K\alpha_2$	877.61	25	0.36	0.43	5.8
38Sr $K\alpha_1$	873.45	24	0.35	0.42	5.7
40Zr $K\alpha_2$	788.51	24	0.35	0.51	6.9
40Zr $K\alpha_1$	784.30	23	0.33	0.49	6.6
41Cb $K\alpha_2$	748.89	21	0.31	0.51	6.9
41Cb $K\alpha_1$	744.65	23	0.33	0.54	7.4
42Mo $K\alpha_2$	712.105		(0.32)*	(0.56)	(7.7)
42Mo $K\alpha_1$	707.831	20	0.29	0.53	7.2
44Ru $K\alpha_2$	646.06	20	0.29	0.63	8.6
44Ru $K\alpha_1$	641.74	20	0.29	0.64	8.7
45Rh $K\alpha_2$	616.37	20	0.29	0.70	9.4
45Rh $K\alpha_1$	612.02	20	0.29	0.70	9.5
46Pd $K\alpha_2$	588.63	20	0.29	0.76	10.3
46Pd $K\alpha_1$	584.27	19	0.28	0.75	10.1
47Ag $K\alpha_2$	562.67	20	0.29	0.83	11.3
47Ag $K\alpha_1$	588.28	19	0.28	0.82	11.1

* The value for Mo $K\alpha_2$ is taken from Allison and Williams,[2] although Spencer,[1] reports no difference between Mo $K\alpha_1$ and Mo $K\alpha_2$.

is typical of other elements in this region of the periodic system.

Unsymmetrical lines are also found in these elements, having been reported by various authors.[13] Larsson noted the asymmetrical nature of the Fe $K\alpha_1$ line, in contrast to the symmetrical Mo $K\alpha_1$. Seljakow, Krasnikow and Stellejsky concluded that the Cu $K\alpha_1$ line is symmetrical, which is not supported by the present results and those of Spencer. They however detected lack of symmetry in 28Ni, 27Co and 26Fe. Bearden and Shaw have also found lack of symmetry in this region. In the present results, asymmetrical lines were noted in the $K\alpha_1$ of 26Fe, 27Co, 28Ni, 29Cu, 30Zn, and 32Ge. An index of the asymmetry may be obtained by giving the ratio of the part of the full width at half maximum lying to the long wave-length side of the maximum ordinate to that part on the short wave-length side. This ratio was: Fe $K\alpha_1$, 1.8; Co $K\alpha_1$, 1.5; Ni $K\alpha_1$, 1.1; Cu $K\alpha_1$, 1.4; and considerably nearer unity for the elements up to Ge. It may be noted that the asymmetry in 28Ni is less than would be expected from its place in the order of atomic numbers. In all these cases the effect consists in a flaring out of the line to the longer wave-lengths.

It may be significant that these anomalies,

[13] A. Larsson, Phil. Mag. **3**, 1136 (1927). Seljakow, Krasnikow and Stellejsky, Zeits. f. Physik **45**, 548 (1927). Spencer, Phys. Rev. **38**, 618 (1931). Bearden and Shaw, Bull. Am. Phys. Soc. **8**, 15 (1933).

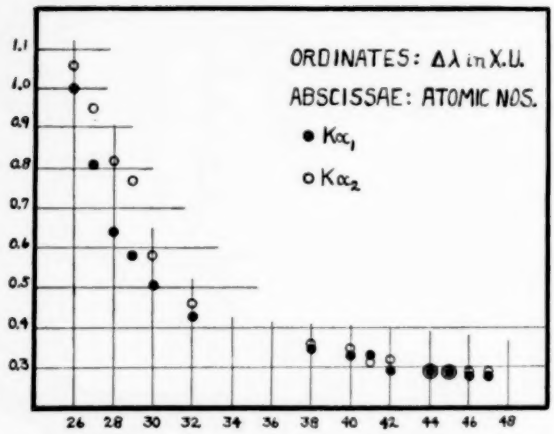

FIG. 4. The full wave-length width at half maximum of $K\alpha_1$ and $K\alpha_2$ as a function of atomic number. The difference in width of $K\alpha_1$ and $K\alpha_2$ for the lower atomic numbers greatly exceeds the experimental error (in most cases about 5 percent).

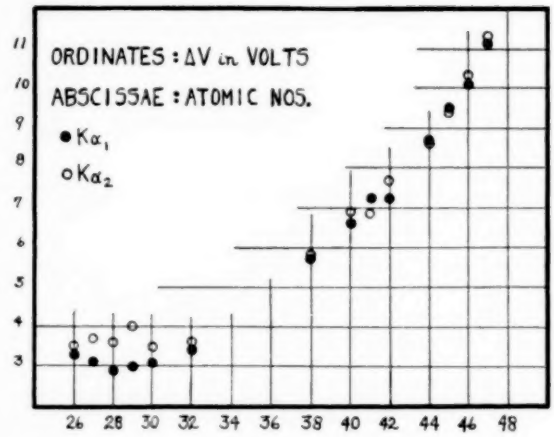

FIG. 5. The full width at half maximum in volts as a function of atomic number.

namely, the difference in width between α_1 and α_2, and the lack of symmetry, occur in a region where the $M_{IV}M_V$ shells are filling as shown by spectroscopic evidence obtained from atoms in the arc and spark. In the solid state, from which the x-ray spectra are obtained, these M shells are probably distorted considerably above 29Cu, where the data from optical spectra indicates that the 3*d* levels have obtained their 10 electrons.

The accuracy of the results has been estimated in a crude way from the variations in the individual runs and the author's opinion of the steadiness of operation of the x-ray tube and electrometer during the taking of the points. The angular widths are estimated as correct to within ± 5 percent, except in the following cases. The data on 26Fe seem upon examination to be less reliable than for the other elements and in this case the accuracy is judged to be ± 10 percent. Because of the many curves taken on copper, the result seems to be correct within ± 3 percent. The same may be said for the Mo $K\alpha$ lines, in view of the many experiments of the author and others on their widths.

Electron Diffraction by Liquids

LOUIS R. MAXWELL,* *Fertilizer and Fixed Nitrogen Division, Bureau of Chemistry and Soils, Washington, D. C.*

(Received May 12, 1933)

Electron interference has been obtained by the transmission of electrons (14 to 30 kv) through thin liquid films of phytol ($C_{20}H_{39}OH$), Nujol and two different grades of Cenco vacuum pump oil. The patterns obtained for these four liquids are all practically the same and are characterized by three complete diffraction rings. The values of $(1/\lambda)\sin\theta/2$ for phytol were found to be 0.108, 0.236 and 0.420. These rings could be produced by diffracting planes of spacings 4.63A, 2.1A and 1.2A. These distances are practically identical with the values obtained by G. W. Stewart for x-ray diffraction in liquid pentadecane ($C_{15}H_{32}$) and tetradecane ($C_{14}H_{30}$). The problem of interpreting the results by a group theory such as proposed by Stewart is the same for electrons as for x-rays.

SINCE the discovery of the wave property of electrons by Davisson and Germer[1] there have been numerous investigations[2] on the diffraction of electrons from various types of crystalline solids. Wierl[3] and others[4] have obtained electron diffraction from gases composed of polyatomic molecules. The present work will deal with the next logical field of investigation, namely, the diffraction of electrons in liquids.

Experimental Arrangement

The essential experimental problem in this work consists in setting up in vacuum a liquid film thin enough for electron diffraction by transmission. This can be accomplished by holding the film in a small wire loop. The liquid to be used must have a low vapor pressure with suitable surface tension and viscosity.

Substances found to be satisfactory for this purpose were phytol[5] ($C_{20}H_{39}OH$), Nujol and Cenco vacuum pump oils (estimated thickness of films about 10^{-4} cm). The arrangement used for photographing the diffraction patterns is similar to the method described by G. P. Thomson[6] and will be reported in detail elsewhere.[7] Electrons (14 to 30 kv) were produced in a cold cathode discharge tube and limited to a fine beam by a series of small holes. After passing through the liquid at approximately normal incidence, their interference pattern was recorded on a photographic plate at a distance of 25 cm.

Results

A typical electron diffraction photograph for phytol is illustrated in Fig. 1*b*. For comparison there are also shown diffraction patterns for solids and gases, gold foil, *c*, and carbon tetrachloride, *d*, respectively. The latter photograph was taken with a slight modification of the apparatus used for the study of liquids. The coherent scattering by phytol is characterized by three complete rings with the intensity decreasing with increasing angle of scattering. The two innermost rings are possibly visible in Fig. 1*b*

* A preliminary report on this work is contained in the regular program of the Washington meeting (April 1933) of the American Physical Society. K. Lark-Horovitz and E. P. Miller reported a paper at this meeting on the x-ray diffraction by liquids which confirmed the results reported to the extent of obtaining for Cenco pump oil the same ratios for $(1/\lambda)\sin\theta/2$ for the rings observed.

[1] C. Davisson and L. H. Germer, Nature **119**, 558 (1927); Phys. Rev. **30**, 705 (1927).

[2] For a review of electron diffraction experiments from crystals, see F. Kirchner, Ergebnisse der Exakten Naturwissenschaften **11**, 64 (1932).

[3] R. Wierl, Ann. d. Physik **8**, 521 (1931); **13**, 453 (1932).

[4] J. Hengstenberg and L. Brú, Anales Soc. Espana. Fis y Quim **30**, 341 (1932); L. Brockway and L. Pauling, Proc. Nat. Akad. **19**, 68 (1933); **19**, 303 (1933); L. R. Maxwell, M. E. Jefferson and V. M. Mosley, Phys. Rev. **43**, 777 (1933).

[5] The writer is indebted to Dr. Frank M. Schertz for preparation of the phytol used.

[6] G. P. Thomson, Proc. Roy. Soc. **A117**, 600 (1928).

[7] S. B. Hendricks, L. R. Maxwell, V. M. Mosley and M. E. Jefferson, J. Chem. Phys., Aug. 1933.

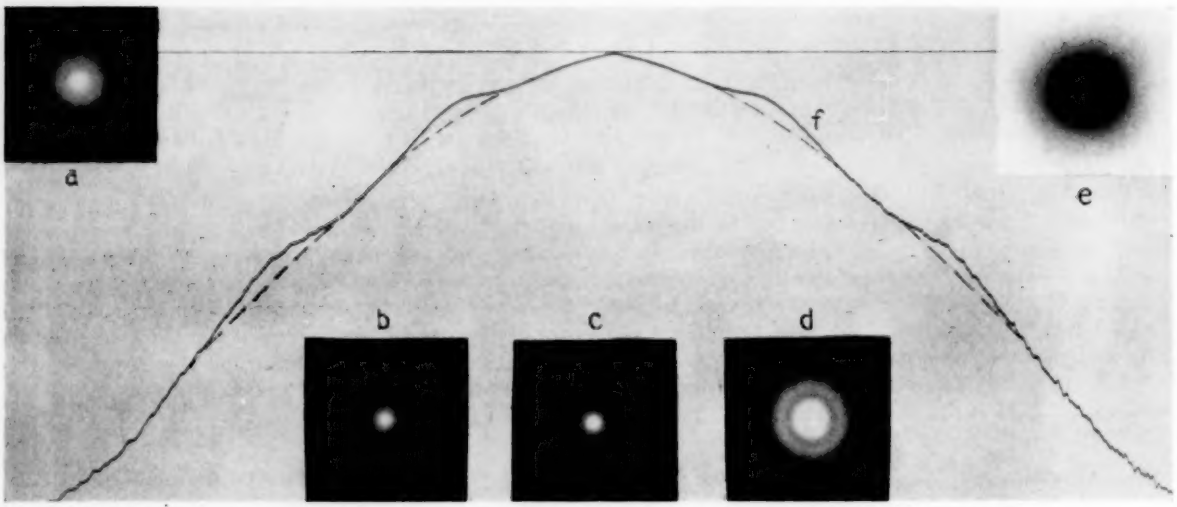

FIG. 1. *a*, print from the negative used for making the record shown in *f* (densitometer ratio 6.8 to 1). *b*, electron diffraction photograph by transmission through thin liquid film of phytol ($C_{20}H_{39}OH$), $\lambda = 0.087$A. *c*, electron diffraction photograph by transmission through gold foil, $\lambda = 0.070$A. *d*, electron diffraction photograph by transmission through carbon tetrachloride vapor, $\lambda = 0.071$A. *e*, electron diffraction photograph by transmission through a thin liquid film of Cenco vacuum pump oil ($\lambda = 0.070$), illustrating the position of the third and outermost diffraction ring not reproduced in *b*, *c*, *d*. *f*, densitometer record obtained from electron diffraction photograph of a Cenco vacuum pump oil film, $\lambda = 0.092$.

while the outermost ring although not too weak for reproduction indivdually, was too faint in comparison with the inner rings to be shown and yet maintain a clear picture of the nature of the pattern at small angles. The pictures illustrated with the exception of 1*e* were made by a single contact print from the original photographs. An important feature of the diffraction from the liquid lies in the appearance of the central spot and the region surrounding it. If one compares this type of diffraction with the photographs, *c* and *d*, it is seen that it resembles the diffraction from the gold foil rather than the scattering from the vapor of CCl_4. In the diffraction from gases, the identity of the central spot is lost because of the intense scattering at small angles, while for solids the contour of the central spot is maintained and the first intense scattering appears at the first diffraction ring given by Bragg's law. Fig. 1*e* shows an electron diffraction pattern for vacuum pump oil giving the same type of pattern and in which all three rings may be seen. In this case the density of the print has been increased in order to show the outer ring, thereby causing a loss of definition at small angles. A typical densitometer record obtained for vacuum pump oil diffraction ($\lambda = 0.092$A) is shown in Fig. 1*a*, *f*.

Table I contains the results obtained for phytol and Cenco vacuum pump oil. The structure of phytol[8] is shown as follows:

Phytol ($C_{20}H_{39}OH$)

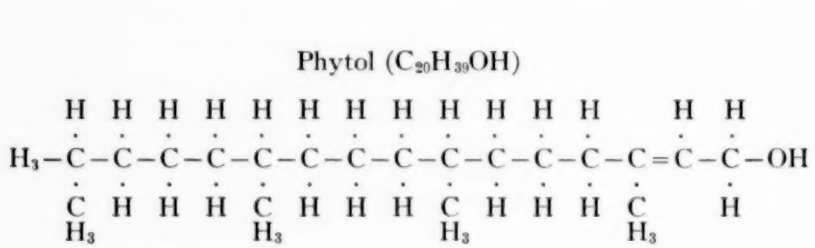

[8] Molecular structure of phytol ($C_{20}H_{39}OH$) by F. Fischer and K. Lowenberg, Ann. d. Chemie **474**, 69 (1928).

TABLE I. *Experimental results for electron diffraction.**

Plate No.	Phytol ($C_{20}H_{39}OH$) λ	(sin θ/2)/λ 1st maximum	2nd maximum	3rd maximum	Vacuum Pump Oil (Cenco No. 11023C) λ	(sin θ/2)/λ 1st maximum	2nd maximum	3rd maximum
1	0.094	0.108			0.104	0.107	0.238	
2	.087	.107	0.237	present	.104	.107	.232	
3	.078	.109	.232	0.425	.079	.111	.235	0.419
4	.076	.105	.233	.414	.078	.106	.232	.406
5	.074	.109	.240	.425	.072	.108	.234	.423
6	.070	.110	.239	.420	.072	.110	.242	.423
7	.069	.110	.235	.419	.069	.107	.231	.402
8					.069	.110	.235	.402
9					.068	.110	.238	.410
10					.068	.111	.236	.406
	Average =	0.108	0.236	0.420	Average =	0.108	0.234	0.412
	"d," 1st order =	4.63A	2.12A	1.19	"d," 1st order =	4.63A	2.13A	1.21A
	"d," 2nd order =		4.24A		"d," 2nd order =		4.27A	

* λ was obtained from readings of a static d.c. voltmeter previously calibrated by electron diffraction from gold foils. Liquids kept at room temperature.

TABLE II. *Electron diffraction results in liquids.*

Substance	1st maximum (sin θ/2)/λ	"d"	2nd maximum (sin θ/2)/λ	"d"	3rd maximum (sin θ/2)/λ	"d"
Phytol (7 plates) $C_{20}H_{39}OH$	0.108	4.63	0.236	2.12	0.420	1.19
Nujol (5 plates)	.103	4.85	.232	2.15	.406	1.23
Cenco Pump Oil (10 plates) No. 11023C (dark brown)	.108	4.63	.234	2.13	.412	1.21
Cenco Pump Oil (5 plates) No. 11021-B (clear)	.105	4.76	.229	2.18	.407	1.23

X-ray diffraction by Stewart: pentadecane ($C_{15}H_{32}$) and tetradecane ($C_{14}H_{30}$); "d" = 4.63; 2.1 and 1.23A.

Values of "d" were computed for the three rings given by the use of Bragg's formula $n\lambda = 2d \sin \theta/2$. The results for all the liquid used are summarized in Table II. All four liquids give the same type of diffraction patterns and the location of the rings is in approximate agreement. The first diffraction ring of Nujol appears at an appreciably smaller angle, thereby causing a somewhat greater spacing of 4.85A. The experimental values shown in Table II are averages taken from several plates (5 to 10). Typical variation between individual plates is represented in Table I. Stewart's x-ray measurements[9] on pentadecane ($C_{15}H_{32}$) and tetradecane ($C_{14}H_{30}$) are also included in this table for comparison with the electron diffraction results.

DISCUSSION

The results obtained can be summarized as follows: (1) All four substances studied gave practically the same diffraction pattern. (2) At small angles the scattering by liquids resembles the diffraction produced by crystalline foils in contrast to coherent scattering from gases. The "background scattering" is greater for liquids than it is for metal foils. (3) Only three rings were observed; these correspond to interplanar spacings of 4.63A, 2.1A and 1.2A. These separations agree very closely with the x-ray results of Stewart on pentadecane ($C_{15}H_{32}$) and tetradecane ($C_{14}H_{30}$).

Interpretation of these results from the standpoint of electron diffraction is approximately similar to the case of x-rays. Stewart[10] has proposed a theory of the structure of liquids which assumes that the molecules form in groups in which the long chain carbon molecules align themselves approximately parallel to each other forming a square

[9] G. W. Stewart, Phys. Rev. **31**, 174 (1928).

[10] G. W. Stewart, ibid., Phys. Rev. **30**, 232 (1927); **31**, 1 (1928); **31**, 174 (1928); **32**, 153 (1928); **32**, 558 (1928).

array in a plane perpendicular to their lengths. On the basis of this theory the average distance between molecules, i.e., the side of the elementary squares, is assumed to be 4.63A. This separation could produce the first diffraction ring observed for electrons. The carbon to carbon distance measured along the axis of these long chain molecules is known to be approximately 1.2A. Diffracting layers with this spacing may be formed by the carbon atoms and this would produce the third maximum observed. G. P. Thomson[11] has obtained electron diffraction from a layer of tap grease on a metal surface which was interpreted as indicating that 2.54A is the distance between alternate diffracting layers of carbon atoms which is consistent with the above conclusions.

This particular model of molecular grouping does not clearly explain the second diffraction ring which indicates a spacing of 2.1A. The use of the Bragg diffraction formula for interpreting the present experiments in terms of a group theory is highly arbitrary. However, the theory has been used to explain the results found for x-ray scattering from series of long chain carbon molecules—primary normal alcohol, liquid normal monobasic fatty acids and the liquid normal paraffins. These compounds are similar in structure to phytol, which is a pure long chain carbon compound, and to the vacumn pump oils and Nujol. The latter substances are made up largely of saturated aliphatic hydrocarbons. Nujol is more nearly a pure compound than the pump oils since the aromatic compounds have been removed by sulphonation.

The writer is indebted to Mr. V. M. Mosley and Dr. S. B. Hendricks for cooperation in this work.

[11] G. P. Thomson and C. A. Murison, Nature **131**, 237 (1933).

The Magnetic Interaction of a Valence Electron with Inner Shells

M. H. JOHNSON, JR.* AND G. BREIT, *Department of Physics, New York University, University Heights*

(Received May 12, 1933)

The magnetic interaction terms between two electrons are well known. By using antisymmetric wave functions the diagonal terms of the energy matrix for this interaction are calculated for an electronic configuration consisting of a valence electron and a closed shell. From the diagonal elements the doublet separation is easily obtained by applying the energy sum rule. The direct integrals, that is, terms which would occur even though the wave functions were not symmetrized for the Pauli principle, yield the expected contribution to the doublet separation; namely the interaction of the spin of the valence electron with the electric field produced by the closed shell. The exchange integrals give a contribution which decreases the doublet separation in the cases examined. They have been evaluated for the *f* terms of Cs I. Their effect is much too small to explain the inversion of the doublets in this spectrum.

INTRODUCTION

IN discussing the doublets of alkalies it is customary to consider the valence electron in a central field of force. The fact that the atom consists of a nucleus and many electrons is usually supposed to be taken care of by treating the closed inner electronic shells as spherically symmetrical distributions of charge. Their only effect in such a consideration is that of changing the central field of force in which the valence electron is moving. It is clear that there is no rigorous argument involved in such reasoning and that the only basis for its acceptance is the success of its results. Such results cannot be claimed, however, to be consequences of quantum mechanics because it does not follow from the general theory that the effect of inner shells is equivalent to a simple charge distribution derivable directly from Schroedinger's charge density. The results themselves are not always in agreement with experiment, for it is known that alkali doublets show inversion and it is also well known that such inversion can be explained on the above picture only if one supposes the effective electric field to be directed towards the nucleus at least in some region of space. Such an inversion of the electric field is inconsistent with the picture itself, as follows from simple electrostatics. We thought it of interest, therefore, to reconsider the problem. We shall see below that the usual central field picture is responsible for one of the terms in the result but that another exchange term is also present. The contributions to the doublet splittings due to the exchange term are usually very small and we may consider the central field picture as justifiable for ordinary cases. We have estimated the exchange terms for Cs *f* terms and we find that their effect is not sufficient to account for the inversion of these doublets. We are not prepared to state that no other inverted doublets can be accounted for by this effect of exchange.

1. THE INTERACTION ENERGY

Using the spin model for the electron and the Thomas correction factors, Heisenberg[1] has set up an expression for the spin-orbit and the spin-spin interactions of a pair of electrons with each other and with the nucleus. This interaction energy may be written (omitting the spin-spin interactions) as

$$H' = 2\mu_0^2(\mathbf{A}'_1 \cdot \mathbf{s}_1 + \mathbf{A}'_2 \cdot \mathbf{s}_2), \tag{1}$$

where

$$\mathbf{A}'_1 = Zr_1^{-3}\mathbf{l}_1 + r^{-3}[(\mathbf{r}_1 - \mathbf{r}_2) \times (2\mathbf{p}_2 - \mathbf{p}_1)] \tag{2}$$

and $\mathbf{A}'_2$ is obtained from the above by interchanging 1 and 2. Here $\mathbf{l}_1$, $\mathbf{s}_1$ are respectively the orbital and spin angular momenta of the first electron in units of $h/2\pi = \hbar$; $\mathbf{r}_1$, $\mathbf{p}_1$ are the

* National Research Fellow.

[1] W. Heisenberg, Zeits. f. Physik **39**, 499 (1927).

vector displacement from the origin and the linear momentum of this electron; Z is the atomic number and r is the distance between the two electrons. It should be noted that the matrices representing $\mathbf{s}$ are one-half of Pauli's σ's. This form of interaction energy may be justified by means of Dirac's equation.[2, 3, 4, 5, 6] This justification is itself not entirely free from speculation. It is, however, at least probable that to a sufficient approximation the interaction energy is given by

$$H' = -(e^2/2)[(\boldsymbol{\alpha}^1\boldsymbol{\alpha}^2)/r + (\boldsymbol{\alpha}^1\mathbf{r})(\boldsymbol{\alpha}^2\mathbf{r})/r^3] \quad (3)$$

which contributes the same amount to the spin-orbit interaction as the second part of (2)

$$\mathbf{A}_1 = r^{-3}[(\mathbf{r}_1 - \mathbf{r}_2) \times (2\mathbf{p}_2 - \mathbf{p}_1)] \quad (4)$$

in most of the configuration space. As long as one is treating the problem by means of radial functions satisfying Schroedinger's equation rather than by means of the radial equations of Darwin-Gordon, there is no advantage[7] in using Eq. (3) since then Eq. (4) is fully equivalent to Eq. (3). The additional terms due to spin-spin interactions which must be added to Eq. (4) are readily seen to have no effect on the interaction with closed shells. The calculation of this effect offers no difficulties and we leave it to the reader.

Using Eqs. (1) and (4) we calculate the doublet splitting using the method of sums. We deal with the states of the valence electron appropriate to strong fields and we describe them by assigning the orbital and spin magnetic quantum numbers m', μ'. We suppose that the atomic wave functions may be described sufficiently well as an antisymmetric combination of products of single electron functions, there being one kind of function for each electron in the atom. The first-order perturbation energy is then

$$W = \sum'_{ab}\{(ab|H'|ab) - (ab|H'|ba)\},$$

where a, b are the electronic states present and the summation is restricted to pairs. For the calculation of doublet splittings the pairs of electrons in inner shells do not matter and we may restrict the summation to

$$W = \sum_b\{(ab|H'|ab) - (ab|H'|ba)\}, \quad (5)$$

where a refers to the valence electron and b to the closed shells so that:

$$a = m', \mu', \quad b = m, \mu. \quad (5')$$

The closed shells are specified here by the principal quantum number n, the azimuthal number l, and the orbital and spin magnetic numbers m, μ. The energy (5) may be broken up into parts, each part referring to a shell with given n, l. We shall suppose that it has been thus broken up and we shall consider the contribution to (5) due to such a shell. In order not to complicate the notation we will call this also W. We have, using (1)

$$\sum_b(ab|H'|ab) = 4\mu_0^2\mu' I_{m'}; \quad \sum_b(ab|H'|ba) = 6\mu_0^2\mu' J_{m'} \quad (6)$$

where

$$I_{m'} = \sum_m \int w_{m'}^*(1) u_m^*(2) A_{1z} w_{m'}(1) u_m(2) d\tau_1 d\tau_2$$

$$J_{m'} = \sum_m \int w_{m'}^*(1) u_m^*(2) B_z w_{m'}(2) u_m(1) d\tau_1 d\tau_2 \quad (6')$$

$$\mathbf{B} = [(\mathbf{r}_1 - \mathbf{r}_2) \times (\mathbf{p}_2 - \mathbf{p}_1)]/r^3 = (\mathbf{A}_1 + \mathbf{A}_2)/3 \quad (6'')$$

and $w_{m'}$, u_m are the Schroedinger orbital wave functions for the valence and shell electron, respectively. The matrix vector character of $\mathbf{A}$, $\mathbf{B}$ shows that

[2] J. A. Gaunt, Phil. Trans. Roy. Soc. **A228**, 151 (1929).
[3] G. Breit, Phys. Rev. **34**, 553 (1929).
[4] G. Breit, Phys. Rev. **39**, 616 (1932).
[5] Fock and Podolsky, Phys. Zeits. d. Sow. **1**, 798 (1932).
[6] Bethe and Fermi, Zeits. f. Physik **77**, 296 (1932).

[7] Since this work was practically completed there arrived a paper by Fock in Zeits. f. Physik **81**, 195 (1933). His considerations are closely related to ours and are in many respects more general. Thus he goes into the influence of exchange on the effective central field which we leave

$$I_{m'}=m'I, \quad J_{m'}=m'J \tag{7}$$

and a simple application of the method of sums shows that the difference in the energies of the two doublet states due to the influence of inner shells is

$$\Delta w=2\mu_0^2(2l'+1)(I-3J/2) \tag{8}$$

where l' is the azimuthal quantum number of the valence electron. In addition the nucleus exerts its usual effect.

2. The Direct Term

According to Eq. (8), part of the doublet splitting is due to the direct integrals I. The term

$$2\mu_0^2(2l'+1)I \tag{8'}$$

in (8) we call the direct term because it would be present even if there were no Pauli principle. We shall now calculate (8') and we shall see that its value is the same as one would expect from simple charge density considerations. We resolve the orbital functions of the valence and the shell electron into their angle and radial factors:

$$w_{m'}=Y_{l'}^{m'}F(r); \quad u_m=Y_l^m f(r) \tag{9}$$

and we normalize each factor to unity:

$$\int_0^{\pi}\int_0^{2\pi}|Y_l^m|^2\sin\theta d\theta d\varphi=\int_0^{\infty}|f(r)|^2r^2dr=1. \tag{10}$$

We have the summation theorem formula for spherical harmonics:

$$\sum_m Y_l^{m*}(1)\,Y_l^m(2)=(2l+1)P_l(\cos\theta_{12})/4\pi \tag{11}$$

where P_l is the Legendre function of order l and θ_{12} is the angle between $\mathbf{r}_1$ and $\mathbf{r}_2$. The summation theorem is applied to the first Eq. (6'). It must be remembered that the operator $\mathbf{p}_2$ in Eq. (4) applies only to $u_m(2)$ and not to $u_m^*(2)$. Thus we introduce a third point 3, use Eq. (11) for $\sum_m u_m^*(3)u_m(2)w_{m'}(1)$ apply the operator A_{1z} to the result and then we let the point 3 approach the point 2 as a limit. We have

$$I_{m'}=[(2l+1)/4\pi]\int w_{m'}^*(1)\{r^{-3}[(\mathbf{r}_1-\mathbf{r}_2)\times(2\mathbf{p}_2-\mathbf{p}_1)]_z P_l(\cos\theta_{23})f_2f_3w_{m'}(1)\}_{3\to 2}d\tau_1d\tau_2.$$

We note that $\lim[(\mathbf{r}_1-\mathbf{r}_2)\times\mathbf{p}_2]_z\cos\theta_{23}=0$ and also that the operation $\mathbf{p}_2$ on f_2 gives rise to a term which disappears on integration over 2. We are left with

$$I_{m'}=\frac{2l+1}{4\pi}\int w_{m'}(1)\left\{\frac{[(\mathbf{r}_2-\mathbf{r}_1)\times\mathbf{p}_2]_z}{r^3}f_2^2d\tau_2\right\}w_{m'}(1)d\tau_1. \tag{12}$$

---

out of account. Fock considers two cases: (a) the non-relativistic, nonspin case in which the electrostatic interaction is considered. This has to do with the calculation of term values irrespective of multiplet structure. (b) He works also with the Diracian form modified by Eq. (3). He shows that in interactions with closed shells only the exchange part of Eq. (3) gives a non-vanishing contribution. Neglecting this he obtains the usual doublet-splitting formula, making use of the Darwin-Gordon radial equations and approximating the solutions of these by means of the Schroedinger radial functions. He also gives a tentative form for the effect of exchange on the doublet splitting which involves the smaller of the Darwin-Gordon functions. This form he regards as uncertain. In this respect we have a more definite result, for we believe that as long as the Darwin-Gordon functions are approximated in the usual way by Schroedinger's function, one may use Eq. (4) instead of Eq. (3). It is furthermore likely that the use of the exact relativistic radial functions matters only for p electrons and even there we expect the difference to be small because the difference between these exact functions and their non-relativistic approximations disappears in regions where the wave functions of the shell and valence electron overlap.

We interpret $(\mathbf{r}_2-\mathbf{r}_1)f_2^2/r^3$ as the electric field at the point 1 due to a charge $-f_2^2 d\tau_2$ at the point 2. Expression (12) is thus the diagonal matrix element with respect to $w_{m'}$ of the quantity $(2l+1)[\mathcal{E}\times\mathbf{p}]_z/4\pi$ where $\mathcal{E}$ is the electric intensity at the valence electron due to a spherically symmetrical distribution of charge having a charge density $-f^2$. This contribution thus corresponds to the central field picture. The interaction of the valence electron spin with the electric field of the nucleus gives rise to a perturbing energy: $2\mu_0^2 Z[\mathbf{r}_1\times\mathbf{p}_1]\cdot\mathbf{s}_1/r_1^3$, which contributes to the doublet splitting the amount $2\mu_0^2(2l'+1)I_N$, where $I_N=I_{Nm'}/m'$.

$$I_{Nm'}=(Z/2)\int w_{m'}^*(1)[\mathbf{r}_1\times\mathbf{p}_1]_z r_1^{-3} w_{m'}(1)d\tau_1. \tag{13}$$

Comparing this with Eq. (12) we see also that the numerical factors are precisely such as one would expect on the charge density picture. The effect of the shell is to decrease the effect of the nucleus. It is convenient to divide the action of the nucleus into parts, each part belonging to a shell. The total nuclear charge Z is then divided into $2(2l+1)$ parts and the contribution of any part to Eq. (13) is combined with the corresponding I as given by Eq. (12). The electric field due to the charge density $-f^2$ in Eq. (12) may be broken up into contributions due to charges $-4\pi f_2^2 r_2^2 dr_2$ at $r_1=0$ for $r_2<r_1$. The sum of the contributions to I due to the shell and the corresponding nuclear charge then becomes, by Eq. (9),

$$(I_N+I)_s=(2l+1)\int_{r_1>r_2}(F_1 r_1)^2 f_2 r_2)^2/r_1^3 dr_1 dr_2. \tag{14}$$

This contribution added to $-3J/2$ and multiplied by $2\mu_0^2(2l'+1)$ gives the doublet splitting due to the closed shell together with the positive charge $2(2l+1)$ on the nucleus. According to Eq. (14) the effect of $2(2l+1)$ charges on the nucleus is modified by the presence of the shell to the extent of obliterating $1/r^3$ outside the shell.

3. The Exchange Term

We evaluate next $J_{m'}$ as given by the second Eq. (6'). Various forms can be given to the result. We first derive a form which involves only the radial functions f, F and the derivative of the valence electron function F. To obtain this we transform the part of $J_{m'}$ due to $\mathbf{p}_1$ in (6''). We integrate by parts, thus transferring the differential operator $\mathbf{p}_1$ from $u_m(1)$ to $w_{m'}^*(2)$. In the result we interchange the variables 1 and 2 and we combine this result with the part of $J_{m'}$ due to $\mathbf{p}_2$ of Eq. (6''). We have

$$J_{m'}=(2l+1)/4\pi\int f_1 f_2 P_l(12)\{[(\mathbf{r}_1-\mathbf{r}_2)\times\mathbf{p}_2]_z/r^3\}[w_{m'}^*(1)w_{m'}(2)-w_{m'}(1)w_{m'}^*(2)]d\tau_1 d\tau_2.$$

Using the second Eq. (7) and the summation theorem (11) we have

$$[(l'(l'+1)(2l'+1))/6]J=\sum_{m'}m' J_{m'}$$
$$=[(2l+1)(2l'+1)/8\pi^2]\int f_1 f_2 P_l(12)\{[(\mathbf{r}_1-\mathbf{r}_2)\times\mathbf{p}_2]_z/r^3\}[\mathbf{r}_2\times\mathbf{p}_2]_z F_1 F_2 P_{l'}(12)d\tau_1 d\tau_2. \tag{15}$$

By symmetry we may replace the product of the two z components of the vector products in the above integral by their scalar product provided we divide the result by three. We then note that

$$[(\mathbf{r}_1-\mathbf{r}_2)\times\mathbf{p}_2]\cdot[\mathbf{r}_2\times\mathbf{p}_2]=-(\mathbf{r}_1\cdot\mathbf{r}_2)\Delta_2+2(\mathbf{r}_1\cdot\nabla_2)+(\mathbf{r}_2\cdot\nabla_2)(\mathbf{r}_1\cdot\nabla_1)-l_2^2,$$

where $\mathbf{l}_2=[\mathbf{r}_2\times\mathbf{p}_2]$ and we find by means of Eq. (15) that

$$J=\frac{2l+1}{8\pi^2 l'(l'+1)}\int f_2 f_2 P_l r^{-3}\left\{l'(l'+1)\left(\frac{r_1}{r_2}\cos\theta-1\right)F_1F_2P_{l'}+\frac{r_1}{r_2}\sin^2\theta P_{l'}'F_1\frac{d}{dr_2}(F_2r_2)\right\}d\tau_1 d\tau_2.$$

The argument of the Legendre function is $\mu=\cos\theta_{12}$. We have

$$\int_{-1}^{+1}(1-\mu^2)P_lP_{l'}'r^{-3}d\mu=\int_{-1}^{+1}(1-\mu^2)P_lP_{l'}'r_1^{-1}r_2^{-1}(\partial/\partial\mu)r^{-1}d\mu$$

$$=-r_1^{-1}r_2^{-1}\int_{-1}^{+1}r^{-1}[-l'(l'+1)P_lP_{l'}+(1-\mu^2)P_{l'}'P_l']d\mu$$

$$=[l'(l'+1)/r_1r_2]\int_{-1}^{+1}r^{-1}\{P_lP_{l'}+P_{l'}[(P_{l'+1}-P_{l'-1})/(2l'+1)]\}d\mu$$

and thus

$$J=\frac{2l+1}{8\pi^2}\int f_1f_2F_1\left\{r_2^{-1}\left(\frac{\partial}{\partial r_2}r^{-1}\right)P_lP_{l'}F_2+\left[\frac{P_lP_{l'}}{r}+P_{l'}\frac{P_{l'+1}-P_{l'-1}}{(2l'+1)r}\right]r_2^{-2}\frac{\partial}{\partial r_2}(F_2r_2)\right\}d\tau_1d\tau_2. \quad (16)$$

Here the angular integrations can be performed by means of Gaunt's integrals for products of three spherical harmonics since

$$P_l'=(2l+1)P_{l-1}+(2l-5)P_{l-3}+\cdots. \quad (16')$$

By means of the expansion

$$1/r=\sum_0^\infty(r_2^n/r_1^{n+1})P_n \quad r_1>r_2$$

the expression (16) reduces to

$$J=(2l+1)\sum_\tau\int_{r_1>r_2}\left\{(l_1l_1'\tau)\left[\left(\tau\frac{r_2^{\tau-2}}{r_1^{\tau+1}}-(\tau+1)\frac{r_2^\tau}{r_1^{\tau+3}}\right)F+G_{12}\frac{r_2^{\tau-2}}{r_1^{\tau+1}}+G_{21}\frac{r_2^\tau}{r_1^{\tau+3}}\right]+[l_1l_1'\tau]\left(G_{12}\frac{r_2^{\tau-2}}{r_1^{\tau+1}}+G_{21}\frac{r_2^\tau}{r_1^{\tau+3}}\right)\right\}dr_1dr_2, \quad (17)$$

where

$$(l,m,n)=\int_{-1}^{+1}P_lP_mP_nd\mu$$

$$=2\frac{[((l+m+n)/2)!]^2(m+n-l)!(l+m-n)!(l+n-m)!}{(l+m+n+1)![((m+n-l)/2)!]^2[((l+m-n)/2)!]^2[((l+n-m)/2)!]^2} \quad (17')$$

is Gaunt's integral[8] while

$$[l_1\,l_1'\,\tau]=\int_{-1}^{+1}P_l'[(P_{l'+1}-P_{l'-1})/(2l'+1)]P_\tau d\mu=[l(l+1)/l'(l'+1)][l_1'\,l_1\,\tau] \quad (17'')$$

can be calculated by means of Gaunt's integrals or usually more simply by using the expression for P_l' as a polynomial in μ and applying the recurrence formula

$$(2n+1)\mu P_n=(n+1)P_{n+1}+nP_{n-1}$$

to express the integrand as a sum of products involving two Legendre functions at a time. In particular for an f electron outside a p shell we have $l=1$, $l'=3$ and

[8] See reference 2, Eq. (14). Note that Gaunt's P_l is l' times the Legendre function used here. Thus Gaunt's form has been divided by l' m' n' for use here.

$$J=\int_{r_1>r_2}\left\{\left(\frac{36}{35r_1^3}-\frac{2r_2^2}{105r_1^5}-\frac{40r_2^4}{21r_1^7}\right)F+\left(\frac{12}{35r_1^3}+\frac{10r_2^2}{21r_1^5}\right)G_{12}+\left(\frac{12r_2^2}{35r_1^5}+\frac{10r_2^4}{21r_1^7}G_{21}\right)\right\}dr_1dr_2, \quad (18)$$

while for an f electron outside a d shell $l'=3$, $l=2$, and

$$J=\int_{r_1>r_2}\left\{\left(\frac{6}{7r_2r_1^1}-\frac{4}{7}\frac{r_2}{r_1^4}+\frac{444r_2^3}{693r_1^7}-\frac{200r_2^5}{77r_1^8}\right)F+\left(\frac{2}{7r_2r_1^2}+\frac{2r_2}{7r_1^4}+\frac{50r_2^3}{77r_1^6}\right)\left(G_{12}+\frac{r_2^2}{r_1^2}G_{21}\right)\right\}dr_1dr_2. \quad (19)$$

4. 5p Shell of Caesium

We begin with the outer shells of Cs for we expect the largest exchange effects will come from these shells. We have to evaluate the integral J of Eq. (18). This is done in three ways. The first is a calculation with a hydrogenic wave function for the 4f electron and an approximate nodeless function for 5p. The second makes use of the same function for 4f but an improved 5p function having nodes. The third uses Hartree's 5p function and a wave function for 4f obtained using Hartree's field by a numerical procedure.

The nodeless function is so chosen as to fit the Hartree 5p function[9] at large distances for we expect that in this region the maximum overlapping between the shell and the valence electron will occur, and hence we expect that the biggest contributions to our integral will be due to this region.

Thus

$$F(x)=2.20\times10^{-4}a_H^{-\frac{1}{2}}x^3e^{-\frac{1}{2}x},$$

$$f(x)=0.418a_H^{-\frac{1}{2}}x^4e^{-1.82x},$$

$$x=r/a_H, \quad a_H=h^2/4\pi^2me^2.$$

Our integral then contains terms of the type

$$J_{nm}=\int_{x_1>x_2}x_1^nx_2^me^{-\gamma(x_1+x_2)}dx_1dx_2,$$

$$\gamma=1.82+.25=2.07.$$

On rotating the coordinate system through 45° the double integral becomes

$$J_{nm}=2\int_0^\infty x^{n+m+1}e^{-2\gamma x}\int_0^x(1-y/x)^m(1+y/x)^ndy/x.$$

Changing variables to $z=y/x$ in the second integral, we find

$$J_{nm}=[2(n+m+1)!/(2\gamma)^{n+m+2}]H_{nm},$$

$$H_{nm}=\int_0^1(1+z)^n(1-z)^mdz.$$

In this way the terms of J are readily evaluated and we find that the doublet splitting[10] due to exchange is decreased by an amount 5×10^{-4} cm^{-1}.

In order to test the error in our approximation to the Hartree function, we have used other approximations in which the part of the function for large r is unchanged but nodes are introduced in the inner part of the function. This is done by replacing x^4 in $f(x)$ by a polynomial in such a way that the inner loops are about the same size as the actual Hartree function. We find that the contribution to the doublet separation is not significantly affected by this change.

Finally we have examined the effect of the charge distribution of the inner shells on the wave function for the valence electron. From Hartree's Z for the various shells, the potential in which the valence electron moves is found by integration. For $x>4$ this potential is inappreciably different from the Coulomb potential. Starting with the hydrogenic solution at $x=4$ we have continued the solution in to $x=1.5$ by means of the method of Wentzel-Kramers-Brillouin. At this point the actual solution is about twice as large as the hydrogenic solution. Since the important contributions to the integral all come from the region where x is large (about $x=3$ or 4) it is probable that this correction cannot alter the order of magnitude of the contribution to the doublet splitting. The point has been examined by means of numerical calculations and it has been found that no important change is produced by using the improved wave function.

[9] We are indebted to Professor Slater for communicating to us tables of the Hartree function for caesium.

[10] The actual doublet separations in the f series of Cs are of the order of 10^{-1} cm^{-1}, since the contribution of the direct integrals I to the doublet splitting is necessarily positive, the exchange integrals must be at least as great as the actual doublet separations if the inversions are due to this effort.

5. 4*d* Shell of Caesium

Since the valence electron function decreases rapidly as x decreases we expect our exchange integrals to be smaller for the 4*d* than for the 5*p* shell. (See Fig. 1 for the 4*d* and 5*p* functions.) If we calculate as before, using the hydrogenic wave function for the valence electron, we find that the effect of the 4*d* shell is about 1/100 that of the 5*p* shell. However if we examine the effective potential energy for the 4*f* valence electron, we find (Fig. 2) that there is a second region of classical motion between $x=0.8$ and

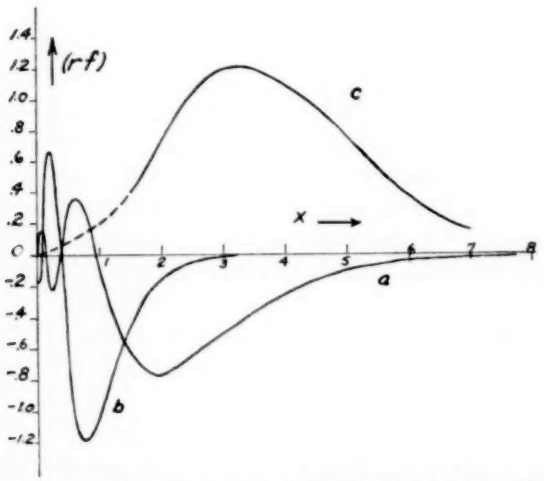

FIG. 1. a, Hartree 5*p* function for Cs1. b, Hartree 4*d* function for Cs1. c, $[(rf)(rF)/r^3]_0 \int^r (rf)(rF)dr$ where f is the Hartree 5*p* function and F is the wave function of the valence electron (see Fig. 2c). The arc under this curve is the contribution of the first term of Eq. (18) to the integral J. The numbers from the graph must be multiplied by 7.18×10^{-7}.

$x=0.3$. We therefore have continued the valence electron function into the origin in the following way. For the region $2>x>0.3$ the effective potential is approximated by the dotted lines in the figure. For the region $0.30>x>0.15$ we assume a constant effective nuclear charge of $Z=32.5$, while for the region $0.15>x>0$ we

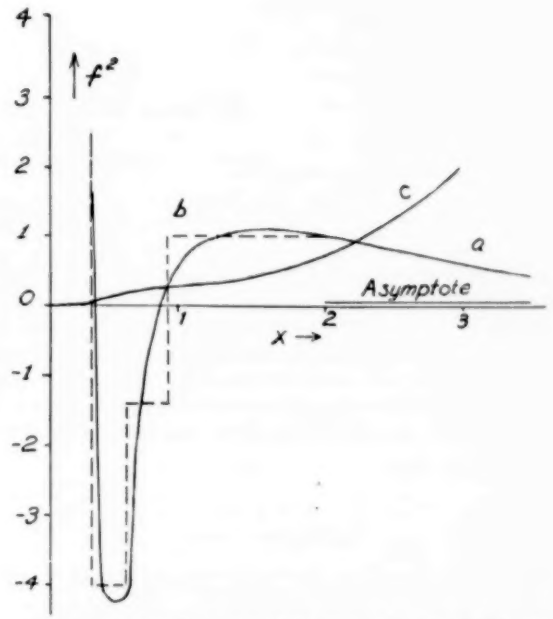

FIG. 2. a, Effective potential energy for the 4*f* electron of Cs1 as computed from Hartree's Z. b, The approximation to the effective potential energy used in the inner region of classical motion. c, Wave function for the 4*f* valence electron of Cs as computed from the above effective potential energy. The figures given by the graph must be multiplied by 4.34×10^{-3} to give the actual wave function.

assume an effective nuclear charge of $Z=54$. The above Z is that used by Hartree. Our use of two different Z's thus introduces a discontinuity only in the derivative of the potential but not in the potential itself. With the solution obtained in this way we have made a numerical estimate of our integrals. This modification increases the effect of the 4*d* shell so that it is of the same order of magnitude as the 5*p* shell.

From these calculations we conclude that for the caesium atom the magnetic exchange effects are unimportant. Though they are of the right sign, they are about a thousand times too small to explain the inversion of the *f* terms in this spectrum.

Zeeman Effect for Perturbed N_2^+ Terms

ALLAN E. PARKER, *Sloane Physics Laboratory, Yale University*

(Received April 10, 1933)

The Zeeman effects for the perturbed terms in the $v=1$ and 3 levels of the upper $^2\Sigma$ state of N_2^+ have been investigated at various field strengths up to 27,000 gauss. At the points of maximum perturbation the Zeeman patterns are doublets for the moderate and high field strengths. At high field strengths the unperturbed lines, of the same K value as the most perturbed lines, also become doublets under the influence of the magnetic field. This is attributed to a Paschen-Back effect. For K values greater than those of the maximum perturbation point, all the lines exhibit an asymmetric broadening in the field. A consideration of the interactions with the perturbing $^2\Pi$ state gives an explanation of the patterns observed.

INTRODUCTION

THE observation and discussion of the Zeeman patterns found for perturbed terms in a $^1\Pi$ state of CO by Watson[1] made it seem worth while to investigate a similar situation for a doublet state. Perturbations have been observed in the $^2\Sigma-{}^2\Sigma$ bands of N_2^+ by Fassbender,[2] by Coster and Brons[3] and by Childs.[4] The transitions which were the subject of the present investigation were the 1,3 and 3,5 bands. The perturbations found by Childs in the $v=0$ level of the upper $^2\Sigma$ state were not investigated since those perturbations occur in high rotational levels which the sources used did not excite.

EXPERIMENTAL PROCEDURE

Two sources were used for obtaining the spectrograms. The first of these was a 15,000 volt a.c. discharge between small copper electrodes in a modified Back chamber mounted on a Weiss magnet. Commercial tank nitrogen was usually flowed through the chamber. At other times a small air leak was used. The pressure in the chamber was approximately one mm as this was found to be the most suitable for enhancing the N_2^+ bands at the expense of the N_2 bands. However the latter were not entirely removed. The second source was a discharge tube similar to that used by Mulliken and Monk[5] in their investigation of the Zeeman effect for helium bands. The method of excitation was the same as before, the discharge taking place in purified helium at a pressure of 30 mm. A small trace (0.01 mm) of nitrogen,[6] obtained from sodium azide, was added to the helium. Under these conditions the N_2 bands were virtually absent.

The spectrograms were taken in the second order of a 21 foot grating mounted stigmatically. The dispersion for this order and region is 2.42 A/mm. Eastman 40 plates were used to obtain the spectrograms, the exposure time for the first source being 24 hours with the magnetic field and 24 hours without it. When using the other source 40 hours were needed instead of 24.

The field strengths used were 4,700, 9,000, 12,600, 19,700, 24,000 and 27,000 gauss. The second source was used for exposures taken at the first, third and fifth field strengths. While using the first source, the field strength was determined from the λ4680 zinc line. Since the second source contained mainly helium, the helium line at 4713A, which is a normal triplet, was available for the determination of the magnetic field's strength when this source was used. The sharpness of the atomic lines gives evidence

[1] W. W. Watson, Phys. Rev. **42**, 509 (1932).
[2] M. Fassbender, Zeits. f. Physik **30**, 73 (1924).
[3] D. Coster and H. H. Brons, Zeits. f. Physik **73**, 747 (1932).
[4] W. H. J. Childs, Proc. Roy. Soc. **A137**, 641 (1932).
[5] R. S. Mulliken and G. S. Monk, Phys. Rev. **34**, 1530 (1929).
[6] T. R. Merton and J. G. Pilley, Phil. Mag. **50**, 195 (1925).

TABLE I. *Zeeman patterns for the 1,3 N_2^+ band.*

$\Delta\nu$ represents the magnitude of the perturbation. The field strength followed by $\Delta\nu_n$ is placed at the top of the various columns. The two measurements indicate the limits of the Zeeman pattern associated with that particular line. If three measurements are given it means that there was a definite alteration of the intensity at the middle of the three points. These measurements, as well as those in Table II, were made only on the lines of the R branches as the corresponding lines in the P branches lie in the immediate vicinity of the head of the bands, thus preventing separation of the pattern associated with one P line from that associated with another P line. − indicates a displacement to lower frequency. The other measurements indicate displacement to higher frequency. All measurements are in cm^{-1}.

K''	J	$\Delta\nu$	12,600 (0.59)	19,700 (0.92)	24,000 (1.12)	27,000 (1.26)
10	10.5	−0.80	0.70 to −0.03	0.08 to	0.78 to −0.09	0.10 to −0.72
10	9.5		0.81 to −0.10	0.02	0.79 to 0.09	0.91 to −0.10
11	11.5	−1.61	1.28 to −0.09	1.24 to 0.19 −0.98 to −1.72	1.06 to 0.35	−0.48 to
11	10.5		0.02 to −0.25	0.60 to −0.16	0.67 to −0.10	0.66
12	12.5	−4.02	1.16 to 0.27 −0.05 to −0.93		1.21 to 0.42 −0.61 to −1.56	
12	11.5		1.10 to −0.36	1.10 to 0.37 to −1.22	1.01 to 0.21 −0.52 to −1.59	1.17 to 0.00
13	13.5	3.83	0.77 to −0.26	−0.36 to −1.10		−0.25 to −1.85
13	12.5		0.34 to −0.45	0.90 to 0.33 −0.37 to −1.06	1.39 to 0.55 −0.37 to −0.95	
14	14.5	2.23	0.25 to −0.46 to −1.27	0.25 to	−0.17 to −0.87	−0.26 to
14	13.5		0.62 to −0.16	−0.05	0.01 −1.60	0.00
15	15.5	1.63	0.30 to −0.51	0.00 to		0.01 to
15	14.5		0.54 to −0.07	−0.03		−0.20
16	16.5	1.33	0.20 to	0.19 to	−0.09 to	−0.01 to
16	15.5		−0.11	−0.08	0.09	−0.06
17	17.5	1.18	0.27 to −0.39			0.15 to −0.14
17	16.5		0.79 to −0.09			−0.01 to −0.42
18	18.5	1.08	0.32 to −0.43	0.32 to	0.15 to	0.05 to
18	17.5		0.65 to −0.09	0.03	0.07	−0.01
19	19.5	0.95		0.01 to		
19	18.5			−0.09		
20	20.5	0.94	0.12 to	0.01 to	−0.09 to	0.00 to
20	19.5		−0.01	0.01	−0.17	−0.01

of the constancy and uniformity of the magnetic field. An iron arc comparison spectrum was also recorded on each plate.

Observed Zeeman Patterns

The N_2^+ bands are a $^2\Sigma - ^2\Sigma$ transition having no appreciable spin doubling for low K values (under 20). Hence we would expect that an external magnetic field would not cause any appreciable change in the band lines. Such has been found to be the case for those bands which do not contain a perturbation. The perturbing level is a $^2\Pi$ level and transitions between a $^2\Pi$ level and a $^2\Sigma$ level do give rise to Zeeman patterns of observable magnitude. Therefore we might expect that at the perturbation points in the N_2^+ bands there would be Zeeman patterns of appreciable size due to the interaction of the $^2\Pi$ and $^2\Sigma$ levels. The spectrograms confirm these expectations.

The bands studied were the 1,3 and 3,5 transitions. The patterns of the lines of only the R branches were measured as the perturbation points in the P branches occur in the vicinity of the heads of the bands and the Zeeman patterns for the P lines overlap too much to permit of determining exactly what the effect of the magnetic field is upon a particular line. Tables I and II give the observed patterns for the R branches of the 1,3 and 3,5 bands, respectively. The patterns for the lowest field strength, 4700 gauss, are not recorded as the effect of such a small field is nearly negligible. Fig. 1, which consists of two microphotometer traces, one of a portion of the R branches in a field of 12,600 gauss and one of the same lines in the absence of an external magnetic field, illustrates the results obtained. From the tables we see that the Zeeman patterns for some lines are doublets and that for many lines they consist of an asymmetric broadening.

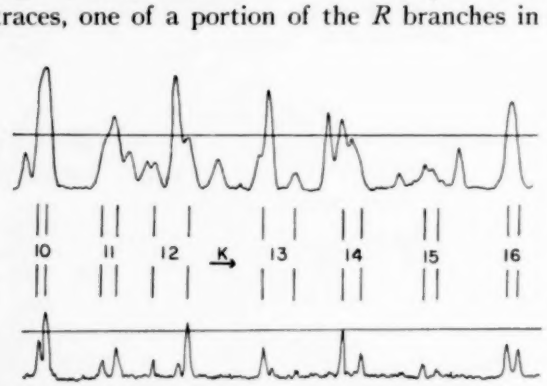

Fig. 1. Microphotometer traces of the perturbation in the 1,3 band. At left the lines are shown with an externally applied field of 12,600 gauss, at right with no external field. The position of the various lines is marked by the K value. These lines are members of the R_1 and R_2 branches.

Let us first consider the perturbation in the 1,3 band, as the situation there is much clearer than it is for the 3,5 band. Here we have but one perturbation in contrast to the two perturbations in the latter. The perturbation in the 1,3 band occurs in the T_1 terms and hence we would expect lines originating on T_1 levels to have appreciable Zeeman patterns. For while normally a $^2\Sigma - ^2\Sigma$ transition with an inappreciable spin doubling in both electronic states would show no Zeeman effect, there is here a strong interaction of the T_1 terms of one of these states with a $^2\Pi_{1/2}$ level which has pronounced Zeeman patterns. And the transitions at the perturbation point originate in levels whose character is partially that of a $^2\Sigma$ state and partially that of a $^2\Pi$ state. Our expectations of appreciable Zeeman patterns are realized as one readily sees on glancing at either the tables or the microphotometer traces. We also see that the T_2 terms are affected by the magnetic field as well as the T_1 terms. At 9000 gauss the R_2 lines are broadened asymmetrically about the no-field position of the line, for those lines in the immediate vicinity of the maximum of the perturbation. As we progress to higher rotational quantum numbers, this broadening takes the form of a block of radiation extending from the R_2 lines to the R_1 lines and on past them for a varying amount. As the field strength is increased the patterns for these high K values more and more closely approach the width of the separation of the R_1 and R_2 lines. And at the highest field strength and highest K value, we see that the patterns are actually a filling in of this gap. The two photometer traces show this phenomenon setting in at $K=16$.

If one assumes that the separation of the T_1 and the T_2 levels is due to spin doubling and computes the Zeeman patterns to be expected on the basis of the expression developed by Hill and published by Almy,[7]

[7] G. M. Almy, Phys. Rev. **34**, 1517 (1929).

TABLE II. *Zeeman patterns for the 3,5 N_2^+ band. (See heading for Table I.)*

K''	J	$\Delta\nu$	12,600 (0.59)	24,000 (1.12)
4	4.5	−0.74	0.47 to −0.14	0.07 to −1.09
4	3.5	−2.00	1.15 to 0.00	0.15 −1.85
5	5.5	−1.03	0.30 to 0.01	
5	4.5	−2.48	1.26 to 0.21	
6	6.5	+0.66	0.09 to −0.59	1.63 to −0.44
6	5.5	−3.14	0.79 to 0.09 0.09 to −0.68	
7	7.5			
7	6.5	−4.35		1.23 to 0.25
8	8.5		1.36 to 0.59 0.59 to −0.40	
8	7.5	−6.75	1.09 to 0.21 0.13 to −0.72	1.11 to −1.13
9	9.5		2.10 to 0.14 to −0.45	
9	8.5	8.12	1.14 to −0.15	
10	10.5		−0.41 to −1.27	1.05 to −1.06
10	9.5	5.59	1.03 to 0.14 to −0.50	3.23 to 2.23 −1.90 to −3.02
12	12.5		0.58 to −0.22	0.60 to −0.34
12	11.5	3.21	0.55 to −0.73	0.25 to −0.87
14	14.5		0.67 to −0.12	
14	13.5	2.37		0.13 to −0.81
16	16.5		1.06 to −0.20	
16	15.5	1.91	0.30 to −0.85	

$$\Delta W = \pm\tfrac{1}{2}\{\nu_0^2 + 4m\nu_0\Delta\nu_n/(K+\tfrac{1}{2}+4\Delta\nu_n^2\}^{\frac{1}{2}},$$

then one finds that there is good agreement between the observed and computed patterns for K greater than 14 at the three highest field strengths.

The patterns of the most interest are those in the immediate vicinity of the perturbation. As previously remarked, the patterns in this region are doublets. At 12,600 gauss the $K=12$, $J=12.5$ line is a doublet. This is the only line which appears as a doublet in the field at this low field strength and it is the most perturbed line. At 19,700 gauss the $K=11$, $J=11.5$ line is a doublet and the $K=12$, $J=12.5$ is not measurable as there is an overlapping atomic line. Furthermore we find that the R_2 lines for $K=12$ and 13 each have patterns at this field strength which are doublets. At 24,000 gauss the lines which were doublets at the previous field strengths are doublets still and there is also evidence that the two lines with $K=14$ become doublets at this field strength. In other words in the immediate vicinity of the perturbation we find that the patterns are doublets for both the T_1 and T_2 terms, that the doubling occurs first in the T_1 (perturbed) terms and that at the higher field strengths the T_2 (unperturbed) terms likewise become doublets. This summarizes the results for the 1,3 band.

In the case of the 3,5 band the situation is complicated by the fact that there are perturbations in both the T_1 and the T_2 terms. The T_1 terms first pass through a perturbation and then the T_2 terms are perturbed. These two perturbation points are at nearly the same K value and the effects of both are present simultaneously. The observations on this band are

much more meager, being mainly taken from the plates at 12,600 and 24,000 gauss, that is those taken with the second type of source.

The perturbation in the T_1 terms is relatively small while that in the T_2 terms is quite large, reaching a maximum displacement of 8.12 cm^{-1} at $K=9$. Much the same results are obtained here as for the 1,3 band. At high field strengths and high K values, the patterns tend to fill in the space between the corresponding R_1 and R_2 lines and agree with the results computed by Hill's equation. And in the immediate vicinity of the perturbation both the R_1 and the R_2 lines appear as doublets in the field.

Discussion

Certain requirements have been established by Kronig[8] as necessary for the existence of a perturbation. Among them is the requirement that the two levels which perturb each other shall have the same J and the same M values. An explanation of the observed Zeeman patterns is possible with this requirement as a guide. There are three findings which need consideration. They are first the existence of doublet patterns for the perturbed terms at the points of maximum perturbation, second the asymmetric patterns of these terms throughout the remainder of the band, and third the existence of any magnetic effect for the unperturbed levels.

Fig. 2a illustrates the situation for a particular K level in the immediate neighborhood of a perturbation. The solid lines are the position of the levels in the absence of an external magnetic field. The dashed lines indicate the position of the $M=0, \pm J$ levels when an external magnetic field has been applied. Childs[4] has estimated the value of the B constant in the perturbing $^2\Pi$ state as approximately 1.5 cm^{-1}. We may assume an A value of 50 cm^{-1} by analogy to the similar $^2\Pi$ level in CN, as these two molecules are isoelectronic. Then by means of Hill's equation for doublet II states,[9] we can compute the spread of the levels in this perturbing state for any field strength. Computation shows that the spread in the region of the perturbation is considerably less than $\Delta\nu_n$. We know that the spread of the levels in the $^2\Sigma$ state is from $+\Delta\nu_n$ to $-\Delta\nu_n$. Hence we see that the spread of levels for a particular K value is much greater in the $^2\Sigma$ than it is in the $^2\Pi$ state. Therefore the levels are drawn as they are. The separation of the levels in the absence of a magnetic field is not known, a fact which is absolutely essential for the quantitative treatment of the problem.

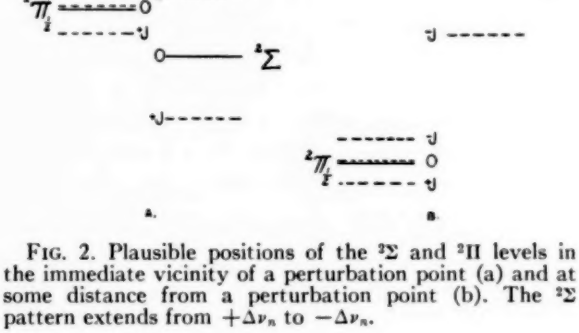

FIG. 2. Plausible positions of the $^2\Sigma$ and $^2\Pi$ levels in the immediate vicinity of a perturbation point (a) and at some distance from a perturbation point (b). The $^2\Sigma$ pattern extends from $+\Delta\nu_n$ to $-\Delta\nu_n$.

Recalling the perturbation requirement that only levels having the same M values perturb each other, we see that in the case illustrated the levels with $M=-J$ are brought closer together and hence the perturbing effect of the one on the other is greatly increased, while those for which $M=+J$ are thrown further apart and the effect is the reverse. Furthermore for the $^2\pi$ state the level $M=0$ will be slightly shifted and its perturbation will also be altered. The region of low intensity (approximately zero intensity) must be caused by the extremely close dependence of the perturbation energy on the separation between levels having the same M value. The asymmetry observed in regions where the perturbation is small is easily understandable as arising from the situation illustrated in Fig. 2b. Here we see that there is very little interaction between the levels in the absence of the field. The interaction of the $M=+J$ levels is practically unaltered by the application of an external magnetic field as the perturbation energy varies only slowly with the distance between the mutually perturbing levels when this distance is large. The drawing

[8] R. de L. Kronig, Zeits. f. Physik **50**, 347 (1928).
[9] E. L. Hill, Phys. Rev. **34**, 1507 (1929).

together of the $M=-J$ levels is so slight as to cause but a small increase in their perturbation energy.

Now the existence of Zeeman patterns for the unperturbed levels (T_2 levels in the $v'=1$ state) following the perturbation is quite unexpected. However it may be accounted for in the following manner. There is no appreciable spin doubling in the unperturbed upper $^2\Sigma$ states of the N_2^+ molecule until quite high rotational quantum numbers are reached. This must mean that the coupling of the electron spin and the magnetic field produced by the rotation of the molecule is quite small. It is so small in fact that a perturbation is required to show the doubling of the $^2\Sigma$ state at low K values. Now the magnetic field which is applied externally is sufficient to cause a partial Paschen-Back effect and uncouple to more or less degree the spin from the magnetic field produced by the rotation of the molecule. Hence the T_1 and the T_2 terms are no longer distinct entities when an external magnetic field has been applied. And the T_2 terms (unperturbed) may share the perturbation which was previously the distinguishing characteristic of the T_1 terms. Thus we see that just as the R_1 lines are doublets in the field at the points of maximum perturbation so will the R_2 lines become doublets, though to a slightly smaller extent.

A quantitative treatment of the problem requires a knowledge of the actual position of the perturbing levels but these data are not available because of the nature and position of the perturbing state.

The author wishes to thank Professor W. W. Watson for his many timely suggestions and for his guidance in this research.

Rotational Analysis of the Perturbed (13,15) $^2\Sigma - {}^2\Sigma$ N_2^+ Band

ALLAN E. PARKER, *Sloane Physics Laboratory, Yale University*

(Received April 10, 1933)

A rotational analysis of the 13,15 $^2\Sigma - {}^2\Sigma$ N_2^+ band has been made. This analysis is of interest as a perturbation is found to occur in the upper state. The rotational analysis gives the following constants: $B_{13}' = 1.54_5$ cm^{-1}, $D_{13}' = -5 \times 10^{-5}$ cm^{-1}, $B_{15}'' = 1.62$ cm^{-1} and $D_{15}'' = -1 \times 10^{-5}$ cm^{-1}. The origin of the band is at 21044.7 cm^{-1}.

INTRODUCTION

AS mentioned in the preceding paper perturbations have been found in the $v = 0$, 1 and 3 levels of the upper $^2\Sigma$ state of the N_2^+ bands. These perturbations arise from an interaction of a $^2\Pi$ state with this $^2\Sigma$ state. Transitions between these two states are forbidden by selection rules and transitions of any intensity between this $^2\Pi$ state and the ground $^2\Sigma$ state lie too far out in the infrared to be observable. So what knowledge is to be obtained of the $^2\Pi$ state must be deduced from a study of the perturbations which it shares with the upper $^2\Sigma$ state.

ROTATIONAL ANALYSIS

In the course of the investigation of the Zeeman effect for perturbed N_2^+ terms[1] already known, use was made of a discharge tube in which the N_2^+ bands were excited while the N_2 bands were not present. Hence observation of N_2^+ bands in regions ordinarily overlain with N_2 bands was possible. It was found that to the red of the $\Delta v = 2$ sequence, there was a band degrading to the red and containing a perturbation. Analysis of this band gives the assignments of the lines shown in Table I. The B values of the two levels are obtained from the combination differences given in Table II. The values of the constants are

$B_{13}' = 1.54_5$ cm^{-1}, $B_{15}'' = 1.62$ cm^{-1},

$D_{13}' = -5 \times 10^{-5}$ cm^{-1}, $D_{15}'' = -1 \times 10^{-5}$ cm^{-1}.

Coster and Brons[2] have shown that the B values of the lower state fit a linear equation. Extrapolation by this equation to $v = 15$ gives the value of B_{15}'' as 1.620 cm^{-1}. This serves to fix the vibrational quantum number of the lower state. A consideration of the B values of the upper state show that they can best be fitted by the equation

$$B_v' = B_0'(1 + \alpha v + \beta v^2)$$

where $\alpha = -0.0101$ and $\beta = -0.00072$. The determination of the upper state vibrational quantum number is based on the position of the band ($\nu_0 = 21044.7$ cm^{-1}) and the B value of this level.

TABLE I. *Rotational assignments for the 13,15 band.*

K''	R_1	R_2	P_1	P_2
0	21,047.80			
1	50.48			
2	53.53		21,038.04	
3	56.15		34.36	
4	58.67		30.85	
5	61.02		27.15	
6	63.20		23.13	
7	65.55	65.28	18.98	
8	67.48	66.91	(15.83)	
9	68.51		10.46	
10	69.90	06.15		05.80
11		00.56		00.01
12	71.48	20,996.44		20,995.52
13	72.53	92.02		90.48
14	73.67	86.42		84.21
15	74.71		81.11	
16	75.71		75.79	
17	76.67		(69.13)	
18	77.16		64.32	
19			58.74	
20			52.34	
21			46.14	
22			39.57	
23			32.74	
24			25.82	
25			18.78	
26			11.56	

[1] A. E. Parker, Phys. Rev. **44**, 84 (1933).

[2] D. Coster and H. H. Brons, Zeits. f. Physik **73**, 747 (1932).

The point of interest in this analysis is the existence of a perturbation in the upper level. Determination of whether the perturbation occurs in the T_1 or the T_2 levels must be made by means of the intensity ratio of lines of the same K value. The ratio of intensities is as $K+1 : K$, the lines originating on the T_1 levels being the stronger. When the separation of the two sets of levels persists into the region where the spin doubling has become appreciable, this is possible as shown by Coster and Brons. This procedure is not applicable here as only the lines of low K value (inappreciable spin doubling) were excited. However, the branch in which the perturbation occurs is not detectable after the perturbation and therefore we may assume that the perturbation is in the T_2 levels. This assignment is of course open to question. In Fig. 1 the separations of the levels in the upper state are plotted against their K values.

TABLE II. *Combination differences for the 13,15 band.*

K''	$\Delta_2F''(K)$	$\Delta_2F'(K)$
1	9.76	
2	16.12	15.49
3	22.68	21.79
4	29.00	27.82
5	35.54	33.87
6	42.04	40.07
7		46.57
8	55.09	
9	61.33	58.03
10	67.95	63.75
11	73.46	
12		75.04
13	85.06	80.51
14	91.42	87.25
15	97.88	93.60
16		99.92
17	111.39	
18	117.93	112.84
19	124.82	

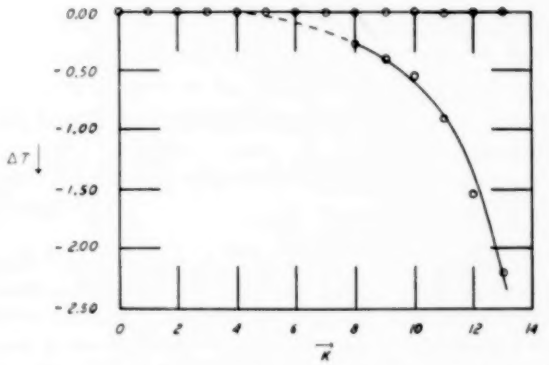

FIG. 1. Separations between the T_1 and the T_2 terms in the $v'=13$ level plotted against K, showing a perturbation in the $T_2(?)$ levels.

We now know that the following vibrational levels of the upper $^2\Sigma$ state are perturbed: the $v=0$, 1, 3 and 13 levels. Furthermore we know that the course of the $^2\Pi$ state's levels is such that in all probability consecutive levels of it perturb the $v=0$ and 1 levels of the $^2\Sigma$ state. That there are two $^2\Pi$ levels intervening between those which perturb the $v=1$ and 3 levels of the $^2\Sigma$ state seems very likely. The spacing of the $^2\Pi$ vibrational levels is considerably smaller than that of the $^2\Sigma$ levels in question and so we need not be at all surprised at the existence of a perturbation in one of the higher vibrational levels of the $^2\Sigma$ state. In fact we might predict, by means of a level diagram, that the $^2\Sigma$ levels from nine on probably contain perturbations and that the $v=5$, 7 and 8 levels probably contain perturbation points in the region of high K values.

The author wishes to thank Professor W. W. Watson for his interest and advice during the course of this analysis.

Pressure Effects of Foreign Gases on the Sodium *D*-Lines

HENRY MARGENAU AND WILLIAM W. WATSON, *Sloane Physics Laboratory, Yale University*

(Received May 2, 1933)

The effects of foreign gases (A, N_2 and H_2) on the *D*-lines of Na have been studied by means of a steel absorption chamber, in which the Na-vapor pressure is kept low while the foreign gas pressure varies between 0 and 17 atmospheres. Temperatures were such that true line contours could be photographed and photometrically evaluated. Results are: (1) The red shift of the absorption maximum varies linearly with the density of the perturbing gas. (2) Study of the line contours reveals marked asymmetries, most pronounced near the base. Asymmetries are to the red in case of A and N_2, slightly to the blue for H_2. (3) Both *D*-lines show the same broadening and shift. (4) The effects can be accounted for theoretically by assuming a distance of closest approach between excited Na and the foreign gas molecules of about 9A. Quantitative results are summarized in Table I.

INTRODUCTION

IN studying the shape and position of spectral lines emitted or absorbed by an atom which is not in an isolated state, two conditions should be clearly distinguished: the optically active atom may be under the influence of perturbing neighbors of its own kind, or it may be perturbed by a foreign gas. Experimentally, very strong broadening and small shifts in the position of the lines are characteristic of the first named effect, while perturbation by foreign gases always produces relatively smaller broadening and larger shifts. The quantum mechanical forces responsible for the first effect are due to "resonance"; in the second case it is mainly the mechanism of nonstatic polarization which provides the forces of interaction, as was shown in an earlier paper[1] by one of the authors. Believing that theory at present furnishes more definite guidance in an experimental study of the effect due to foreign gases than it does in connection with resonance broadening, we have devoted this investigation entirely to the former problem. Absorption lines are chosen in preference to emission lines, of course, because of the difficulties attending the precise determination of the thermodynamic state in which emission occurs.

Much of the earlier work on problems similar to this was done with the main object of determining the "number of resonators" absorbing the line in question (*f*-values).[2, 3] For this purpose, the exact position and the details of the shape of the line are inessential and have not been determined with great precision. Füchtbauer and Schell[4] have measured the absorption of the *D*-lines in nitrogen and compared their results with the theory of Lorentz, which does not explain the most interesting and important features of the phenomenon, namely the asymmetries and the shifts. They also worked in a very limited pressure range, not exceeding 2 atmospheres. Minkowski[5] obtained some interesting data on the shape of the *D*-lines perturbed by a large number of foreign gases from which the asymmetry of the lines is especially apparent. He finds that all gases except H_2 and He broaden predominantly toward the red, while the latter two produce noticeable blue asymmetries. Theory leads one to expect a shift toward the red in all these cases; hence there arises the question as to whether, in the case of H_2 and He, a blue asymmetry is coupled with a red shift. This will be verified presently, and a qualitative explanation will be given. Minkowski's measurements do not expose, however, the true contour of the absorption lines, for their centers were completely absorbed. His pressures are confined to

[1] H. Margenau, Phys. Rev. **40**, 387 (1932).

[2] C. Füchtbauer and Hofmann, Ann. d. Physik **43**, 96 (1914). (Work on Cs-lines.)

[3] H. Bartels, Ann. d. Physik **65**, 143 (1921). (Cs-lines.)

[4] Füchtbauer and Schell, Phys. Zeits. **14**, 1164 (1913).

[5] R. Minkowski, Zeits. f. Physik **55**, 16 (1929).

values below one atmosphere. This pressure range was also studied by Korff,[6] who used H_2 and He as perturbing gases.

Further papers deal more specifically with the effect of foreign gases on the integrated (total) absorption and demonstrate the existence of quenching. Different gases behave differently in reducing the total absorbed intensities, as was shown by Stuart,[7] Kunze[8] and others.

Very careful and significant measurements were made by Füchtbauer, Joos and Dinkelacker[9] ten years ago. They observed the contours of the absorption curves for Hg 2537 in their entirety and produced an interesting set of data, suitable as a basis for theoretical analysis. Besides determining shift and half width, they also showed the quenching effect of several foreign gases. Their findings were first discussed from a theoretical point of view in reference one and proved to be in substantial agreement with current notions of intermolecular forces.

Meanwhile a complex of theories on the broadening of spectral lines has been developed. Confining attention only to those theories which have a direct bearing on the specific problem at hand, two principal methods of calculation appear to be prevalent. The first proceeds on the basis of an analysis of the potential energy curves[10] representing the interaction between the active atom and its perturber. This method permits one, by applying the Franck-Condon principle together with statistical considerations, to account for the main experimental results.[11, 12, 13] In the first of these papers, an evaluation of the intermolecular forces here encountered in terms of dispersion *f*-values was also given. The alternative mode of approach[14, 15] considers the active atom as absorbing continuously, but with a varying frequency which depends on the distance of the perturbers. The calculation is then a Fourier analysis of the electric moment of the atom, written as a function of the time. The former point of view leads to results capable at least of rough quantitative comparison with experiment and places emphasis on the main experimental features: shift and asymmetry of the lines. While our experimental results are independent of any chosen interpretation, the former method of reasoning will be employed in their discussion. It turns out that none of the observed features are contradictory to the basic assumptions of references 11 and 13.

To be of aid to any theory, the experimental data on pressure broadening must include observations on the entire absorption contour, which requires an adjustment of foreign gas pressure and temperature of absorbing gas for every exposure. The lines of an alkali metal were chosen for this investigation because both broadening and shift could be expected theoretically to be larger than for most other substances, which is verified. It seemed interesting, furthermore, to find out whether the two components of the Na-doublet suffer equal pressure effects or not. Finally, it remained to be seen what forces between the excited Na-atom and the gas molecule, together with the simple model used in references 11 and 13; would have to be assumed to account for the observed shifts and line contours. The interpretation also leads to an approximate value for the distance of closest approach between the excited Na-atom and the foreign molecule. Measurements at pressures greater than atmospheric appeared necessary to increase the accuracy of measurement. High pressures do not invalidate the application of theory in any essential way, for one can easily convince himself that the molecular forces even at the highest pressures used in this work remain approximately additive. An experimental verification of this assumption may be seen in the absence of departures from the linear dependence of shift and width on densities.

Experimental Procedure

The absorption tube used in these experiments was a steel pipe 33 inches long, $1\frac{5}{8}$ inches outside diameter and with a 1 inch bore. Glass windows 1 cm thick were held on the ends by means of

[6] S. A. Korff, Astrophys. J. **76**, 124 (1932).
[7] H. A. Stuart, Zeits. f. Physik **32**, 262 (1925).
[8] P. Kunze, Ann. d. Physik **8**, 500 (1931).
[9] C. Füchtbauer, G. Joos and O. Dinkelacker, Ann. d. Physik **71**, 204 (1923).
[10] First suggested qualitatively by Jablonski, Zeits. f. Physik **70**, 723 (1931).
[11] H. Margenau, Phys. Rev. **40**, 387 (1932).
[12] M. Kulp, Zeits. f. Physik **79** (1932).
[13] H. Margenau, Phys. Rev. **43**, 199 (1933).
[14] V. Weisskopf, Zeits. f. Physik **75**, 287; **77**, 398 (1932).
[15] W. Lenz, Zeits. f. Physik **80**, 423 (1933).

overlapping nuts of $\frac{5}{16}$ inch steel threaded on to the tube. Considerable trouble was experienced in constructing gaskets which would continue to be pressure-tight after the absorption tube had been heated to 200°C and then cooled. This difficulty was almost completely overcome by the use of lead rings $\frac{3}{32}$ inch in thickness, their lateral expansion when compressed being hindered by short sections of thin-walled steel tubing which fitted tightly into the main tube and the end-nuts. An opening near one end, closed by a nut with a piece of annealed copper for a gasket, served for the introduction of the sodium. A side tube near the other end connected to the nitrogen, argon, or hydrogen tank, the vacuum pump, and the pressure gauge. The latter read to 200 lbs. full-scale and was carefully calibrated. The absorption tube could be kept at any desired temperature by means of a three-section electric furnace somewhat longer than the tube. A thermometer was placed in each section of the furnace.

In preparation for the taking of the spectrograms the apparatus was first evacuated and the tube heated with a blow-torch to free it of water vapor. The gas being used was then allowed to stream in slowly through a heated coil of copper tubing filled with copper filings. When atmospheric pressure was reached, metallic sodium was introduced into the tube through the small opening from which the gas was escaping all the while. In this way the pieces of sodium were but slightly oxidized on the surface. Next the tube was again evacuated, heated with the blow-torch until the sodium boiled, and then tipped so that the clean liquid sodium ran down its entire length. Gas was then admitted through the hot copper tube to atmospheric pressure, the valve to the vacuum pump closed, the furnace adjusted around the tube, and its temperature raised to about 200°C. Under these conditions the sodium vapor was so dense as to cause the D-lines to be very completely absorbed. The tube was then slowly filled with the foreign gas to a pressure of 200 lbs./in.^{2} as read on the gauge. After taking the spectrogram at this highest pressure, the gas pressure and temperature were reduced and other spectrograms were taken at convenient pressure intervals. At each pressure the temperature of the furnace was adjusted so that the absorption was less than total in the center of the D-lines in order that true line contours would be registered. With practice this adjustment could be checked by visual inspection of the lines.

A Pointolite lamp served as the source of continuous spectrum, a single lens being employed to produce a much-enlarged image of the tungsten bead on the slit of the spectrograph. The latter was a 21-foot concave grating in a stigmatic mounting giving a dispersion of 2.25A per mm at 5890A in the second order. The exposure times varied from 6 to 10 minutes. On each plate exposures of a half and a quarter of this time, all other variables being held constant, were placed as blackening marks for the purpose of calibrating the density gradations in the absorption lines. Both Eastman Hypersensitive Panchromatic and Eastman Type 4-D plates were used. The former were found to have a longer linear section for the density *vs.* log (It) curve and a lower threshold, thus necessitating but little correction to the microphotometer trace to get the true absorption curve, but their large plate grain proved troublesome. We therefore adopted the type 4-D emulsion together with a borax developer, the combination giving a very small plate grain. A more detailed determination of the characteristic curve of these plates, however, showed them to require care in calibrating the microphotometer deflections. A neon spectrum was superposed on a portion of the main exposure on each plate as a comparison. Ne has two lines 5881.896A and 5902.475A, one on either side of the D-lines which serve as convenient standards. Finally, on each spectrogram a fine scratch was drawn parallel to the spectral lines between the two Na lines, and its "wave-length" determined with the comparator by reference to the Ne standard lines, to serve as an additional reference point on the microphotometer traces.

Each spectrogram was run through a Koch-Goos recording microphotometer using the 1 : 40 ratio to give the maximum enlargement. Because of this enlargement two traces were necessary for each spectrogram, one covering the 5881 Ne line, the D_2 absorption band and the scratch above referred to, the other recording the region from the 5902 Ne line through the D_1 absorption band to about the center of the D_2 band. In

FIG. 1. Microphotometer traces of D_2 broadened by argon. *Small peak:* trace for an argon pressure of 1.85 atm.; *large peak:* trace for a pressure of 17.8 atm. Reference line (Ne, λ5881.896), exactly superposed on the two traces, appears on extreme left. (Lower trace is slightly out of focus in the reproduction.)

addition the deflections of the microphotometer for the three blackening marks and for the clear portion of each plate were recorded. To illustrate the character of the microphotometer curves obtained, we give in Fig. 1 a superposition of two traces of the D_2 line perturbed by argon at relative densities d (cf. below) of 1.21 and 9.16, respectively. The large shift of the maximum of absorption to longer wave-length and the marked asymmetry of the absorption curve for the higher density of argon are to be noted.

For the computation a trace of each microphotometer curve was made on millimeter cross-section paper, smoothing out of course the slight irregularities due to plate grain. In each instance where necessary this curve was transformed into a true absorption intensity curve by means of the known photographic density curve. The wave-length dispersion on each of these traces being known from the interval between the peaks due to the two reference standards, the wave-length of the maximum of the absorption for each D-line was computed by interpolation. Drawing the base line beneath each absorption maximum for the position of the trace if no absorption were present, the levels for one-half and for one-quarter of the interval to the absorption peak were marked, the widths of the absorption band at these two points determined in millimeters, and the conversion to wave numbers made. These last measurements are the half-widths and quarter-widths referred to below. Since at the highest densities of the foreign gases the absorption on the red side of the D_2-line is beginning to merge with the blue side of the D_1-line, allowance for this overlapping was necessary in order to get the true line-widths.

EXPERIMENTAL RESULTS

It is clear that the effect of the foreign gases does not depend on their pressure, but on their concentration. A convenient unit of the concentration is the density of the amount of perturbing gas used in the experiment at 0°C and 1 atm. The density measured in this unit will be called "relative density." To convert pressures as read on the gauge into relative densities, two corrections had to be applied. First, because the gauge was slightly above room temperature with the gas in the absorption tube at approximately 200°C, account had to be taken of thermal transpiration. If the perturbing gas were ideal and equilibrium existed, this could be done by use of the simple formula: $P_1/P_2=(T_1/T_2)^{\frac{1}{2}}$, where P_1 and T_1 are pressure and temperature in the absorption tube, P_2 and T_2 refer to the gauge. To test this relation, the tube was filled at room temperature and a reading of the pressure taken. After heating the tube the pressure was read again on the cool gauge, and finally the initial temperature was restored to insure that no leak had occurred. In this way the validity of the above relation was verified to within the experimental errors of pressure and temperature measurements, and the formula applied thereafter. The second step involved the reduction to density at 0°C and was made by means of van der Waals equation—although, except for the highest pressures, the deviation from the law for perfect gases is inappreciable.

The results indicate clearly that the two D-lines behave alike with respect to shift, width and asymmetry, as was concluded on theoretical grounds.[11] The shift, plotted against relative densities in Figs. 2 and 3, is seen to be proportional to the density of the perturbing gas, as

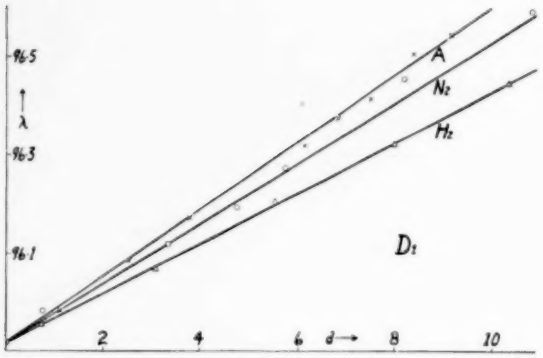

FIG. 2. Wave-length of maximum of D_1 *vs.* relative density of perturbing gas.

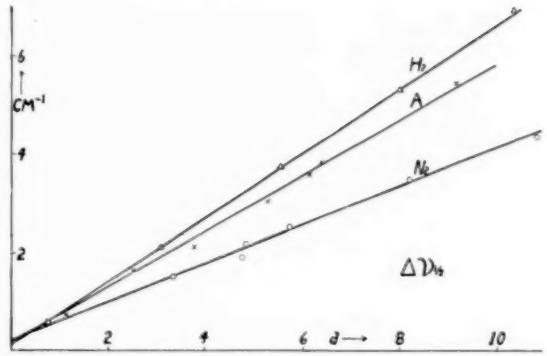

FIG. 4. Half widths (averages for D_1 and D_2) *vs.* relative density of perturbing gas.

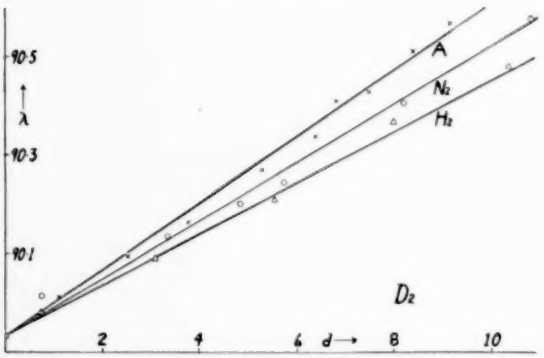

FIG. 3. Wave-length of maximum of D_2 *vs.* relative density of perturbing gas.

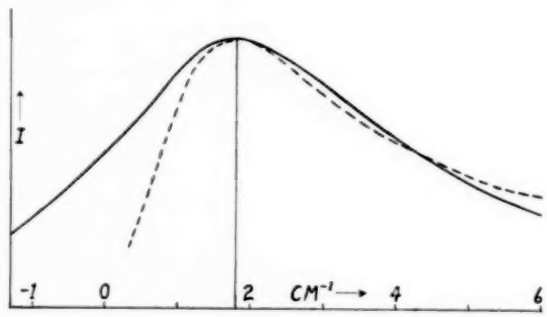

FIG. 5. *Solid curve:* Absorption contour of D_1 broadened by 17.8 atm. of argon pressure. *Dashed curve:* Corresponding theoretical curve.

was found by Füchtbauer and his collaborators for the Hg line. All shifts are to the red. Regarding the unperturbed position of the *D*-lines it may be noted that the values plotted in Figs. 2 and 3 are slightly different from those given by Wood and Fortrat[16] (5889.933 and 5895.917A as against W. and F.'s 5889.963 and 5895.930A). Nevertheless our unshifted wave-lengths fall in line with the other points of the diagram distinctly better than do those of Wood and Fortrat. It may be, therefore, that a small constant error affects the absolute values of all the wave-lengths plotted in the figures. In Füchtbauer's[9] experiment, the shift of the Hg-line was about 0.126 cm^{-1} per unit relative density of argon; the corresponding displacement for the Na-lines is 0.196 cm^{-1}. Because of the longer wave-length of the Na-lines, this makes the measured wave-length shift for the Na-lines more than 8 times as large as that for Hg, which increases considerably the accuracy of measurement. An upper limit for the pressures used was set by the incipient overlapping of the *D*-lines. At 18 atmospheres, this became so strong that corrections became necessary, indicating the futility of continuing to greater densities, although this was originally planned.

The exact shape of the broadened lines is exhibited in Fig. 1 (uncorrected for plate characteristic) and Fig. 5 (solid curve, representing the absorption coefficient, i.e., const. × log (absorbed intensity)) as a function of the wave number. In the case of N_2 and A, the asymmetries to the red are very pronounced; they grow especially strong near the base of the line. H_2 produces a slight but unmistakable asymmetry to the blue. Following the usual convention, we have chosen the "half width" to convey a measure of the broadening produced by the different gases. Half width is defined as the wave number or wave-length interval in which the absorption coefficient is equal to or greater than one-half

[16] R. W. Wood and R. Fortrat, Astrophys.J. **43**, 73 (1916).

its maximum value. In Fig. 4, these half widths are plotted against relative densities. Since the corresponding values for D_1 and D_2 were found to be equal within the error of their determination, separate graphs for the two lines were thought unnecessary, hence the average half width was plotted in all cases. The best curves through the experimental points are straight lines.

To give an indication of the asymmetries, the ratio of the red "half" to the blue "half" of the half widths should be given. By these terms we wish to designate the two portions of the half width range on the two sides of the maximum. The ratio begins, as might be expected, with the value 1 at zero densities and grows to 1.3 and 1.45, respectively for N_2 and A at the highest pressures used in this experiment; for H_2 it falls to 0.96. Hydrogen, though producing the smallest shift, broadens most effectively in toto. It appears, however, that the broadening on the red side of the line alone maintains with respect to N_2 and A the same order as the shift. The large line width in the case of H_2 is best thought of as produced by additional broadening to the blue. A possible theoretical interpretation of this phenomenon will be considered later.

Comparing our results again with those of Füchtbauer, Joos and Dinkelacker on the Hg-line, we find that the D-lines are broadened by a given gas almost twice as strongly as is the Hg-line (using as a measure the half width intervals in wave numbers). Table I contains a summary of our data. $\Delta\lambda/d$ represents the shift of the line per unit relative density in A, $\Delta\nu/d$ the average of this shift for the 2 D-lines, expressed in wave numbers, and $\Delta\nu_{1/2}/d$ is the half width of the lines per unit relative density of the corresponding gas. The numbers are simply the slopes of the lines in Figs. 2 to 4. The variation of the total absorption ($\int(n\kappa)d\nu$) was not investigated because it depends very critically on the number of Na atoms within the absorption tube. This was difficult to determine since deviations from exact equilibrium between Na-vapor and liquid in the large volume of our tube at high pressures may well be expected to occur.

TABLE I.

	$\Delta\lambda/d$			
	D_1	D_2	$\Delta\nu/d$	$\Delta\nu_{\frac{1}{2}}/d$
A	0.068A	0.068A	0.196 cm^{-1}	0.57 cm^{-1}
N_2	0.061A	0.059A	0.173 cm^{-1}	0.39 cm^{-1}
H_2	0.051A	0.052A	0.148 cm^{-1}	0.65 cm^{-1}

THEORETICAL DISCUSSION OF RESULTS

Various assumptions have been made in the literature about the actual shape of pressure broadened lines. Among the simplest possible theoretical contours are the "dispersion" curve and the error curve. The asymmetries demonstrate, of course, that neither assumption is correct. Nevertheless it might be possible to characterize the general trend of the absorption contour by one of these two simple types; in fact this procedure has been largely followed by experimental investigators who, in stating line widths, assumed the line to be a simple dispersion curve in accordance with Lorentz' theory of broadening. This hypothesis is capable of being tested simply. Let us call the wave number range in which the absorption coefficient is equal to or larger than $\frac{1}{4}$ of its maximum value, the quarter width of the line, and denote it by $\Delta\nu_{1/4}$. Then the ratio $\Delta\nu_{1/4}/\Delta\nu_{1/2}$ is a simple characteristic for each of the two simple types of curve just mentioned. Experiment, too, gives a value for this ratio which is essentially independent not only of the density used (quarter widths are roughly proportional to the relative densities in our experiment) but even of the broadening gas. The values of this ratio were found to be 1.61, 1.59, 1.65, respectively, for A, N_2 and H_2.—The dispersion curve has the form (ω is angular frequency):

$$I(\omega)=1/[(\omega-\omega_0)^2+1/\tau^2];$$

it gives a half width $\Delta\omega_{1/2}=1/\tau$, and a quarter width $\Delta\omega_{1/4}=3^{\frac{1}{2}}/\tau$. Hence $\Delta\omega_{1/4}/\Delta\omega_{1/2}=3^{\frac{1}{2}}=1.73$. On the other hand, an error function

$$I(\omega)=\text{const. } e^{-(\omega-\omega_0)^2/a^2}$$

has a half width $\Delta\omega_{1/2}=a(\log 2)^{\frac{1}{2}}$ and a quarter width $\Delta\omega_{1/4}=a(\log 4)^{\frac{1}{2}}$, yielding a ratio $\Delta\omega_{1/4}/\Delta\omega_{1/2}=2^{\frac{1}{2}}=1.41$. The experimental ratio lies between these two values, indicating that neither assumption is strictly correct, even if asymmetries are disregarded.

A feature worthy of explicit mention is apparent from Fig. 1. The intensity in the high

density curve at the point which corresponds to the maximum of the undisplaced line is surprisingly small. The effect of foreign pressures is not adequately described by referring to it as unsymmetrical broadening; the outstanding characteristic seems to be a very real displacement of the line. We feel, therefore, that any theory designed primarily to account for the broadening, and compelled afterwards to correct for asymmetries and displacements, misses the central part of the phenomenon. In the subsequent discussion we shall make use of the theoretical considerations proposed in the other papers,[11, 13] which are free from this objection, and analyze the effect of argon on the D-lines in somewhat greater detail.

Following the reasoning in reference 13, we have attempted to fit the expression given in Eq. (17) of that paper to the experimental contour of the D-lines perturbed by 17.8 atmospheres of argon at a temperature of 250°C (relative density = 9.16). The result is given in Fig. 5, where the solid line represents the experimental curve, the dashed line being Eq. (17), with $R_1 = 8.5$A and $\beta = 345$. This choice of constants produced the correct shift as well as the correct half width. The graphical evaluation of the theoretical curve is somewhat tedious, and it might be that a slightly different choice would have given a better fit. But the imperfection of the model (cf. below) used in the calculation would render further numerical refinement meaningless. R_1 is to be interpreted as the distance of closest approach between an excited Na-atom and the (unexcited) A-atom. The meaning of β is this: if the interaction energy between a normal Na-atom and an A-atom is given by $-a/R^6$, where R is the distance between the two measured in A-units (higher powers in $1/R$ are neglected!), and the corresponding energy between an excited Na-atom ($3\ ^2P$-state) and A is $-b/R^6$, $\beta = b - a$. The value of β here obtained is about twice as great as that found by the use of f-values as outlined in reference 13, but a reasonable change in the choice of f's would remove the discrepancy.

An application of these simple notions to the interaction between a Na-atom and an N_2-molecule is probably more risky. It leads to a value between 9 and 10A for R_1.

The meaning of the discrepancies in Fig. 5 is best understood if reference is made to the diagram in Fig. 6. Curve c gives the qualitative

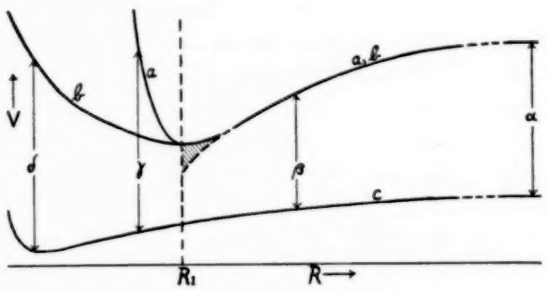

FIG. 6. Qualitative interaction curves demonstrating the mechanism of broadening and shift.

trend of the interaction energies between normal Na and a foreign gas atom or molecule as a function of the distance of separation, while curves a or b refer to an excited Na-atom. In the calculation, the upper curves have been replaced for simplicity by the dotted one, which rises vertically at R_1. Hence in the simplified model, only transitions to the right of R_1 can occur, all of which have smaller energies than α, the transition at an infinite separation. The model can therefore not account for blue broadening. It also magnifies the extreme red transitions by inserting the shaded area into the diagram, which explains the divergence at the red end in Fig. 5. The relatively small blue broadening apparent in the experimental contours we wish to ascribe to transitions occurring to the left of R_1, like γ.

For A and N_2 the upper curve is probably similar to a, while it is not unlikely that H_2 corresponds more nearly to b. For H_2, therefore, our model is particularly inadequate. The situation is then approximately this: Since the average of all possible transitions has a frequency smaller than α, the center of gravity of the broadened line is displaced to the red. Nevertheless, the distribution of frequencies within the broadened line may well be nearly symmetrical if sufficient weight is assigned to the transitions of type δ; or if the latter are particularly strong (the Boltzmann factor would render transitions at small values of R relatively more numerous) there can be a blue asymmetry superimposed on a red shift.

The Infrared Spectrum of Carbon Dioxide. Part II

ARTHUR ADEL AND DAVID M. DENNISON, *University of Michigan*

(Received June 2, 1933)

The interaction between the vibration and rotation of the CO_2 molecule is discussed. It is shown that the fine-structure lines will exhibit a convergence which depends upon certain of the anharmonic potential constants. The convergence factors are compared with the experimental data of the resolved bands and an excellent agreement is found, which leads to a determination of the anharmonic constants. Combining these results with those of Part I, the complete potential function for CO_2 is obtained. A simple analytic function for the potential is proposed which contains but four constants. It is shown that this function agrees satisfactorily with the experimental potential for small displacements. The range of the validity of the analytic function is discussed and one of the heats of dissociation of CO_2 is obtained.

INTRODUCTION

A PREVIOUS paper by this title, Part I,[1] was concerned with an analysis of the vibrational levels of the linear and symmetrical molecule O—C—O. The Hamiltonian governing the vibrational motions of the molecule was shown to have the form,

$$H = H_0 + \lambda H_1 + \lambda^2 H_2,$$

where

$$H_0 \equiv (2\pi^2/h)\{2\omega_2 p_\sigma^2 + \omega_2 p_\rho^2 + \omega_3 p_\xi^2 + (\omega_2/\rho^2) p_\varphi^2\} + (h/2)\{2\omega_2\sigma^2 + \omega_2\rho^2 + \omega_3\xi^2\},$$

$$\lambda H_1 \equiv (2\pi^2\Delta/h) p_\sigma^2 + h\{(\Delta/2)\sigma^2 + a\sigma^3 + b\sigma\rho^2 + c\sigma\xi^2\},$$

$$\lambda^2 H_2 \equiv (\omega_3/2\omega_2 I)\rho^2 p_\xi^2 + h\{d\sigma^4 + e\rho^4 + f\xi^4 + g\sigma^2\rho^2 + h\sigma^2\xi^2 + i\rho^2\xi^2\}.$$

The quantities σ, ρ, and ξ are dimensionless variables corresponding to the normal coordinates q, r, and z, respectively.

A system having the Hamiltonian H_0 was solved rigorously and to this system, λH_1 and $\lambda^2 H_2$ were applied as first and second order perturbations. An expression was thus obtained for the vibrational energy levels $W = W_0 + \lambda W_1 + \lambda^2 W_2$ which was shown to be in excellent agreement with the observed positions of the levels.

The immediate dependence of the energy W was upon eleven derived constants whose connections with the twelve constants of H were given explicitly. Thus the positions of the vibrational levels furnish but eleven data and it is necessary to find some new relation before the twelve constants of the potential energy may be determined. This new relation may be found from an analysis of the interaction between the vibration and rotation of the molecule. It will be shown that this interaction, just as in the case of a diatomic molecule, leads to a convergence in the band lines; that is, to a term in the fine-structure formula proportional to the square of the ordinal number of the line. The analysis, in addition to fixing the values of the twelve energy constants, serves to correlate the convergence factors of all the CO_2 bands which have thus far been resolved.

THE INTERACTION BETWEEN ROTATION AND VIBRATION

The interaction between vibration and rotation can be divided into two parts which may be described in the following way. The centrifugal forces occasioned by the rotation of the molecule pull the atoms away from their old equilibrium positions to new ones in the anharmonic force field. The frequencies with which the atoms oscillate about their new positions of rest differ from the corresponding frequencies of the non-rotating molecule by amounts which are measured by the anharmonicity of the field; that is, in first order by the coefficients a, b and c, and in higher order by d, e, f, g, h and i. It is thus

[1] Adel and Dennison, Phys. Rev. **43**, 716 (1933).

apparent that the frequencies of vibration are slightly dependent upon the rotational state of the molecule, giving rise to a convergence factor in the fine-structure formula. This part of the mutual perturbations may be thought of as the effect of rotation upon vibration.

The reverse phenomenon; namely, the perturbation of rotation by vibration is independent of the anharmonic nature of the force field. To the present degree of approximation, the moments of inertia of the molecule must be considered as functions of the normal coordinates. The consequent periodic fluctuation of the moments of inertia distorts the rotational frequency to a new value. It is clear that this mechanism also induces a convergence of fine-structure lines. It is to be noted that a consequence of the effect of the vibration is to distort the molecule into a slightly asymmetrical rotator with three different, and in this instance variable, moments of inertia.

The three moments of inertia of the molecule depend upon the normal coordinates in the following manner,

$$C=\mu r^2, \quad B=(m/2)(a+q)^2+\mu z^2, \quad A=B+C.$$

The wave equation describing the system may be easily obtained. It consists of two parts. The first of these is independent of the rotation and was the equation treated in Part I. The second part of the wave equation contains terms relating both to the rotation of the molecule and to the interaction between vibration and rotation. It may be written,

$$\begin{aligned}&[\partial^2/\partial\vartheta^2+\cot\vartheta(\partial/\partial\vartheta)+(A_e/C_e+\cot^2\vartheta)\partial^2/\partial\varphi^2\\&\quad+\csc^2\vartheta(\partial^2/\partial\psi^2)-2\cot\vartheta\csc\vartheta(\partial^2/\partial\varphi\partial\psi)\\&\quad+8\pi^2A_eW/h^2]U+(\mu r^2/I)F(\varphi,\vartheta,\psi;\partial^2/\partial\vartheta^2,\\&\quad\partial^2/\partial\varphi^2,\partial^2/\partial\psi^2;\partial^2/\partial\vartheta\partial\varphi,\partial^2/\partial\vartheta\partial\psi,\partial^2/\partial\varphi\partial\psi)U\\&\qquad\qquad=0,\end{aligned}$$

where $1/A_e=\frac{1}{2}(1/A+1/B)$ and $1/C_e=1/C-\frac{1}{2}(1/A+1/B)$. It is evident that the first group of terms constitute the wave equation for a symmetrical rotator with effective moments of inertia A_e and C_e. The remaining terms, grouped as $(\mu r^2/I)F$, have no counterpart in the symmetrical rotator equation and are the purely asymmetrical rotator terms. These terms would introduce effects characteristic of the difference between the energy levels of the symmetrical and asymmetrical rotators. They would give rise to a splitting of the fine-structure lines into multiplets whose separation would be a function of the small coefficient $(\mu r^2/I)$. The bands of CO_2 observed in the Venus atmosphere are very finely resolved but they show no trace of multiplicity or even of unsharpness. We may, therefore, on purely *a priori* grounds discard the group of terms $(\mu r^2/I)F$. An exact analysis, moreover, confirms this conclusion and shows that they will, to the present order of approximation, furnish no contribution to the energy levels.

The wave equation involving the angles ϑ, φ, ψ may now be integrated and we can show that the interaction energy (and hence the convergence) may be considered as due wholly to those terms which mark the difference between the symmetrical rotator with effective moments of inertia A_e and C_e and the rigid, linear model of CO_2 with moment of inertia I. Expanding $1/A_e$ and $1/C_e$ in powers of the normal coordinates we may, upon introduction of the quantum numbers of angular momentum J and l, express the interaction in the form of a perturbing potential energy.

$$V_I=\frac{h^2}{8\pi^2I}[J(J+1)-l^2]\left[\frac{-3q^2}{a^2}+\frac{\mu}{I}(r^2+z^2)+\frac{2q}{a}\right].$$

The most significant term is the one linear in q, for it marks the removal of the oxygen atoms to new positions of equilibrium. As will become evident, it is immediately responsible for the introduction of the anharmonic coefficients a, b and c. The terms, quadratic in q, r and z giving the remainder of the interaction, express the variation of the principal moments of inertia with the phase of vibration.

When considered as a portion of the potential energy of the molecule, V_I is inconsistent with the assumption of normal coordinates because of the presence of the stretching term proportional to q. A transformation must, therefore, be effected from the coordinate q to a normal coordinate x. q and x satisfy the relation $q-x=\delta$, where

$$\delta=(h^2/8\pi^2I)(J(J+1)-l^2)/4\pi^2\omega_2^2(2Im)^{\frac{1}{2}}$$

is the linear displacement of equilibrium. Transforming the cubic anharmonic potential from its dependence upon q to its new dependence upon x, we find the final form of the interaction function to be,

$$V_I = -(h^2/8\pi^2 I)[J(J+1)-l^2][-3(m/2I+\alpha/4\pi^2\omega_2^2(2mI)^{\frac{1}{2}})x^2+(\mu/I-\beta/4\pi^2\omega_2^2(2mI)^{\frac{1}{2}})r^2 + (\mu/I-\gamma/4\pi^2\omega_2^2(2mI)^{\frac{1}{2}})z^2],$$

where

$$\alpha x^3 = a\sigma^3, \quad \beta x r^2 = b\sigma\rho^2, \quad \gamma x z^2 = c\sigma\xi^2.$$

That is to say, we have $V_I = C_1\sigma^2 + C_2\rho^2 + C_3\xi^2$ and as a consequence the correction to the energy of a rotation vibration level can be found from the zeroth order energy of vibration of the molecule by a comparison of the coefficients in V_I with the corresponding coefficients in

$$V_0 = (h/2)(2\omega_2\sigma^2+\omega_2\rho^2+\omega_3\xi^2).$$

In other words, since the contribution of V_0 is

$$h\{2\omega_2(V_1+\tfrac{1}{2})+\omega_2(V_2+1)+\omega_3(V_3+\tfrac{1}{2})\},$$

the contribution of V_I is

$$E_I = (h^2/8\pi^2 I)[J(J+1)-l^2][(V_1+\tfrac{1}{2})\{3h/8\pi^2 I\omega_2+(3h/4\pi^2 m\omega_2)(\alpha/4\pi^2\omega_2^2(2mI)^{\frac{1}{2}})\} + (V_2+1)\{-h/4\pi^2 I\omega_2+(h/4\pi^2\mu\omega_2)(\beta/4\pi^2\omega_2^2(2mI)^{\frac{1}{2}})\} + (V_3+\tfrac{1}{2})\{-h/4\pi^2 I\omega_3+(h/4\pi^2\mu\omega_2)(\gamma/4\pi^2\omega_2^2(2mI)^{\frac{1}{2}})\}].$$

We have now computed the energy shift of a rotation-vibration level resulting from the interaction between rotation and vibration. To pass from the corrected energy levels to the corrected positions of the fine-structure lines the selection rules for J and l must be introduced. For a parallel band $\Delta J = \pm 1$ and $\Delta l = 0$. Representing by N the ordinal number of the fine-structure line, the correction to the N-th line of a parallel band produced in a transition from the ground state is

$$\Delta\nu = (h/8\pi^2 Ic)[\{PV_1+QV_2+RV_3\}N^2+\{P(V_1+1)+Q(V_2+2)+R(V_3+1)\}N],$$

where P, Q, and R are the respective coefficients of $(V_1+\frac{1}{2})$, (V_2+1), and $(V_3+\frac{1}{2})$ within the bracket [ ] of the above expression for E_I. Similar expressions obtain for the corrections to the fine-structure of a perpendicular band.

The interpretation of $\Delta\nu$ follows at once from a correlation with the empirical expression for the positions of the fine-structure lines in a band. In the empirical formula $\nu = K_0+K_1N+K_2N^2$, K_1 is the major interval between fine-structure lines, while K_2 fixes the convergence which is superimposed upon the spacing determined by K_1. This suggests the division of $\Delta\nu$ into two sections—the one linear and the other quadratic in N. That is to say, the interaction between rotation and vibration not only is the cause of convergence, but it alters the major interval as well. Thus, the measured separation of lines is

$$K_1 = h/4\pi^2 Ic + \text{linear part of } \Delta\nu.$$

The quantity $\Delta\nu$ is, therefore, essential to a precise determination of the moment of inertia of the molecule.

Putting the numerical values of the known constants into $\Delta\nu$, we find:

$$\Delta\nu = 0.390[(0.00175+0.000112a)V_1+(-0.00117+0.0000372b)V_2 + (-0.00033+0.000019c)V_3]N^2+0.390[(0.00175+0.000112a)(V_1+1) + (-0.00117+0.0000372b)(V_2+2)+(-0.00033+0.000019c)(V_3+1)]N.$$

Of the twenty-eight bands which have now been observed in the infrared spectrum of carbon dioxide, only five are sufficiently well resolved for the present analysis. These are the active fundamentals and the three Venus bands. The observed positions are:[2]

$$\nu_2 = 667.5 + 0.780\,N + 0.0005\,N^2; \quad \nu_3 = 2350.1 + 0.780\,N - 0.0035\,N^2;$$

$$5\nu_3 = 11496.5 + 0.769\,N - 0.0153\,N^2; \quad 5\nu_3 + (\nu_1, 2\nu_2)\begin{cases} 12672.5 + 0.769\,N - 0.0150\,N^2 \\ 12774.7 + 0.769\,N - 0.0156\,N^2. \end{cases}$$

(For sources of data see Part I.)

The band ν_2 possesses the theoretical convergence: $0.390(-0.00117 + 0.0000372b)N^2$. From the vibrational analysis of Part I the value 72.9 cm^{-1} was obtained for $|b|$. Obviously the convergence demands that b be positive and the value $b = 72.9$ cm^{-1} yields the convergence factor $+0.0006\ N^2$, in excellent agreement with the observed value $+0.0005\ N^2$.

Of the two bands ν_3 and $5\nu_3$, the photographic one, $5\nu_3$, is the more accurately resolved. For this reason $5\nu_3$ will be used to compute the value of c which will then serve to predict the convergence of the fundamental ν_3. From the equation

$$0.390(-0.00033 + 0.000019c)5\ N^2\ cm^{-1} = -0.0153\ N^2\ cm^{-1}$$

the value $c = -202.1$ cm^{-1} is found. The calculated convergence $-0.0031\ N^2$ agrees very well with the measured value $-0.0035\ N^2$ for the ν_3 fundamental.

The convergences for the combination bands at 12,672.5 and 12,774.7 cm^{-1} are given by the respective linear combinations:

$$\{0.43[0.390(0.00175 + 0.000112a)] + 0.57(0.00120) - 0.0153\}N^2$$

$$\{0.57[0.390(0.00175 + 0.000112a)] + 0.43(0.00120) - 0.0153\}N^2$$

since the resonance degeneracy of the molecule described in Part I must be taken into account. Equating the first expression to the observed datum $-0.0150\ N^2$, the value -36.2 cm^{-1} for the anharmonic constant a is found. When this is substituted into the second expression the value $-0.0153\ N^2$ is obtained, which may be compared with the observed constant $-0.0156\ N^2$.[3]

The moment of inertia of CO_2 may be determined from any of the resolved infrared bands. It appears, however, that the $5\nu_3$ band should yield the most reliable value since it is the most accurately resolved band. In making the computation the correction arising from the convergence factor must be applied to the coefficient of N in the fine-structure formula. The observed major interval of the $5\nu_3$ band is 0.769 cm^{-1}. It follows that:

$$0.769\ N = hN/4\pi^2 Ic - 0.0031(V_3 + 1)N,$$

where $V_3 = 5$. We obtain $I = 70.1 \times 10^{-40}$ gram cm^2, a value which is in good accord with the value 70.2×10^{-40} as determined from the rotational Raman effect of CO_2.[4]

The Potential Energy Function of CO_2

The analysis of the interaction between rotation and vibration has yielded values for the coefficients a and c. Combining these data with the x's and ν's it becomes possible to determine the remaining anharmonic coefficients; namely, d, e, f, g, h, i. The equations used in this evaluation are given on pages 719 and 720 of Part I and are simply the connections between the constants of the vibrational energy and the constants of the vibrational potential. The results of this calculation are listed in Table I, together with the zeroth and first order constants of the potential.

ω_1, ω_2, ω_3, b, and c are the most accurately known of the twelve constants, with a probable

[2] Due to the fact that the oxygen nucleus has zero spin, half of the fine-structure lines of CO_2 are missing. The above formulae represent the observed positions of the lines when N takes on the values $+1, +3, +5, +7$, R-branch; $-2, -4, -6, -8$, P-branch.

[3] We are very much indebted to Professor E. F. Barker for the following information. He has recently resolved the two infrared bands $\nu_3 - (\nu_1, 2\nu_2)$ at 10μ, and from the convergence factors which he obtains, the two values of a -38.6, -36.6 may be computed. We shall adopt the mean value -37.0.

[4] Houston and Lewis, Proc. Nat. Acad. 17, 229 (1931).

TABLE I.

ω_1 1361 cm^{-1}	a −48.8	d 7.8, 5.3	g −9.9
ω_2 673	b 72.9	e 2.0	h 7.7
ω_3 2378	c −202.1	f 2.4	i −12.3

error of about ½ percent. The value of a is probably known to within 5 percent while the remaining constants may well be in error by as much as 10 percent to 15 percent. Two values are given for d, one obtained from the constant x_{11} and the other from the expression for ν_1. We should regard the latter determination as the more accurate. It is to be noted that the least accurately known constants are the smallest in magnitude; namely, the coefficients of the second order potential. The behavior of the molecule, however, is determined chiefly by the zeroth and first order potentials. Consequently, we believe that the potential energy of the carbon dioxide molecule for small displacements will be represented to within a few wave numbers by the data in Table I. An attempt will now be made to approximate this potential energy by means of an analytic function with a fewer number of constants.

It seems probable that each of the two oxygen nuclei are bound to the carbon nucleus by a force field having a potential minimum. The success of the Morse potential function for diatomic molecules suggests that we connect the carbon with each of the oxygens by a Morse function. The constants of these two functions will, of course, be identical. The valencies of the two oxygen atoms are satisfied by the carbon atom and we might accordingly expect that the two oxygen atoms will repel one another. From analogy with the repulsion forces of homopolar atoms we shall attempt to approximate this potential by an expression of the form Ae^{-Bq}. Thus,

$$V=[De^{-2a(r_1+\epsilon)}-2De^{-a(r_1+\epsilon)}]+[De^{-2a(r_2+\epsilon)}-2De^{-a(r_2+\epsilon)}]+Ae^{-Bq}.$$

The distances between the nuclei are given by $a/2+r_1$, $a/2+r_2$, and $a+q$, as shown in Fig. 1,

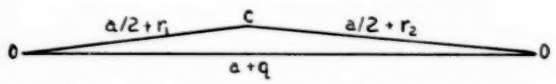

FIG. 1. Configuration of the carbon dioxide molecule.

and completely define the configuration of the system. The quantities r_1 and r_2 are connected with the normal coordinates by the relations

$$r_1=q/2+r^2/a+z, \quad r_2=q/2+r^2/a-z$$

and V may be rewritten as follows, where $y=q/2+r^2/a$,

$$V=2De^{-a(\epsilon+y)}\cosh 2\alpha z-4De^{-a(\epsilon+y)}\cosh \alpha z+Ae^{-Bq}.$$

The equilibrium condition

$$\partial V/\partial q=\partial V/\partial r=\partial V/\partial z=0 \quad \text{at} \quad q=r=z=0$$

yields the relation $2\alpha^2\epsilon D=AB$. ϵ can thus be evaluated in terms of α, D, A and B, and the potential V is seen to depend upon these four parameters only.

For the purpose of comparison with the terms of the series potential already obtained for CO_2, we must expand $V(r_1r_2q)$ about the point $q=r=z=0$, and all terms through the quartic must be retained. Powers of ϵ higher than the first may be neglected, and the expansion yields the following term by term comparison,

$$\pi^2m\omega_1^2=\tfrac{1}{2}\{AB^2+D\alpha^2(1-3\alpha\epsilon)\},$$

$$2\pi^2\mu\omega_2^2=4\epsilon D\alpha^2/a,$$

$$2\pi^2\mu\omega_3^2=2D\alpha^2(1-3\alpha\epsilon),$$

$$a=\{(D\alpha^3/4)[(7\alpha\epsilon/3)-AB^3/6]\}R^3,$$

$$b=\{2D\alpha^2(1-3\alpha\epsilon)/a\}RS^2,$$

$$c=\{D\alpha^3(7\alpha\epsilon-3)\}RT^2,$$

$$d=\{AB^4/24+(D\alpha^4/96)(7-15\alpha\epsilon)\}R^4,$$

$$e=\{2D\alpha^2(1-3\alpha\epsilon)/a^2\}S^4,$$

$$f=\{D\alpha^4(7-15\alpha\epsilon)/6\}T^4,$$

$$g=\{D\alpha^3(7\alpha\epsilon-3)/2a\}R^2S^2,$$

$$h=\{D\alpha^4(7-15\alpha\epsilon)/4\}R^2T^2,$$

$$i=\{2D\alpha^3(7\alpha\epsilon-3)/a\}S^2T^2, \text{ where}$$

$$R=(1/2\pi)[h/m\omega_2]^{\frac{1}{2}},$$

$$S=(1/2\pi)[h/\mu\omega_2]^{\frac{1}{2}},$$

$$T=(1/2\pi)[h/\mu\omega_3]^{\frac{1}{2}}.$$

For the determination of α, D, B and A, it is desirable to employ the four best known of the

constants $\omega_1 \cdots i$. ω_1, ω_2, ω_3 and c are evidently the data required. (The constant b is unsuited for the fourth relation as will be seen in the general discussion to follow.) In this way we obtain,

$$\alpha = 1.81\text{A}^{-1}, \quad B = 1.086\text{A}^{-1}, \quad \epsilon = 0.061\text{A}.$$

$$D = 168350 \text{ cm}^{-1}, \quad A = 62600 \text{ cm}^{-1}.$$

By using these values, the remaining anharmonic constants can be predicted and the suitability of the generalized Morse function will be indicated by the agreement between these values and the corresponding ones obtained earlier in the paper. The comparison is contained in Table II.

TABLE II.

	Infrared analysis	Generalized Morse function
a	-37.0 cm^{-1}	-36 cm^{-1}
b	72.9	102
d	5.3, 7.8	1.1
e	2.0	4.6
f	2.4	4.1
g	-9.9	-8.9
h	7.7	12.4
i	-12.3	-17.7

The agreement shown in Table II is, in several respects, satisfactory. The anharmonic constants are correctly given by $V(r_1r_2q)$ as regards order of magnitude and as regards algebraic sign. It is apparent, however, that their numerical values diverge by amounts which are certainly in excess of the experimental errors. Perhaps the principal objection to the function we have chosen is that it belongs to the class of central force potentials which have, in the past, shown themselves to be incapable of describing the potential functions of polyatomic molecules. There are certain consequences of the central force assumption which are completely independent of the restricted form $V(r_1r_2q)$. This assumption imposes certain restrictions upon the anharmonic constants which are listed below:

$$b/\omega_3^2 = 2\pi^2\mu RS^2/a; \quad e/\omega_3^2 = 2\pi^2\mu S^4/a^2$$

$$i/g = 4T^2/R^2; \qquad f/h = 2T^2/3R^2.$$

It is because b is already specified by the central character of the forces that it may not be used in determining the constants of the generalized Morse function.

The fact that the four relations given above are not accurately fulfilled by the actual constants of the molecule proves that the true force function cannot be wholly central in character. On the other hand, the fact that they are approximately fulfilled leads us to the belief that to this extent the potential energy of CO_2 can be represented by a central force function such as $V(r_1r_2q)$.

Our purpose in introducing $V(r_1r_2q)$ was to find a function which possesses definite physical significance and whose constants might be evaluated from the infrared data. The function we have chosen does fairly well represent the potential energy of CO_2 for small displacements of the particles. The question now arises as to whether it will also furnish some measure of the potential for large displacements and of the heats of dissociation of the molecule.

Suppose, for example, that we consider the dissociation of CO_2 into CO and O, where we must suppose that the products of the dissociation are probably not in the normal state. For this purpose we assume that one of the oxygen atoms is slowly removed to infinity; the distance between the remaining C and O remaining constant. This can be accomplished by letting q and z become infinite while preserving the relation $z = q/2$. The energy required for this operation is $D - A$, but the residual CO molecule is not in its normal state since $a/2$ is no longer its equilibrium distance, but rather $(a/2) - \epsilon$. The heat of dissociation is thus equal to

$$2De^{-\alpha\epsilon} - De^{-2\alpha\epsilon} - A.$$

Upon substituting the values of the constants, we obtain for the heat of dissociation 103,750 cm^{-1} or 300 calories/mol. In order to compare this figure with an experimental determination of the heat of dissociation we would require more detailed information about the excited states of CO and O than appears to be now available.

Multiplets in the Spectra of O III, O IV, O V and C III

P. GERALD KRUGER AND W. E. SHOUPP, *Department of Physics, University of Illinois*

(Received May 25, 1933)

The spectra of oxygen and carbon have been photographed in the region 100A to 650A with a twenty-one foot grazing incidence vacuum spectrograph. A hot spark was used as the light source. Transitions between $2s^22p3d\ ^3D^0$, $^3P^0$, $2s^22p3s\ ^3P^0$ and $2s^22p^2\ ^3P$ of O III terms were observed. The separation of the levels arising from the lowest electron configuration is thus fixed. Nebular lines fit these term differences very well. In O IV the quartet intercombinations $2s2p^2\ ^4P$ to $2s^23s\ ^4P^0$, $2s2p3d\ ^4D^0$, $^4P^0$ have been found. This connects the two quartet systems and a revised term table is given. The $\Delta\nu$ separations of three O V triplets have been measured but do not agree too well with other data. Two C III triplets, previously observed by Bowen as doublets, have been resolved and fit the calculated $\Delta\lambda$'s.

INTRODUCTION

THE spectra of ionized oxygen are well known and a list of term values has been collected and published in *Atomic Energy States* by Bacher and Goudsmit. Most of these energy levels have been determined from spectra lines observed above 600A.[1, 2, 3, 4, 5, 6, 7] Some, as in the case of Fowler,[3] have been fixed by observing single lines which in the present analysis have been found to be the multiplets suggested by the previous classification. Examples of such lines are λλλ303A, 305A and 374A. Ericson and Edlén[8] reported a large number of O III, O IV and O V lines in the region 150A to 700A, but did not publish their classification.

EXPERIMENTAL

The oxygen spectra were developed while attempting to excite B by using powdered boron (probably B_7O) with oxygen as an impurity, and H_3BO_3 in copper shell electrodes. The electrodes were used in a "hot spark" light source. The electrical connections were made in the usual way, power being supplied by an 80 kv kenetron bridge set. About 0.05 mf capacity was in the circuit. With this mode of excitation two sparks per sec., each spark having a duration of about 1/30 sec., for a total time of two hours was sufficient to give a well developed spectrum. The oxygen lines were also obtained while using bismuth trioxide in copper shell electrodes to excite the Bi spark spectra.

A twenty-one foot grazing incidence vacuum spectrograph[9] which was constructed by the Mann Instrument Company of Cambridge, Mass., was used to photograph the spectra. The angle of incidence was 87°. The grating was ruled, 30,000 lines per inch, on glass by R. W. Wood and H. M. O'Bryan at Johns Hopkins University.

RESULTS FOR O III

Table I gives the intensity, wave-length, wave number and classification of the lines observed in the O III multiplets. The term differences ($\Delta\nu$) observed in these multiplets agree very well with those observed by other workers while studying the O III spectrum at longer wave-lengths. The starred wave-lengths in the table were taken from an unpublished list of oxygen standard lines which have been determined by B. Edlén at Upsala in 1931. With the help of the multiplet transitions in Table I it is possible to fix the deepest terms ($2s^22p^2\ ^3P_{0,\,1,\,2}$), with respect to the higher terms ($2s^22p3s\ ^3P^0$, etc.), more accurately than before. For this reason a revised term table has been included (Table II). This table is

[1] Miliul, Comptes Rendus **183**, 1035 (1926).
[2] Bowen, Phys. Rev. **29**, 241 (1927).
[3] Fowler, Proc. Roy. Soc. **A117**, 317 (1928).
[4] Freeman, Proc. Roy. Soc. **A124**, 654 (1929).
[5] Freeman, Proc. Roy. Soc. **A127**, 330 (1930).
[6] Bowen and Millikan, Phys. Rev. **26**, 150 (1925).
[7] Edlén, Nature **127**, 744 (1931).
[8] Ericson and Edlén, Zeits. f. Physik **59**, 656 (1929).
[9] Kruger, Rev. Sci. Inst. **4**, 128 (1933).

TABLE I. *New multiplets of O III.*

Int.	λ	ν	Classification
4	374.4344	267,069.5	$2s^22p^2\ ^3P_2-2s^22p3s\ ^3P_1^0$
2	374.3319	267,142.6	$2s^22p^2\ ^3P_1-2s^22p3s\ ^3P_0^0$
1	374.1658	267,261.0	$2s^22p^2\ ^3P_1-2s^22p3s\ ^3P_1^0$
*10	374.0740	267,326.8	$2s^22p^2\ ^3P_2-2s^22p3s\ ^3P_2^0$
2	374.0075	267,374.3	$2s^22p^2\ ^3P_0-2s^22p3s\ ^3P_1^0$
5	373.8046	267,519.4	$2s^22p^2\ ^3P_1-2s^22p3s\ ^3P_2^0$
		(326,929.4)	$2s^22p^2\ ^3P_2-2s^22p3d\ ^3D_1^0$
2	305.8293	326,979.8	$2s^22p^2\ ^3P_2-2s^22p3d\ ^3D_2^0$
*10	305.7610	327,052.8	$2s^22p^2\ ^3P_2-2s^22p3d\ ^3D_3^0$
1	305.6970	327,121.3	$2s^22p^2\ ^3P_1-2s^22p3d\ ^3D_1^0$
5	305.6481	327,173.6	$2s^22p^2\ ^3P_1-2s^22p3d\ ^3D_2^0$
3	305.5909	327,234.8	$2s^22p^2\ ^3P_0-2s^22p3d\ ^3D_1^0$
*7	303.7920	329,172.6	$2s^22p^2\ ^3P_2-2s^22p3d\ ^3P_2^0$
1	303.6903	329,283.2	$2s^22p^2\ ^3P_2-2s^22p3d\ ^3P_1^0$
1	303.6151	329,353.6	$2s^22p^2\ ^3P_1-2s^22p3d\ ^3P_2^0$
1	303.5067	329,482.1	$2s^22p^2\ ^3P_1-2s^22p3d\ ^3P_1^0$
1	303.4526	329,540.7	$2s^22p^2\ ^3P_1-2s^22p3d\ ^3P_0^0$
1	303.4014	329,596.4	$2s^22p^2\ ^3P_0-2s^22p3d\ ^3P_1^0$

the same as that in Bacher and Goudsmit when 60.53 cm^{-1} has been subtracted from all terms above and including the $2s^22p\ 3s$ terms in Bacher and Goudsmit. The $2s^22p^2\ ^1D_2$ and $^1S_0$ terms can be fixed equally well by taking the values for the transitions $2s^22p^2\ ^1D_2-2s^22p3s\ ^1P_1^0$ and $2s^22p^2\ ^1S_0-2s^22p3s\ ^1P_1^0$ from the wave-lengths in Edlén's unpublished list. They are 395.558A (252,807.4 cm^{-1}) and 434.975A (229,898.3 cm^{-1}), respectively. The corrected term value of $2s^22p3s\ ^1P_1^0$ is 273,087.04 cm^{-1}. This gives $2s^22p^2\ ^1D_2$ a value 20,279.6 cm^{-1} and $^1S_0$ a value 43,188.7 cm^{-1} as given in Table II.

Wright[10] has observed O III nebular lines of

λ(air)	4363.21A	ν(vac)	22,912.49 cm^{-1}
	4958.91A		19,967.12 cm^{-1}
	5006.84A		20,160.11 cm^{-1}

Becker and Grotrian[11] have assumed that these nebular lines represent transitions between the $2s^22p^2\ ^3P_{2,\,1}$, $^1D_2$, $^1S_0$ terms. By then calculating the predicted wave-length for the center of density of λλ374.3A and 305.7A,[3] and taking into account the theoretical intensity of the components of all transitions of $^3P-{}^3P^0$ and $^3P-{}^3D^0$ it is found these calculated values fit the experimental value within the limit of error. It is concluded that the classification is correct.

[10] Wright, Publ. of the Lick Obs. **13**, Part VI (1918).

[11] Ergebnisse der Exakten Naturwissenschaften **7**,61–4.

TABLE II. *Partially revised term table for O III.**

Term	Term value with respect to $2s2p^2\ ^3P_0=0$
$2s^22p^2\ ^3P_0$	0
$2s^22p^2\ ^3P_1$	113.5
$2s^22p^2\ ^3P_2$	305.4
$2s^22p^2\ ^1D_2$	20,279.6
$2s^22p^2\ ^1S_0$	43,188.7
$2s^22p3s\ ^3P_0^0$	267,255.9
$2s^22p3s\ ^3P_1^0$	267,374.3
$2s^22p3s\ ^3P_2^0$	267,632.2
$2s^22p3d\ ^3D_1^0$	327,234.8
$2s^22p3d\ ^3D_2^0$	327,287.1
$2s^22p3d\ ^3D_3^0$	327,360.1
$2s^22p3d\ ^3P_2^0$	329,476.9
$2s^22p3d\ ^3P_1^0$	329,596.4
$2s^22p3d\ ^3P_0^0$	329,655.0

* Terms arising from the $2s2p^3$ configuration are correct as given in *Atomic Energy States*, Bacher and Goudsmit with respect to the term values in this table. All terms above and including the $2s^22p3s$ terms have a value too high by 60.53 cm^{-1} with respect to the values in the above table.

Since all of the components of the transitions $2s^22p^2\ ^3P_{2,\,1,\,0}-2s^22p3s\ ^3P^0{}_{2,\,1,\,0}$ and $2s^22p^2\ ^3P_{2,\,1,\,0}-2s^22p3d\ ^3D^0{}_{3,\,2,\,1}\ ^3P^0{}_{2,\,1,\,0}$ have been found during the present study, it is no longer necessary to assume that the nebular lines are the above suggested transitions. A direct check can be made from the term table. This follows from Table III.

TABLE III. *Comparison of term differences in* $2s^22p^2\ ^3P_{2,\,1}$ $^1D_2$, $^1S_0$ *terms and nebular lines.*

Term difference in cm^{-1}	ν cm^{-1} of nebular lines
$^1S_0-{}^1D_2=22{,}909.1$	22,912.49
$^1D_2-{}^3P_2=19{,}974.2$	19,967.12
$^1D_2-{}^3P_1=20{,}166.1$	20,160.11

RESULTS OF O IV

Table IV gives the wave-lengths of lines resulting from $2s2p^2$, $^4P-2s2p3s\ ^4P^0$ and $2s2p3d$ $^4D^0$, $^4P^0$ transitions. This enables the two quartet systems (listed separately in Bacher and Goudsmit) to be connected. A revised quartet term table is given in Table V. Freeman[5] observed the doublets 279.935A, 279.632A and 238.575A, 238.362A as single lines and gave them the correct classification. Edlén[8] has also observed the 238A doublet. The starred wave-lengths were taken from Edlén's unpublished list of oxygen standards.

TABLE IV. *New multiplets of O IV.*

Int.	λ obs.	ν obs.	calc. ν	Classification
20	279.935	357,225.8		$2s^22p\ ^2P_{3/2} - 2s^23s\ ^2S_{1/2}$
10	279.632	357,612.8		$2s^22p\ ^2P_{1/2} - 2s^23s\ ^2S_{1/2}$
3	272.3181	367,217.5	367,221.6	$2s2p^2\ ^4P_{5/2} - 2s2p3s\ ^4P_{3/2}^0$
3	272.2808	367,267.9	367,265.5	$2s2p^2\ ^4P_{3/2} - 2s2p3s\ ^4P_{1/2}^0$
1	272.1859	367,396.0	367,400.6	$2s2p^2\ ^4P_{3/2,\ 1/2} - 2s2p3s\ ^4P^0_{3/2,\ 1/2}$
10	272.1327	367,467.8	367,466.5	$2s2p^2\ ^4P_{5/2} - 2s2p3s\ ^4P_{5/2}^0$
4	272.0818	367,536.5	367,535.6	$2s2p^2\ ^4P_{1/2} - 2s2p3s\ ^4P_{3/2}^0$
5	271.9964	367,651.9	367,647.5	$2s2p^2\ ^4P_{3/2} - 2s2p3s\ ^4P_{5/2}^0$
*20	238.575	419,155.4		$2s^22p\ ^2P_{3/2} - 2s^23d\ ^2D_{5/2,\ 3/2}$
10	238.362	419,530.0		$2s^22p\ ^2P_{1/2} - 2s^23d\ ^2D_{3/2}$
			(428,031.3)	$2s2p^2\ ^4P_{5/2} - 2s2p3d\ ^4D_{3/2}^0$
1	233.6022	428,078.1	428,078.0	$2s2p^2\ ^4P_{5/2} - 2s2p3d\ ^4D_{5/2}^0$
*8	233.5660	428,144.5	428,142.6	$2s2p^2\ ^4P_{5/2} - 2s2p3d\ ^4D_{7/2}^0$
			(428,183.4)	$2s2p^2\ ^4P_{3/2} - 2s2p3d\ ^4D_{1/2}^0$
1	233.5272	428,216.0	428,212.3	$2s2p^2\ ^4P_{3/2} - 2s2p3d\ ^4D_{3/2}^0$
4	233.5016	428,262.8	428,259.0	$2s2p^2\ ^4P_{3/2} - 2s2p3d\ ^4D_{5/2}^0$
1.5	233.4669	428,326.3	428,318.4	$2s2p^2\ ^4P_{1/2} - 2s2p3d\ ^4D_{1/2}^0$
1	233.4548	428,348.3	428,347.3	$2s2p^2\ ^4P_{1/2} - 2s2p3d\ ^4D_{3/2}^0$
*10	231.3020	432,335.2	432,330.5	$2s2p^2\ ^4P_{5/2} - 2s2p3d\ ^4P_{5/2}^0$
3	231.2433	432,445.0	432,443.9	$2s2p^2\ ^4P_{5/2} - 2s2p3d\ ^4P_{3/2}^0$
4	231.2053	432,516.0	432,511.5	$2s2p^2\ ^4P_{3/2} - 2s2p3d\ ^4P_{5/2}^0$
1	231.1475	432,624.2	432,624.9	$2s2p^2\ ^4P_{3/2} - 2s2p3d\ ^4P_{3/2}^0$
2	231.1087	432,696.8	432,704.1	$2s2p^2\ ^4P_{3/2} - 2s2p3d\ ^4P_{1/2}^0$
4	231.0777	432,757.9	432,759.9	$2s2p^2\ ^4P_{1/2} - 2s2p3d\ ^4P_{3/2}^0$
1	231.0333	432,838.0	432,839.1	$2s2p^2\ ^4P_{1/2} - 2s2p3d\ ^4P_{1/2}^0$

TABLE V. *Revised term table for O IV quartets.*

Term	Term value with respect to $2s2p^2\ ^4P=0$	Term	Term value with respect to $2s2p^2\ ^4P=0$
$2s2p^2\ ^4P_{1/2}$	0	$2s2p3d\ ^4F_{3/2}^0$	423,719.5
$2s2p^2\ ^4P_{3/2}$	135	$2s2p3d\ ^4F_{5/2}^0$	423,798.3
$2s2p^2\ ^4P_{5/2}$	316	$2s2p3d\ ^4F_{7/2}^0$	423,910.7
$2p^3\ ^4S_{3/2}^0$	160,100	$2s2p3d\ ^4F_{9/2}^0$	424,064.8
$2s2p3s\ ^4P_{1/2}^0$	367,400.5	$2s2p3d\ ^4D_{1/2}^0$	428,318.4
$2s2p3s\ ^4P_{3/2}^0$	367,535.6	$2s2p3d\ ^4D_{3/2}^0$	428,347.3
$2s2p3s\ ^4P_{5/2}^0$	367,782.5	$2s2p3d\ ^4D_{5/2}^0$	428,394.0
$2s2p3p\ ^4D_{1/2}$	386,887.4	$2s2p3d\ ^4D_{7/2}^0$	428,458.6
$2s2p3p\ ^4D_{3/2}$	386,966.2	$2s2p3d\ ^4P_{5/2}^0$	432,646.5
$2s2p3p\ ^4D_{5/2}$	387,101.7	$2s2p3d\ ^4P_{3/2}^0$	432,759.9
$2s2p3p\ ^4D_{7/2}$	387,311.4	$2s2p3d\ ^4P_{1/2}^0$	432,839.1
$2s2p3p\ ^4S_{3/2}$	403,029.8		
$2s2p3p\ ^4P_{1/2}$	407,399.7		
$2s2p3p\ ^4P_{3/2}$	407,494.2		
$2s2p3p\ ^4P_{5/2}$	407,623.3		

TABLE VI. *Triplets of O V.*

Int.	λ obs.	ν obs.	Δν	Classification
*10	215.2000	464,684.0		$2s2p\ ^3P_2-2s3s\ ^3S_1$
			305.8	
5	215.0585	464,989.8		$2s2p\ ^3P_1-2s3s\ ^3S_1$
			125.0	
2	215.0007	464,114.8		$2s2p\ ^3P_0-2s3s\ ^3S_1$
*50	192.9100	518,376.4		$2s2p\ ^3P_2-2s3d\ ^3D_{3,2,1}$
			291.2	
25	192.8017	518,667.6		$2s2p\ ^3P_1-2s3d\ ^3D_{3,2,1}$
			134.6	
10	192.7517	518,802.2		$2s2p\ ^3P_0-2s3d\ ^3D_{3,2,1}$
8	151.5689	659,766.0		$2s2p\ ^3P_2-2s4d\ ^3D_{3,2,1}$
			300.0	
*2	151.5000	660,066.0		$2s2p\ ^3P_1-2s4d\ ^3D_{3,2,1}$
			126.3	
0	151.471	660,192.3		$2s2p\ ^3P_0-2s4d\ ^3D_{3,2,1}$

Table VI lists three triplets of O V and their $\Delta\nu$ separations. These are different from those previously reported.[6, 7] The $2s2p\ ^3P_2-{}^3P_1$ term separation is probably 306 cm^{-1} but $^3P_1-{}^3P_0$ is more nearly 125 cm^{-1} than the previously reported value 135 cm^{-1}. The lines at 192.9A representing the $2s2p\ ^3P_{2,1,0}-2s3d\ ^3D_{3,2,1}$ transition do not have the above separations but this is probably because of the small splitting of the ^3D terms which are unresolved. In the 150A triplet the separations are again essentially those of the $2s2p\ ^3P_{2,1,0}$ states.

Two C III triplets which were previously observed as doublets by Bowen[12] have been resolved and are listed in Table VII. The observed Δλ's check the calculated Δλ's so that Bowen's classification is substantiated.

TABLE VII. *Triplets of C III.*

Int.	calc λ's	calc Δλ's	obs Δλ's	Classification
6	535.430			$2s2p\ ^3P_2^0-2s3s\ ^3S_1$
		0.161	0.167	
3	535.269			$2s2p\ ^3P_1^0-2s3s\ ^3S_1$
		0.068	0.065	
1	535.201			$2s2p\ ^3P_0^0-2s3s\ ^3S_1$
10	459.634			$2s2p\ ^3P_2^0-2s3d\ ^3D_{3,2,1}$
		0.118	0.113	
6	459.516			$2s2p\ ^3P_1^0-2s3d\ ^3D_{2,1}$
		0.050	0.053	
3	459.466			$2s2p\ ^3P_0^0-2s3d\ ^3D_1$

[12] Bowen, Phys. Rev. **38**, 128 (1931).

A Comparison of the Nuclear Theories of Heisenberg and Wigner. I

CARL ECKART, *University of Chicago*

(Received May 17, 1933)

The energy levels of Wigner's proposed equation for protons and neutrons in nuclei are compared with those of Heisenberg's equation, after the latter has been simplified by the omission of all interaction terms except those between protons and neutrons. It is assumed for the purpose of comparison, that Wigner's potential energy function is identical with Heisenberg's exchange energy $-J$. It is shown that the lowest energy level of Wigner's equation must be lower (more stable) than the lowest level of Heisenberg's equation, except in the case of H^2, for which they are the same. This does not exclude the possibility that Heisenberg's equation may give as good a value for the ratio of the mass defects of He^4 and H^2 as Wigner's equation, since the assumption above is not necessary except for the statement of the theorem. It is also shown that Heisenberg's equation probably predicts that the nuclei H^3 and He^3 are unstable.

I.

THE major forces holding the atomic nucleus together seem to be those exerted by protons on neutrons so that, for a first approximation, all others may be neglected. There are at least two ways in which these forces may be described: Heisenberg[1] has proposed that they be considered as arising from an exchange energy so that they are analogous to the valence forces in H_2^+; Wigner[2] proposes to treat them as arising from an ordinary potential energy. Depending on the point of view, different wave equations are obtained.

Wigner's is a simple Schroedinger equation; in the case of the nucleus H^3 it is

$$T\psi - J(r_{13})\psi - J(r_{23})\psi = W_S\psi, \qquad \text{S}$$

where

$$T = -(h^2/8\pi^2 M)(\nabla_1^2+\nabla_2^2+\nabla_3^2). \qquad (1)$$

In this equation the particles 1 and 2 are the neutrons, while 3 is the proton. The two kinds of particles are treated as having the same mass M; W_S does not include the energy responsible for the mass defect of the neutron. The function $-J(r)$ is the potential energy function.

Characteristic of the Heisenberg theory is the fact that it does not specify which particles are neutrons and which protons. Therefore the wave function must be a hyper-function; in the example of H^3 it has three components $\psi_1\psi_2\psi_3$. Of these, ψ_i determines the probability density in configuration space when particle i is a proton. Correspondingly, the wave equation consists of three simultaneous equations:

$$\begin{aligned} T\psi_1 - J(r_{12})\psi_2 - J(r_{13})\psi_3 &= W_H\psi_1, \\ T\psi_2 - J(r_{23})\psi_3 - J(r_{12})\psi_1 &= W_H\psi_2, \\ T\psi_3 - J(r_{13})\psi_1 - J(r_{23})\psi_2 &= W_H\psi_3. \end{aligned} \qquad \text{H}$$

In both theories the precise form of the function J is as yet unknown, though Wigner has assumed a particular form for the purpose of a numerical calculation. It seems likely that any other reasonable assumption will lead to essentially the same results. No numerical results have as yet been obtained from Eqs. (H).[3] For the purpose of comparing the two equations it is convenient to suppose that J is the same function in each. This will be done in the following, with the expressed reservation that it will be necessary to abandon this identity in order to secure agreement with experimental facts. It is probably justified to suppose that J is

[1] W. Heisenberg, Zeits. f. Physik **77**, 1 (1932); **78**, 156 (1932); **80**, 587 (1933).

[2] E. Wigner, Phys. Rev. **43**, 252 (1933).

[3] In Part I, the designations, Eq. (S) and Eqs. (H), will be used in a general sense to refer to equations for any nucleus which are based on the same principles as the particular examples in the text. In Part II, the particular examples will be meant.

essentially positive in sign in both Eqs. (S) and (H).[4]

The numerical results which Wigner has obtained from Eq. (S)[3] are rather impressive. He shows that it is possible to choose the function J in a reasonable manner and in such a way that the calculated ratio of the mass defects of He^4 and H^2 is greater than 14 (empirical value = 17), while yet leaving the ratio of the mass defects of H^3 and H^2 not much greater than 2. This latter ratio is unknown, but from the rarity (or non-existence?) of H^3 it is inferred to be small.

It is therefore of interest to see if the Heisenberg theory can give as good an account of the empirical facts. To investigate this variational methods seem the only ones available. They lead to a result for H^3 without numerical calculation; this will be shown in detail below. The numerical calculations for He^4 have not yet been completed; they will be published at a later date.

A general theorem has also been discovered, which seems likely to be of considerable value in discussing the Eqs. (H). This theorem reads: *The lowest energy level of Eq. (S) is necessarily lower* (more stable) *than the lowest level of Eq. (H)*, except in the case of H^2 for which nucleus they are equal. It seems probable that this theorem may be generalized to read "corresponding levels" rather than "lowest levels."

Hence, if Wigner's assumption for the function J be substituted in Eqs. (H), the ratio of the mass defects of He^4 and H^2 must come out less than if Eq. (S) were made the basis of the calculation. However, this result does not imply that the Eqs. (H) cannot fit the facts, since another function J may be chosen. Thus, if Wigner's parameter ρ be diminished, it seems probable that the ratio will be increased, just as in the case of Eq. (S).[5] The parameter ρ is essentially the distance beyond which the interaction of the proton and neutron is sensibly zero; hence it is possible to conclude that this distance must be supposed to be smaller according to Heisenberg's theory than according to Wigner's. In both cases it will be of the order of magnitude of the classical radius of the electron, e^2/m_0c^2.

In the matter of the ratio of the mass defects of H^3 and H^2 the theorem leads to a more conclusive result. Here Wigner's value of 2 is essentially independent of the form of J and therefore the Eqs. (H) must inescapably lead to a smaller value. It will be shown in Part II that it is probable that the Eqs. (H) do not even possess a negative energy level in this case. This would account for the failure to find this isotope of hydrogen.

The theorem will always be of value in arguments of the following nature: Wigner's theory of the nucleus strongly resembles the theory of complex molecules; its wave functions possess the same symmetry properties and it is probable that its "Aufbau Prinzip" is the same. To a certain extent therefore, its predictions may be supposed to be known and because of the theorem, will place restrictions on guesses as to the predictions of Heisenberg's theory. If the Wigner theory predicts that a certain nucleus will be unstable, the Heisenberg theory must predict the same thing, but not necessarily conversely.

II.

The general theorem stated above will be proven only for the special case of H^3, but the outline of the general proof will be obvious. The first step is to separate the coordinates of the center of mass and set the total linear momentum equal to zero. This is equivalent to considering only solutions which depend on $x_{13}=x_1-x_3$ and $x_{23}=x_2-x_3$, etc., but are independent of $X=(x_1+x_2+x_3)/3$, etc. For such functions,

$$T=-(h^2/4\pi^2M)(\nabla_{13}^2+\nabla_{23}^2+\nabla_{13}\cdot\nabla_{23}), \tag{2}$$

[4] After the foregoing had been written, a paper by E. Majorana [Zeits. f. Physik **82**, 137 (1933)] came to my attention in which it is proposed to alter the Eqs. (H) by changing the sign of the terms in J. This will alter the symmetry character, etc., of the lowest state but will leave the validity of the theorem stated below unaffected. This may be seen from the fact that the inequality (4) remains true when its left side is replaced by its absolute magnitude; the argument then proceeds without change.

[5] Wigner, reference 2, p. 256, last line.

which is an Hermitian operator. Hence the variational equation from which the Eqs. (H) are derived may be written down at once:

$$W_H \int\int \{\sum \psi_i^2\} dv_{13} dv_{23} = \int\int \{\sum \psi_i T \psi_i - 2\sum\sum J(r_{ij}) \psi_i \psi_j\} dv_{13} dv_{23}, \tag{3}$$

$$dv_{13} = dx_{13} dy_{13} dz_{13}, \text{ etc.}$$

Now it is readily seen from Eqs. (H) that it is not possible for the identity $\psi_1 \equiv \psi_2 \equiv \psi_3$ to exist; hence (since J is essentially positive)

$$2\int\int J(r_{12}) \psi_1 \psi_2 dv_{13} dv_{23} < \int\int J(r_{12})(\psi_1^2 + \psi_2^2) dv_{13} dv_{23}, \text{ etc.} \tag{4}$$

and therefore $W_H > \lambda$ where λ is defined by,

$$\lambda \int\int \{\sum \psi_i^2\} dv_{13} dv_{23} = \int\int \{\sum \psi_i T \psi_i - \sum\sum J(r_{ij})(\psi_i^2 + \psi_j^2)\} dv_{13} dv_{23}. \tag{5}$$

In Eq. (5), the ψ_i are supposed to satisfy Eqs. (H); therefore the inequality will become more pronounced if they are allowed to vary until λ assumes its minimum value. This will occur when

$$T\psi_1 - [J(r_{12}) + J(r_{13})]\psi_1 = \lambda\psi_1, \quad T\psi_2 - [J(r_{23}) + J(r_{12})]\psi_2 = \lambda\psi_2, \quad T\psi_3 - [J(r_{13}) + J(r_{23})]\psi_3 = \lambda\psi_3. \tag{6}$$

The last of these equations is precisely Eq. (S) and therefore the minimum value of λ is W_S. It will be noted that W_S is in general considerably smaller than W_H.

To obtain an upper limit for W_H, it is merely necessary to substitute any trio of functions into Eq. (3). The closeness of the limit will be increased if the trio has the appropriate permutational symmetry; for spin = 3/2, this is

$$\psi_1 = \varphi(\underline{231}), \quad \psi_2 = \varphi(\underline{312}), \quad \psi_3 = \varphi(\underline{123});$$

for spin = 1/2,

$$\psi_1 = \varphi(321) - \varphi(231), \quad \psi_2 = -\varphi(132), \quad \psi_3 = \varphi(123).$$

The closeness of the limit will be further increased if the functions are good approximations to the solutions of Eqs. (H), but there is no guide to this goal. It is therefore not in conflict with known facts to take φ as the solution of Eq. (S) for its lowest level; since this function is symmetric in 1 and 2, it leads to no result for spin = 3/2. For spin = 1/2, it results in

$$\psi_1 = 0, \quad \psi_2 = -\psi(\overline{132}), \quad \psi_3 = \psi(\overline{123}).$$

On substituting these functions into Eq. (3):

$$W_H \int\int (\psi_2^2 + \psi_3^2) dv_{13} dv_{23} = \int\int \{\psi_2 T \psi_2 + \psi_3 T \psi_3 + 2J(r_{23}) \psi(\overline{132}) \psi(\overline{123})\} dv_{13} dv_{23}. \tag{7}$$

It should be noted that $\psi(\overline{123})$ is probably positive for all values of the coordinates[6]; hence each integral in Eq. (7) is positive and a positive upper limit for W_H has been obtained. This makes it probable that the Eqs. (H) have no negative energy levels in this particular case.

In conclusion, it may be remarked that this result can be applied immediately to He^3 since the Eqs. (S) and (H) for this nucleus are identical with those for H^3. The repulsion between the two protons of He^3 will make the instability even more certain.

---

[6] Wigner, reference 2, Eq. (6).

Magnetized Spheroid Immersed in a Permeable Medium

LEIGH PAGE, *Sloane Physics Laboratory, Yale University*

(Received June 2, 1933)

The effect of immersing a permanently magnetized spheroid with a uniform intensity of magnetization parallel to its axis of symmetry in a magnetic medium of constant permeability μ is investigated. If γ is the ratio of the field strength H in the absence of the medium to that in the presence of the medium, it is found that γ changes from 1 for a disk to $(2\mu+1)/3$ for a sphere and then to μ for a needle. This is contrary to the generally accepted statement that $\gamma=\mu$ for a magnet of any shape.

IN a recent number[1] of *The Proceedings of the Physical Society of London*, L. R. Wilberforce has shown the falsity of the general notion that the magnetic field H of a permanent magnet immersed in a medium of constant permeability μ is reduced in the ratio $1:\mu$ by the presence of the medium. He has investigated in detail the field of a uniformly magnetized sphere immersed in such a medium, and finds that, if H_1 designates the magnetic intensity at any point outside the sphere when no medium surrounds it and H_μ the magnetic intensity at the same point when the sphere is immersed in a medium of permeability μ, then $H_\mu=H_1/\gamma$, where $\gamma=(2\mu+1)/3$.

The object of the present paper is to investigate the field of a spheroid, magnetized with constant intensity of magnetization I parallel to its axis of symmetry, when immersed in a magnetic medium of constant permeability μ. The spheroid is of especial interest, because the limiting case of a prolate spheroid of length great compared with its diameter of cross section corresponds to a long magnetic needle, whereas the limiting case of an oblate spheroid of thickness small compared with its diameter of cross section approximates the thin magnetic shell used so much in elementary circuit theory.

Boundary Conditions

As the spheroid is uniformly magnetized, $\nabla\cdot\mathbf{I}=0$ in its interior and hence magnetic poles are confined entirely to its surface. Consequently the magnetic potential V is a solution of Laplace's equation in the interior of the sphere as well as outside. The boundary conditions to be satisfied as we pass from the sphere across its surface into the permeable medium in which it is immersed are (1) that the tangential component of the magnetic intensity **H** shall be continuous, and (2) that the normal component of the magnetic induction **B** shall be continuous. The first is equivalent to the condition that the magnetic potential V shall be continuous at the surface.

If we use the superscripts o and i to indicate quantities outside and inside the sphere respectively, the first condition becomes

$$V^o=V^i \tag{1}$$

at the surface.

If the x axis is taken along the axis of symmetry of the spheroid, the constant intensity of magnetization **I** in its interior can be expressed in terms of a potential by the identity $\mathbf{I}=\nabla(Ix)$. So if we introduce the three orthogonal families of coordinate surfaces $f(x, y, z)=\xi$, $g(x, y, z)=\eta$, $h(x, y, z)=\phi$, the first being a family of confocal hyperboloids of revolution, the second a family of confocal spheroids of which the one $g(x, y, z)=\eta_0$ coincides with the surface of the magnet, and the third a family of planes through the x axis making angles ϕ with the xy plane, then the second boundary condition becomes

$$-\mu\left(\frac{\partial V^o}{\partial\eta}\right)_{\eta_0}=-\left(\frac{\partial V^i}{\partial\eta}\right)_{\eta_0}+4\pi I\left(\frac{\partial x}{\partial\eta}\right)_{\eta_0}. \tag{2}$$

In addition the usual boundary conditions at infinity must be satisfied.

[1] L. R. Wilberforce, Proc. Phys. Soc. (London) **45**, 82 (1933).

Prolate Spheroid

The two families of confocal orthogonal conicoids necessary for coordinate surfaces are the hyperboloids of two sheets

$$x^2/c^2\xi^2-\rho^2/c^2(1-\xi^2)=1, \tag{3}$$

and the prolate spheroids

$$x^2/c^2\eta^2+\rho^2/c^2(\eta^2-1)=1, \tag{4}$$

where $\rho^2\equiv y^2+z^2$. Solving for x and ρ we have

$$x=c\xi\eta, \quad \rho=c[(1-\xi^2)(\eta^2-1)]^{\frac{1}{2}}. \tag{5}$$

Evidently $-1\leqslant\xi\leqslant 1$, $1\leqslant\eta\leqslant\infty$. When $\eta\gg 1$, $\rho=c\eta(1-\xi^2)^{\frac{1}{2}}$, $(\rho^2+x^2)^{\frac{1}{2}}=c\eta$, and, if θ is the angle which the radius vector makes with the x axis, $\xi=\cos\theta$.

As symmetry shows that the potential V is not a function of ϕ, Laplace's equation[2] becomes

$$\frac{\partial}{\partial\xi}\left\{(1-\xi^2)\frac{\partial V}{\partial\xi}\right\}+\frac{\partial}{\partial\eta}\left\{(\eta^2-1)\frac{\partial V}{\partial\eta}\right\}=0. \tag{6}$$

The solutions we need to satisfy the boundary conditions given above are

$$V^o=A\xi\left\{\frac{1}{2}\eta\log\frac{\eta+1}{\eta-1}-1\right\}, \tag{7}$$

$$V^i=B\xi\eta, \tag{8}$$

where A and B are constants to be determined by the boundary conditions.

From (1) we have

$$B=A\left\{\frac{1}{2}\log\frac{\eta_0+1}{\eta_0-1}-\frac{1}{\eta_0}\right\}, \tag{9}$$

and from (2)

$$A\left\{\frac{1-\mu}{2}\log\frac{\eta_0+1}{\eta_0-1}-\frac{1}{\eta_0}+\frac{\mu\eta_0}{\eta_0^2-1}\right\}=4\pi cI. \tag{10}$$

As the eccentricity ϵ of the magnetized spheroid is $1/\eta_0$, the last equation can be written

$$A=\frac{4\pi cI}{\frac{1-\mu}{2}\log\frac{1+\epsilon}{1-\epsilon}-\epsilon+\frac{\epsilon\mu}{1-\epsilon^2}}. \tag{11}$$

[2] Jeans, *Electricity and Magnetism*, 5th edition, p. 255. There is a misprint in the equation given by Jeans.

Now (7) shows that the field strength at any point is proportional to A. Hence, if we denote by γ the ratio of the field H_1 in the absence of a surrounding medium to the field H_μ when the magnet is immersed in a medium of constant permeability μ,

$$\gamma=\frac{A_1}{A_\mu}=\frac{\frac{1-\mu}{2}\log\frac{1+\epsilon}{1-\epsilon}-\epsilon+\frac{\epsilon\mu}{1-\epsilon^2}}{\frac{\epsilon^3}{1-\epsilon^2}},$$

or, in better form,

$$r\equiv\frac{\gamma-1}{\mu-1}=\frac{1}{\epsilon^2}\left\{1-\frac{1-\epsilon^2}{2\epsilon}\log\frac{1+\epsilon}{1-\epsilon}\right\}. \tag{12}$$

This relation shows that the ratio r is a function only of the eccentricity of the spheroidal magnet, that is, of its shape. For $\epsilon=0$ (sphere), $r=2/3$ in agreement with Wilberforce's result, and the derivative of r with respect to ϵ vanishes. On the other hand, for $\epsilon=1$ (needle), $r=1$ and the derivative is infinite. So only in the case of the needle shaped magnet is γ equal to μ, and as the derivative is infinite any slight departure from the limiting form produces a large change in the value of γ.

As the reader can easily verify, the field far from the magnet has the potential

$$V^o=M\cos\theta/\gamma(x^2+\rho^2), \tag{13}$$

where M is the magnetic moment $(4/3)\pi c^3\eta_0(\eta_0^2-1)I$ and γ is given by (12).

Oblate Spheroid

In this case the conicoids required are hyperboloids of one sheet and oblate spheroids. They may be obtained from (3) and (4) by the substitutions $c=ik$, $\eta=-i\chi$, giving the hyperboloids

$$-x^2/k^2\xi^2+\rho^2/k^2(1-\xi^2)=1, \tag{14}$$

and the oblate spheroids

$$x^2/k^2\chi^2+\rho^2/k^2(\chi^2+1)=1, \tag{15}$$

where $\rho^2\equiv y^2+z^2$ as before. In this case

$$x=k\xi\chi, \quad \rho=k[(1-\xi^2)(\chi^2+1)]^{\frac{1}{2}}, \tag{16}$$

and $-1\leqslant\xi\leqslant 1$, $0\leqslant\chi\leqslant\infty$. For large χ, ξ approaches $\cos\theta$.

By making the same substitutions in (7), (8), (9) and (10),

$$V^o = A\xi\{\chi \cot^{-1}\chi - 1\}, \tag{17}$$

$$V^i = B'\xi\chi, \tag{18}$$

where $B' = -iB$, and

$$B' = A\{\cot^{-1}\chi_0 - 1/\chi_0\}, \tag{19}$$

$$A\left\{(1-\mu)\cot^{-1}\chi_0 - \frac{1}{\chi_0} + \frac{\mu\chi_0}{\chi_0^2+1}\right\} = 4\pi kI. \tag{20}$$

In this case the eccentricity ϵ of an elliptical section is $1/(\chi_0^2+1)$ and we find

$$r \equiv \frac{\gamma-1}{\mu-1} = \frac{1}{\epsilon^2}\left\{\frac{(1-\epsilon^2)^{\frac{1}{2}}}{\epsilon}\cot^{-1}\frac{(1-\epsilon^2)^{\frac{1}{2}}}{\epsilon} - (1-\epsilon^2)\right\}. \tag{21}$$

For $\epsilon = 0$ (sphere), $r = 2/3$ as before and the derivative of r with respect to ϵ vanishes. But, for $\epsilon = 1$ (disk), $r = 0$ and the derivative becomes infinite. Consequently $\gamma = 1$ irrespective of μ in the case of the uniformly magnetized disk, and the permeability of the medium in which the disk is immersed has no effect at all on the field. It is a reasonable inference that this statement holds also for the thin magnetic shell of constant strength used as the equivalent of a current circuit in calculations of the latter's magnetic field. As the derivative of r is infinite for $\epsilon = 1$, any slight departure from the limiting flat spheroid causes γ to change markedly.

The field at a great distance from the spheroid is given by (13) with M equal to $(4/3)\pi k^3\chi_0(\chi_0^2+1)I$ and γ taken from (21).

Collected Results

Computing r from (12) and (21) for various values of the eccentricity, we find the results given in Table I.

These results are illustrated graphically in Fig. 1. It is to be noted that the curve is very flat in the neighborhood of zero eccentricity, and that the ratio $(\gamma-1)/(\mu-1)$ does not depart very greatly from the value 2/3 which it has for the sphere until the eccentricity becomes large either in the prolate or in the oblate sense. Hence it is a fair inference that γ does not differ very much from the value $(2\mu+1)/3$ appropriate to the sphere for an irregular shaped magnet of any form such that the linear dimensions are all of the same order of magnitude. In any event it is clear from the manner in which γ is determined from the boundary conditions (1) and (2) that the effect of immersing a permanently magnetized body of any shape in a magnetic medium of constant permeability is to reduce the field everywhere in the same ratio, this ratio being a function of the permeability of the medium and of the geometrical configuration of the body alone.

Table I.

ϵ	$r=\frac{\gamma-1}{\mu-1}$ (Prolate)	$r=\frac{\gamma-1}{\mu-1}$ (Oblate)
0.00	0.67	0.67
0.20	0.67	0.66
0.30	0.68	0.65
0.40	0.69	0.64
0.50	0.70	0.63
0.60	0.72	0.61
0.70	0.75	0.57
0.80	0.79	0.52
0.90	0.85	0.44
0.95	0.89	0.35
1.00	1.00	0.00

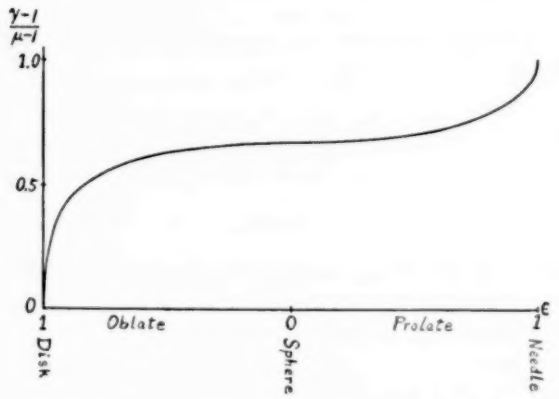

Fig. 1. Values of $(\gamma-1)/(\mu-1)$ as a function of eccentricity.

Demagnetizing Field

Since B in (8) and B' in (18) are functions of μ only through A, the uniform demagnetizing field in the interior of a spheroidal magnet is diminished by the presence of a surrounding per-

meable medium in the same ratio $1 : \gamma$ as is the field outside the magnet. For the thin disk, therefore, the demagnetizing field and the magnetic induction inside are unaffected by the presence of a permeable medium outside, while in the case of the needle the effect of a medium with $\mu > 1$ is to decrease the demagnetizing field in the ratio $1 : \mu$ and hence increase the induction. Of course the magnetic induction inside the magnet is $H^i + 4\pi I$ while that outside is μH^0.

The Temperature Dependence of Young's Modulus for Nickel

JERROLD ZACHARIAS, *Department of Physics, Columbia University*

(Received April 10, 1933)

A new method is described for the measurement of Young's modulus and its variation with temperature below 400°C. The method is applied to single crystals of pure nickel and to hard drawn, polycrystalline, commercial nickel between 30°C and 400°C. The variation of Young's modulus with temperature in these substances depends on the previous thermal history of the sample. Between 30° and 200° Young's modulus for *annealed* specimens decreases about 13 percent. This is followed by an increase to the Curie point of about 6 percent and above the Curie point by a linear decrease. For *hard drawn* specimens and specimens *quenched* at 1100° the minimum is wholly absent. Young's modulus decreases continuously to the Curie point, where the temperature coefficient changes abruptly.

THE object of this research is the measurement of Young's modulus for various specimens of nickel as a function of temperature between 30°C and 400°C. The specimens are rods of circular cross section, 5 mm to 7 mm in diameter and 3 cm to 8 cm long. The observations here reported yield the fundamental frequencies of free longitudinal vibration of the rods. The values of these quantities are related to the corresponding values of Young's modulus by the formula:[1]

$$G_1 = \rho_1 f_n^2 (4L_1^2 + 2\pi^2\sigma^2 r^2) \qquad (1)$$

where G_1 = Young's modulus for the direction of the cylinder axis, f_n = fundamental frequency of free longitudinal vibration, ρ_1 = density of the material, L_1 = length of the rod, σ = Poisson's ratio, and r_1 = radius of the rod.

THEORY

1. The vibrating system

The specimen forms one part of a composite piezoelectric oscillator of the sort described by Quimby.[2] A quartz rod of square cross section equal in area to that of the specimen is so cut from a crystal that the optic axis is perpendicular to one pair of opposite sides and an electric axis to the other. The latter pair is coated with gold leaf. One end of the nickel rod is thinly copper plated and covered with a molten mixture of copper oxide and boric oxide. The rods are then cemented together in a vacuum, under pressure, at a temperature of 600°C.

The oscillator is supported by fine wires and a sinusoidal potential difference is established between the coatings of gold leaf. The electric field in the quartz is accompanied by a piezoelectric stress proportional thereto. In consequence of this harmonically varying stress, a stationary state of forced longitudinal vibration is established in the composite rod.

The present method demands an expression relating the time derivative of the space average strain in the quartz to the frequency of the exciting voltage.

It is assumed that the equations which describe the propagation of the disturbance in the quartz and nickel are, respectively:[2]

$$\partial^2 u/\partial t^2 = V_2^2 \partial^2 u/\partial x^2, \qquad (2)$$

and

$$\partial^2 u/\partial t^2 = V_1^2 \partial^2 u/\partial x^2 + Q_1 \partial^3 u/\partial t \partial x^2, \qquad (3)$$

where u is the particle displacement in the direction of x (Fig. 1), and V_1, V_2 and Q_1 are independent of u, x and t. The form of these equations implies: (1), Hooke's law; (2), absence of internal friction in the quartz; and (3), pure longitudinal vibration.

If the potential difference, E, is of the form,

$$E = E_0 e^{int},$$

then the piezoelectric stress, Π, is of the form,[3]

[1] Rayleigh, *Theory of Sound*, 2nd edition, vol. I, p. 252.

[2] S. L. Quimby, Phys. Rev. **25**, 558 (1925).

[3] W. G. Cady, Phys. Rev. **19**, 1 (1922).

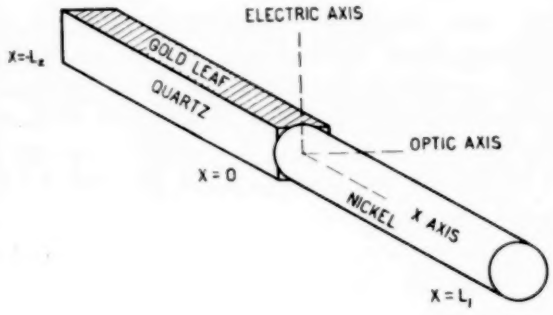

FIG. 1.

$\Pi = \Pi_0 e^{int}$. The expressions

$$u_2 = e^{int}\{A_2 e^{ikx} + A_2' e^{-ikx}\}, \tag{4}$$

and

$$u_1 = e^{int}\{A_1 e^{(\alpha+i\beta)x} + A_1' e^{-(\alpha+i\beta)x}\} \tag{5}$$

are solutions of Eqs. (2) and (3) respectively provided

$$k = n/V_2, \qquad \beta = n(1-3\lambda^2/8)/V_1,$$
$$\alpha = \beta\lambda(1-\lambda^2/4)/2, \quad \lambda = nQ_1/V_1^2,$$

and λ^4 is small compared with unity.

The constants A_1, A_1', A_2, A_2' are evaluated with the aid of equations expressing continuity of total force and velocity at the boundaries. Thus at $x = -L_2$

$$G_2(\partial u/\partial x)_2 + \Pi = 0$$

at $x = 0$

$$q_2\{G_2(\partial u/\partial x)_2 + \Pi\} = q_1\{G_1(\partial u/\partial x)_1 + \rho_1 Q_1(\partial^2 u/\partial x \partial t)_1\},$$

and

$$(\partial u/\partial t)_2 = (\partial u/\partial t)_1,$$

and at $x = L_1$

$$G_1(\partial u/\partial x)_1 + \rho_1 Q_1(\partial^2 u/\partial x \partial t)_1 = 0.$$

In these expressions the subscripts 1 and 2 refer to conditions in the nickel and the quartz, respectively, and q_1 and q_2 denote the cross-sectional areas of the rods. Accordingly the displacement in the quartz is given by Eq. (4) where

$$\begin{aligned} A_2 &= \Pi_0\{iM(1-e^{iy})(e^{z+iw}+e^{-(z+iw)}) - (iN-P)(e^{z+iw}-e^{-(z+iw)})\}/\Delta, \\ A_2' &= \Pi_0\{iM(1-e^{-iy})(e^{z+iw}+e^{-(z+iw)}) + (iN-P)(e^{z+iw}-e^{-(z+iw)})\}/\Delta, \end{aligned} \tag{6}$$

and

$$\Delta = 4iM\{M \sin y \cosh (z+iw) - (iN-P)\sinh (z+iw)\},$$

$$P = nf_n m_1 \lambda(1-\lambda^2/8),$$

$$N = 2nf_n m_1(1+\lambda^2/2),$$

$$M = 2nf_q m_2,$$

$$z = \alpha L_1 = \pi f\lambda(1-5\lambda^2/8)/2f_n,$$

$$w = \beta L_1 = \pi f(1-3\lambda^2/8)/f_n,$$

$$y = kL_2 = \pi f/f_q,$$

$$f = n/2\pi,$$

f_q = fundamental frequency of free longitudinal vibration of quartz rod alone, m_1 = mass of nickel rod, m_2 = mass of quartz rod.

If $\dot{\bar{s}}$ denote the time derivative of the average strain in the quartz, then,

$$\dot{\bar{s}} = \frac{\partial}{\partial t}\int_{x=0}^{x=-L_2} \frac{\partial u}{\partial x}\, dx. \tag{7}$$

2. The electric current

The observed quantity in the present experimental method is the variation with frequency of the amplitude of the current which flows between the electrodes on the quartz when the amplitude of the applied potential difference is kept constant. Van Dyke[4] has shown that this current is related to $\dot{\bar{s}}$ by the formula

$$I = \dot{E}C - \epsilon A\dot{\bar{s}}, \tag{8}$$

where I = current between the electrodes on the quartz, C = the electrostatic capacity between the electrodes, ϵ = the appropriate piezoelectric constant, and A = a geometrical constant.

It follows from Eqs. (4), (6), (7) and (8) that over the range of frequencies for which $\tan^4 y$, $\tan^4 w$, $\lambda^2 \tan^2 y$ and $\lambda^2 \tan^2 w$ are small compared with unity, the current I may be expressed in the form:

$$I = E_0 e^{int}\{inC + 1/(R+iX)\}, \tag{9}$$

[4] Van Dyke, Proc. I.R.E. **16**, 742 (1928).

where

$$R=(aL_2/4A\epsilon^2q_2)(1-\tan^2 y/2-\tan^2 w)(\pi f_n m_1\lambda),$$

$$X=(aL_2/2A\epsilon^2q_2)(1-\tan^2 y/2)$$
$$\times\{(m_2f_q\tan y+m_1f_n\tan w+m_1f_n\lambda^2\Lambda/4)\},$$

$$\Lambda=w-\pi w\tan w-\pi^2m_1f_n\tan y/4m_2f_q,$$

and a = distance between electrodes.

The equation,

$$X=0 \qquad (10)$$

defines a set of "resonance frequencies." Let one of these be denoted by f_0. Then as the frequency

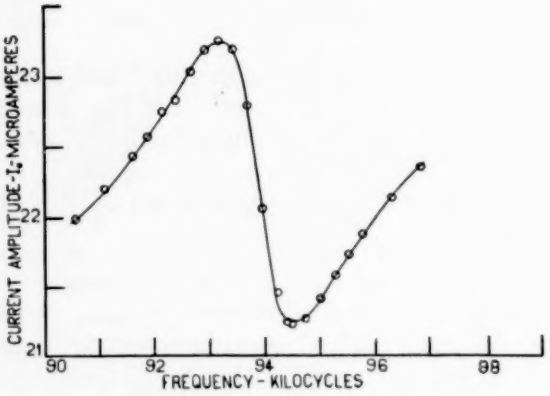

FIG. 2. Typical frequency-current curve.

is increased through f_0 the amplitude of I passes through a maximum and a minimum. The frequency, f_0, lies between the frequencies which correspond to these maximum and minimum values of I.

A typical frequency-current curve is shown in Fig. 2. The points indicate observed values of the current amplitude, denoted by I_0; the line is a graph of this quantity as given by Eq. (9). If $f_q=f_0\pm4000$ cycles, then the frequency, f_0, is related to the frequencies and currents corresponding to the maximum and minimum of this curve as follows: Let I_0', I_0'', f', f'', denote the current amplitudes and frequencies corresponding to the maximum and minimum respectively. Then

$$f_0=f'+(f''-f')I_0'/(I_0'+I_0''). \qquad (11)$$

Furthermore, from Eq. (9)

$$\lambda^2=4(1-m_2/m_1)^2(f''-f_0)(f_0-f')/f_n^2. \qquad (12)$$

λ and f_n are calculated with the aid of Eqs. (10), (11), and (12) together with a value of f_q obtained from observations on an oscillator which consists of the quartz rod alone. In fact, f_0 is given by Eq. (11) and λ by Eq. (12) with an approximate value of f_n. The values of f_0, f_q, and λ so obtained are substituted in Eq. (10) and this is solved for f_n.

APPARATUS AND EXPERIMENTAL METHODS

1. Electrical

To complete the calculations described in the preceding section it is not necessary to know the value of the quantity I_0; the ratio I_0/E_0 suffices. Fig. 3 indicates the arrangement used to supply the alternating potential difference, and to measure its frequency and the quantity I_0/E_0. The potential difference across the quartz is supplied through an amplifier by a vacuum tube oscillator. Its frequency is measured by comparison with the output of a piezoelectric clock.[5] The method of comparison is described elsewhere.[6] I_0/E_0 is measured as follows: r_1 (Fig. 3) is a resistance whose magnitude is negligible in comparison with the impedance of the quartz oscillator. The magnitude of the parallel re-

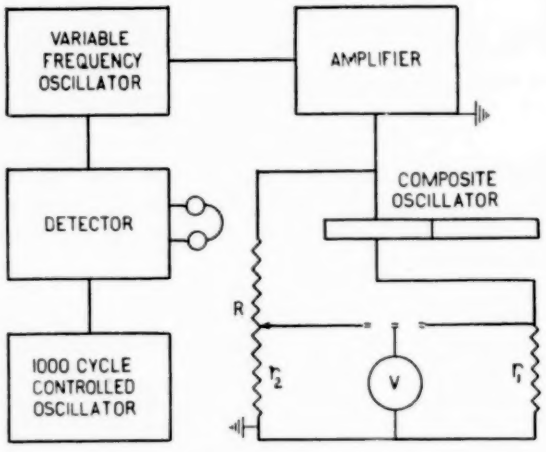

FIG. 3. Circuit diagram.

sistance r_2 is adjusted with the aid of a vacuum tube voltmeter, V, until the potential difference across r_2 is equal to that across r_1. Then

$$I_0/E_0=r_2/Rr_1. \qquad (13)$$

[5] Hull and Clapp, Proc. I.R.E. **17**, 267 (1929).
[6] S. L. Quimby, Phys. Rev. **39**, 345 (1932).

2. Magnetic and thermal

The composite oscillator lies in a fused silica boat on two fine wires located at nodes of vibration. The boat is situated at the center of a horizontal electric furnace about which is wound a solenoid. An astatic magnetometer is mounted above the solenoid and over the specimen. Prior to each observation the specimen is demagnetized with a diminishing alternating current in the solenoid.

The temperature of the specimen is measured with a Chromel P—Alumel thermocouple together with a Leeds and Northrup Type K potentiometer. The junction of the couple is placed about a millimeter from the free end of the specimen.

Experimental Results

The nickel from which the specimens are prepared is of two kinds, first, commercial nickel, initially in the form of hard drawn rods supplied by the International Nickel Company, and second, Mond nickel purified by the method of Fink and Rohrman.[7] The chemical analysis of the commercial nickel is as follows, where the numbers show the percent of impurity present: C, 0.11; Cu, 0.13; Fe, 0.41; Mn, 0.02; Si, 0.09; S, 0.005; Co, 0.3–0.4. The purified nickel is initially spectroscopically pure except for traces of copper and silver. The material is melted in an evacuated molybdenum resistance furnace[8] and single crystals are grown from the melt. Spectroscopic and chemical analyses of such specimens reveal contamination by copper (less than 0.003 percent) and by molybdenum (0.11 percent) and the absence of the following possible impurities: Al, C, Cr, Co, Fe, Mn, Si, Ag.

Observations are reported upon specimens with the following designations and thermal histories:

A. Commercial nickel, heated to 700°C and cooled slowly;

B. Commercial nickel, annealed at 900°C for two hours and cooled slowly;

C. Commercial nickel, annealed at 1100°C for two hours and cooled slowly;

D. A single crystal of purified nickel, cooled slowly from 1450°C;

E. A single crystal of purified nickel, reheated to 1100°C and quenched in water;

F. Commercial nickel, annealed at 1100°C for two hours, cooled slowly, reheated to 1100°C and quenched in water.

1. Young's modulus

The curves of Fig. 4 exhibit the temperature dependence of Young's modulus for specimens A

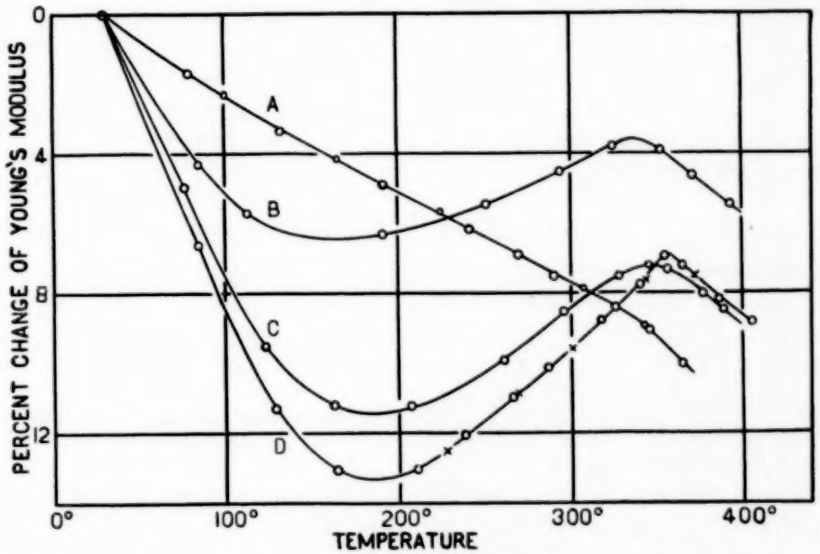

Fig. 4. Temperature dependence of Young's modulus for specimens *A* to *D*.

[7] Fink and Rohrman, Trans. Electrochem. Soc. **57**, 325 (1930); **58**, 403 (1930); **59**, 359 (1931).

[8] A description of the apparatus used in the production of the crystals is given in Phys. Rev. **39**, 345 (1932).

to D inclusive. The ordinates of these curves are $100(G_{30}-G_t)/G_{30}$ percent, where G_t denotes the value of Young's modulus at t°C. The circles represent observations taken between room temperature and 400°C and the crosses observations taken between 400°C and room temperature. Numerical values for the single crystal (curve *D*) are given in Table I. The observed values of Young's modulus at 30°C for the remaining specimens are given in Table II.

TABLE I. *Values of Young's modulus and its variation with temperature for a single crystal of nickel.*

T(°C)	$G_t\times10^{-11}$ dynes/cm²	$G_{30}-G_t/G_{30}$ ×100 percent	T(°C)	$G_t\times10^{-11}$ dynes/cm²	$G_{30}-G_t/G_{30}$ ×100 percent
33°	20.71	0.24	354°	19.33	6.91
84°	19.39	6.60	365°	19.26	7.21
129°	18.42	11.28	386°	19.04	8.27
164°	18.06	13.01	405°	18.94	8.79
211°	18.06	13.00	371°	19.00	7.48
238°	18.26	12.04	342°	19.17	7.68
267°	18.48	10.98	301°	18.78	9.56
287°	18.65	10.16	268°	18.50	10.90
317°	18.94	8.76	226°	18.18	12.44
340°	19.16	7.73	30°	20.76	0.00

TABLE II. *Values of Young's modulus for other specimens of nickel.*

Designation	Length at 30°C cm	Diameter cm	G_{30} dynes/cm²
A	8.118	0.48	21.41
B	6.666	0.48	19.86
C	7.820	0.48	20.77
D*	2.860	0.67	20.76
E	2.598	0.51	21.38
F	2.800	0.48	23.01

* The direction cosines of the cylinder axis with respect to the tetragonal axes of the crystal are 0.071; 0.68; 0.73.

These results indicate that the nature of the temperature dependence of Young's modulus below the Curie point is largely determined by the previous thermal history of the nickel at temperatures considerably above the Curie point. It appears that whether the nickel be pure or impure, single- or polycrystalline, the internal state characterized by a maximum at the Curie point and a minimum below it is produced by annealing at temperatures above 600°C. The difference between these maximum and minimum values of the modulus increases as the annealing temperature is raised. Further evidence in support of these conclusions is afforded by the following experiment: An annealed rod of impure polycrystalline nickel and a single crystal of the pure nickel were quenched at 1100°C. The behavior of both these specimens, as shown in Fig. 5, is substantially that of the hard drawn rod A.*

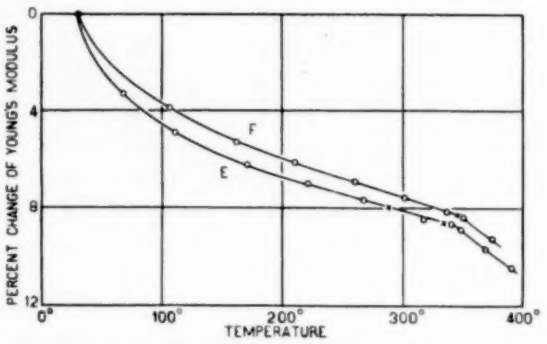

FIG. 5. Temperature dependence of Young's modulus for specimens *E* and *F*.

2. Internal friction

The coefficient of internal friction in solids is best defined by the relation

$$W=\xi S_0^2, \tag{14}$$

where W = energy loss per cm³ per cycle, ξ = coefficient of internal friction, and S_0 = amplitude of elastic stress. The relation (14) was first suggested by Kimball and Lovell.[9] The quantity ξ is related to the logarithmic decrement of free longitudinal vibration in a rod by the formula

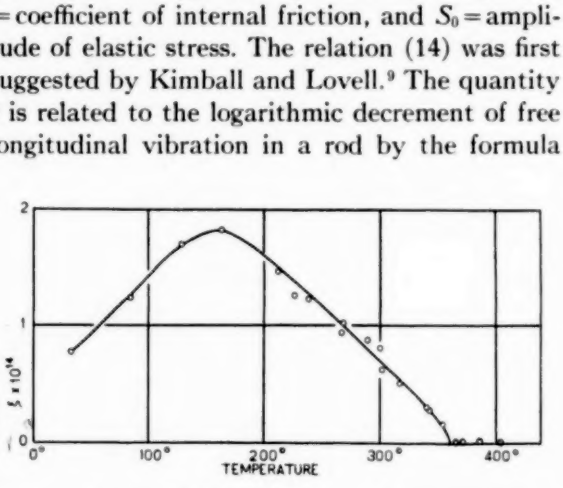

FIG. 6. Variation of internal friction with temperature in a single crystal specimen.

$\delta=\xi G$, and to the quantity λ by the formula $\pi\lambda=\xi G$.

* These results are in qualitative agreement with measurements of the torsion modulus of nickel by W. Möbius, Phys. Zeits. **33**, 411 (1932).

[9] Kimball and Lovell, Phys. Rev. **30**, 954 (1927).

The present experimental method does not yield precise values of ξ, particularly when that quantity is small. However, the observed variation of ξ with temperature in the single crystal specimen is so striking that the results seem worth reporting at this time. They are shown in Fig. 6. A more complete study of this phenomenon is now in progress.

Discussion of Method

Since the present method for measuring Young's modulus has not yet come into general use, it is appropriate here to present the results of experiments designed to establish its validity.

The resonance curves, of which that shown in Fig. 2 is typical, show that Eq. (9) correctly describes the electrical behavior of the composite oscillator.

The quantity f_q is the frequency of free longitudinal vibration of the quartz rod alone and is measured in the manner described by Cady.[10] It follows that the only quantities appearing in Eq. (10) which are not independently measured are f_n and λ. The values of the quantity f_n calculated with this equation should be characteristic of the rod itself. This conclusion is verified by the results of the following experiments. (1), Different quartz rods affixed to the same specimen yield the same values of f_n. (2), Values of f_n are calculated from observations on a nickel rod 28 cm long, at all the resonance frequencies of the system between 20,000 and 120,000 cycles per second. The results are given in Table III. Only those values of f_n which are calculated from resonance frequencies near $0.5f_q$ and $1.5f_q$ deviate appreciably from the average. These deviations may be ascribed in part to the layer of adhesive and in part to the fact that the areas of the quartz and nickel rods are not matched at the interface. It appears that both these effects are negligible over a wide range of resonance frequencies lying above and below f_q. This conclusion, as far as it concerns the adhesive, is confirmed by a theory** in which the adhesive is treated as one part of a tripartite oscillator. A theoretical accuracy is gained by utilizing in the calculation of f_n a value of f_0 which lies near to f_q. (3), Table IV shows the percent change of Young's modulus with temperature for specimen *A* as calculated from observations taken at three different harmonic resonance frequencies. While, as has been stated, the observations at 90 kilocycles are the most precise, the result constitutes a further confirmation of the method. (4), The small circles of curve A (Fig. 4) represent data taken on the same rod after resticking to the same quartz rod.

Table III.

f_0 cycles/sec.	f_n cycles/sec.	$\bar{f}_n - f_n$ cycles/sec.
17,643	9294	− 1
25,884	9287	− 8
32,931	9273*	−22
39,706	9294	− 1
47,622	9290	− 5
56,280	9296	+ 1
65,137	9297	+ 2
74,027	9298	+ 3
82,810	9298	+ 3
91,230	9295	0
98,671	9292	− 3
105,134	9283*	−12
$f_q = 68087$	$\bar{f}_n = 9295$	

* Not included in average.

[10] W. G. Cady, Proc. I.R.E. **10**, 83 (1922).

The absence in these test experiments of any evidence of systematic error indicates that the present method yields in f_n a number which is characteristic of the specimen rod alone. A very detailed study of the elastic behavior of the composite oscillator† shows that the relation of this quantity to Young's modulus for the material is, in fact, given by Eq. (1).

Precision of Measurements

1. Temperature

The longitudinal temperature gradient in the furnace is less than 0.2° per cm. The junction of the thermocouple is within 2 mm of the free end of the specimen. Calibrations of the couple against the melting points of tin, lead and zinc before and after the observations agree to 1° at 327.3°C and to 1.5° at 419.5°C.

** This theory shows that the "sandwich" type of oscillator described by Quimby (6) is the worst that can be designed for the present purpose.

† This will appear as part of a paper shortly to be published by Lewis Balamuth.

TABLE IV.

Temp. °C	f_q cycles /sec.	f_0 cycles /sec.	$G_{30}-G_t/G_{30}$ ×100 percent	f_0 cycles /sec.	$G_{30}-G_t/G_{30}$ ×100 percent	f_0 cycles /sec.	$G_{30}-G_t/G_{30}$ ×100 percent
30	87,650	63,950	0.00	90,368	0.00	115,830	0.00
79	87,640	63,540	1.65	89,690	1.69	115,060	1.69
132	87,610	63,145	3.34	89,043	3.34	114,337	3.28
192	87,540	62,750	4.94	88,440	4.84	113,620	4.84
241	87,440	62,450	6.15	87,930	6.15	113,034	6.17
290	87,280	62,100	7.52	87,410	7.40	112,420	7.40
325	87,150	61,810	8.63	86,990	8.41	111,900	8.41
345	87,060	61,630	9.25	86,756	8.99	111,550	9.09
369	86,930	61,334	10.44	86,390	9.88	111,038	10.08

2. Density and length

The densities of the specimens are determined at room temperature to 0.1 percent by the method of hydrostatic weighing. The length at 30°C is measured to 0.1 percent and the change of length with temperature to 400°C is measured to one percent of its value. Within this limit of accuracy the thermal expansions of single and polycrystalline specimens are the same. It is therefore assumed that the crystals expand equally in all directions, and hence that the fractional change in density is three times the fractional change in length.

3. Magnetization

The astatic magnetometer is sufficiently sensitive to show that the intensity of magnetization of the smallest specimen is less than 1.4 e.m.u. Magnetizations of this magnitude produce no detectable effect on the phenomenon.

4. Frequency

The frequency of the vacuum tube oscillator can be determined to one part in 100,000. The uncertainty in the frequency measurements arises from the flatness of the maximum and minimum of the resonance curve (Fig. 2). The consequent uncertainty in Young's modulus is not greater than 0.2 percent.

The major portion of the present work was done while the author held the Tyndall Fellowship and the Barnard Fellowship at Columbia University. In addition he wishes to acknowledge his indebtedness to Dr. Colin G. Fink and Dr. F. A. Rohrman who donated the pure nickel from which the crystals were grown; to Dr. Andrew Dingwall who made the spectroscopic analyses of the specimens; and to Dr. S. L. Quimby who suggested the problem and who followed the progress of its solution with helpful counsel and encouragement.

LETTERS TO THE EDITOR

Prompt publication of brief reports of important discoveries in physics may be secured by addressing them to this department. Closing dates for this department are, for the first issue of the month, the twentieth of the preceding month; for the second issue, the fifth of the month. The Board of Editors does not hold itself responsible for the opinions expressed by the correspondents.

General Form of the Equation of State for a Monoatomic Ideal Gas

The April first issue of the *Physical Review* contains, on page 552, an article by Uehling and Uhlenbeck in which a general expression, valid for all statistics, of the equation of state for a monoatomic ideal gas is used (Eq. (16), p. 555). In a letter that the authors wrote to the Editor of this *Journal*[1] which I did not notice before, they say that, as far as they knew, the above equation did not appear in the literature. It may be worth while to remember that I reached the same result in 1928[2]: precisely $pv = NkT\varphi(Tv^{2/3})$, where φ is an arbitrary function of its argument $Tv^{2/3}$. I could also prove that, for all statistics, to the adiabatic invariants $pv^{5/3}$, $Tv^{2/3}$ correspond the other $Jv^{1/3}$, where J is the mean value of the absolute values of the molecular momenta. The equation of state can be written: $pv = NkT \cdot f(Jv^{1/3})$, where f is an arbitrary function of its argument $Jv^{1/3}$.

Observing that the physical dimensions of $Jv^{1/3}$ are those of an action, one is led to introduce a universal constant with the same physical dimensions of an action. This may be avoided by making the supposition $f=1$; but in this case we obtain the particular equation of Boyle and Gay-Lussac.

G. POLVANI

Milano, Italy,
Physical Institute of Royal University,
May 29, 1933.

[1] Uehling and Uhlenbeck, Phys. Rev. **39**, 1014 (1932).
[2] Polvani, Nuovo Cimento **5**, 331 (1928).

The Equivalence of Mass and Energy

An experimental test of the relationship $\Delta E = C^2\Delta m$ is possible for two modes of nuclear disintegration when the results of recent mass-spectrograph measurements of the masses of the lithium isotopes[1] are considered in conjunction with the disintegration experiments of Cockcroft and Walton[2] and of Lewis, Livingston and Lawrence.[3]

The experiments of Cockcroft and Walton with lithium show that the lithium isotope of mass number seven under bombardment by high energy protons may capture a proton and that the resulting nucleus may disintegrate into two α-particles. The α-particles of range 8.4 cm which appear for protons of 270 kilo-volts energy have an energy of $8.6_2\times10^6$ electron-volts. The gain in energy in the reaction is $16.9_7\times10^6$ e-volts, an energy equivalent to 0.0182 mass units on the O^{16} scale if $\Delta E = C^2\Delta m$. Taking Aston's values[4] for the mass of helium and hydrogen and the author's value, 7.0146 ± 0.0006 for Li^7, the mass change is $0.018_1\pm0.0006$ in the reaction which may be represented as $Li^7+p\rightarrow 2\alpha$. Within the probable error of the measurements the equivalence of mass and energy is satisfied.

Recently Lewis, Livingston and Lawrence have reported some remarkable disintegration experiments wherein the H^2 nucleus was the bombarding particle. In the case of lithium, α-particles of two ranges, 8.2 and 14.8 centimeters, were observed as the products of disintegration. The bombarding particles were H^2 nuclei of 1.33×10^6 e-volts energy. Extrapolation of the range-energy data for α-particles secured by Rutherford, Ward and W. B. Lewis[5] yields 12.5×10^6 e-volts for the energy of the α-particles of greatest range. Under the assumption that it is the Li^6 isotope which captures an H^2 nucleus and disintegrates into two α-particles, the process may be indicated as $Li^6+H^2\rightarrow 2\alpha$. If one makes the additional assumption that momentum is conserved, the gain in energy in the reaction is 23.7×10^6 e-volts, equivalent to 0.025_3 mass units on the O^{16} scale is $\Delta m = \Delta E/C^2$.

Taking Aston's value for the mass of helium and the writer's values for H^2 and Li^6, the mass change is $0.023_8\pm0.0004$ unit. This measured mass change does not agree satisfactorily with the mass equivalent of the energy change in the disintegration. A more strict comparison must wait on values which include the probable error in the determination of the ranges of the α-particles.

KENNETH T. BAINBRIDGE

Bartol Research Foundation
of the Franklin Institute,
Swarthmore, Pennsylvania,
June 16, 1933.

[1] K. T. Bainbridge, Phys. Rev. **44**, 56 (1933).
[2] J. D. Cockcroft and E. T. S. Walton, Proc. Roy. Soc. **A137**, 229 (1932).
[3] Gilbert N. Lewis, M. Stanley Livingston and Ernest O. Lawrence, Bull. Am. Phys. Soc. **8**, No. 4, 13 (1933).
[4] F. W. Aston, Proc. Roy. Soc. **A115**, 487 (1927).
[5] E. Rutherford, F. A. B. Ward and W. B. Lewis, Proc. Roy. Soc. **A131**, 684 (1931).

Space Density of Cosmic-Ray Particles

A portion of the primary cosmic radiation entering our earth exists in the form of charged particles. If it exists in this form in interstellar space, its existence necessitates a certain volume density of particle radiation there. The object of the present note is to show that this density is large enough to insure that if the particles were all of one sign, there would exist differences of potential of enormous amounts between points in space separated by distances which are relatively small on an astronomical scale.

Suppose $\alpha ds d\omega$ is the number of cosmic-ray particles crossing the element of area ds within a solid angle $d\omega$, whose axis is perpendicular to ds. Then the number of rays crossing ds within the solid angle $\sin\theta d\theta d\varphi$ is $\alpha\cos\theta\sin\theta d\theta d\varphi ds$, where θ is measured from the normal to ds. The number of these to be found at any instant within the cylindrical element of volume $dsdx$, of length dx perpendicular to ds is $\alpha\cos\theta\sin\theta d\theta d\varphi dx ds/c\cos\theta$, where c is the velocity of light. The total space density (number of particles per cc) contributed by the particles from all directions, including both sides of ds is

$$D=\frac{2\alpha}{c}\int_0^{2\pi}d\varphi\int_0^{\pi/2}\sin\theta d\theta=\frac{4\pi\alpha}{c},$$

a result analogous to the well-known corresponding formula in heat radiation.

If the particles all have a charge e, the volume density ρ of electricity which they constitute is

$$\rho=4\pi\alpha e/c.$$

At any point in interstellar space let us draw a sphere with center O and radius R. The field at any point inside the sphere, and so the potential difference between the center and any point P on the boundary is composed of a part resulting from the electricity outside the sphere, and a part resulting from that inside. The difference of potential V between P and O caused by the latter is

$$V=\frac{4}{3}\pi\rho\int_0^R\frac{r^3}{r^2}dr=\frac{8\pi^2 e\alpha R^2}{3c}.$$

Now if the potential difference between P and O is reduced below V by the field caused by the charge outside the sphere, the corresponding difference of potential will be increased by a practically equal amount in the case of the difference of potential between O and a point Q diametrically opposite to P. In case one has any doubts on this point, imagine the sphere R surrounded by a concentric sphere S of radius large compared with R. The electricity between S and R produces no field inside R, and the field resulting from the more distant electricity outside S produces a field, which is sensibly uniform inside R.[1] The result of these considerations is to the effect that there will be points on R which differ in potential from the center O by an amount comparable with V.[2]

Now if we take for α a value no larger than that corresponding to the earth's surface for cosmic rays, i.e., $\alpha=0.7\times10^{-2}$; and if we express V in volts and replace R by the value R_0 measured in light years, we have

$$V=\frac{300\times8\pi^2\times4.7\times10^{-10}\times0.7\times10^{-2}\times(3\times10^{10}\times365\times86400)^2R_0^2}{3\times3\times10^{10}},$$

$$V=7.7\times10^{17}R_0^2 \text{ volts}.$$

Thus V amounts to about 7.7×10^{17} volts for $R_0=1$ light year. Since α should probably be taken as larger than the above value for a point outside the atmosphere,[3] the above value of V certainly represents a lower limit. A sphere one light year in radius is a relatively small sphere as astronomy counts distances. Hence, we see that the assumption of particles of only one sign in sufficient amount to account for cosmic-ray intensities would lead to conclusions prohibited by the possibilities of nature. Of course the presence of charges of both signs would alleviate the difficulty without the necessity of assuming that both signs of charge had energy sufficient for cosmic rays. Such a situation would presumably prevail if positive and negative particles were created in space or were released from atoms existing there. Any attempt to picture particles of one sign as emanating from the stars or other heavenly bodies would result in a condition in which the particles would become bound to their respective stars as a sort of space charge unless both signs of charged particles were emitted.

In conclusion it may be remarked that the author's recent suggestion[4] as to the possibility of the emission of high energy charged particles by the heavenly bodies is by no means limited to particles of one sign.

W. F. G. Swann

Bartol Research Foundation
of The Franklin Institute,
Swarthmore, Pennsylvania,
June 16, 1933.

[1] We wish to avoid any vague statements based upon implications that O is the "center" of an infinite distribution of charge.

[2] It is not contended that there is a unique solution of the problem for a charge which extends to infinity in some unspecified manner. There most certainly is not. The potential difference between O and the sphere R will depend upon the specific problem. All that is maintained is that there are points on the sphere of radius R for which the potential differs from that at O by the amount specified.

[3] It will be recalled that in line with the conclusions of G. Lemaitre and M. S. Vallarta, Phys. Rev. **43**, 87 (1933), the intensity at the earth's surface should be equal to that at infinity except, of course, for absorption.

[4] W. F. G. Swann, Phys. Rev. **43**, 217 (1933).

A Study of Images of Small Areas Formed with Feeble Light

In a previous note[1] the speculative suggestion was advanced that faint light may be incapable of forming a distinct image of a very small area. This suggestion arose from consideration of an analogy of the indetermination principle, in which e would play the part of h, electric field, the part of momentum, and area that of distance. The photographic study described in the present note was begun some time ago, in association with S. A. Korff, and has been continued this year, with a more sturdy camera. The source of light is a pinhole in a dark room, the pinhole being illuminated from behind, through a blue filter. At a distance of 2.5 meters is placed a stage micrometer (a glass slide having numerous fine scratches forming a scale of tenth-millimeters). This slide is photographed in transmitted light from the pinhole.

Half a dozen plates have been obtained, including a score or so of exposures for varying degrees of feeble light, ranging in duration from an hour or two up to twelve days. Examination of these images under a low-power microscope indicates that there is a slight but slowly increasing lack of sharpness as the illumination is made feebler (and the exposure longer). The scratches on the stage micrometer are only a few thousandths of a millimeter in width, and are too small to appear ideally sharp even with the best focus, being several times smaller than the limited resolving power of the lens can define. However with bright light the best focus can be picked to within 0.005 inch. When the illumination from the pinhole is reduced to about what would be produced by a star of magnitude minus one, a three days' exposure is required, on a process plate, and the blurring of the image at best focus seems equivalent to that produced with bright light at, roughly, 0.025 inch away from best focus. (Focal distance, 30 cm; effective aperture about 2 cm.) The corresponding circle of confusion indicated for the feeble light is, as regards order of magnitude, that given by a quantitative application of the suggestion of the previous note.

This result is merely tentative, and the experiment is being continued here. Mechanical warping of the camera, because of temperature changes in the dark room during the long continuous exposures with faint light, might account for the observed blurring. Check tests with intermittent bright light, however,—each such exposure having been continued for several days while the temperature changed about 5–10°F—seem to negative this explanation, all bright light exposures at best focus having resulted in relatively sharp images. A shorter-focus lens, operated in a constant temperature room, will yield more secure results. Since the radius of the hypothetical circle of confusion with feeble light theoretically varies inversely only as the fourth root of the intensity, it is profitable to work with very small objects and with images on finegrained, although insensitive, plates.

J. Q. Stewart and A. M. Skellett

Princeton University,
June 20, 1933.

[1] J. Q. Stewart, Phys. Rev. **34**, 1289 (1929).

The Asymmetry of the Cosmic Radiation at Swarthmore

Attempts to detect a directional asymmetry in the distribution of the cosmic radiation near sea level at geomagnetic latitudes greater than 44° have, until now,[1, 2, 3] shown no differences greater than the probable errors of the measurements, but latitude intensity measurements[4, 5] and the azimuthal measurements on Mt. Washington,[6] geomagnetic latitude 57°, barometer 59 cm, together with confirming results at Mexico City,[7, 8] geomagnetic latitude 29°, indicated that a slight asymmetry should persist above geomagnetic latitude 50°. Consequently, we have made a more accurate determination of the east-west differences at various zenith distances at Swarthmore, geomagnetic latitude 51°, and find the east intensity to be 3 percent lower than the west at 30° from the zenith with smaller differences at other angles. The experimental arrangement and order of observations* were the same as were used in the Mexico studies. By obtaining a large number of determinations extending over prolonged counting periods, the probable error has been reduced so that the result may be regarded as definite. The combined data are contained in Table I, and the east-west differences are represented graphically in the figure. The probable error of an E–W difference as indicated in the last column of the table and by a vertical line in the figure is calculated as the square root of the sum of the squares of the larger of the probable errors R or R'.

In order to compare the magnitude of the asymmetry here with that in Mexico the latter results have been reduced to the same scale by a comparison of the sensitivity of the two instruments and are thus plotted as the dotted curve of Fig. 1. The difference between the two curves is significant in showing the effect of atmospheric absorption on the rays which produce the asymmetries at the respective latitudes. The rays which are involved in the east-west differences at the higher latitude are obviously softer than those at the lower latitude for the maximum difference appears at 30° from the zenith at

[1] B. Rossi, Nuovo Cimento **8**, March, 1931.

[2] Johnson and Street, Phys. Rev. **41**, 690 (1932).

[3] S. A. Korff has also found no E–W difference greater than 4 percent at Pasadena. Minutes of the Salt Lake City Meeting of the American Physical Society, June, 1933.

[4] A. H. Compton, Phys. Rev. **43**, 387 (1933).

[5] J. Clay, Proc. Amsterdam Acad. **31**, 1091 (1928).

[6] Johnson, J. Frank. Inst. **214**, 689 (1932); Johnson and Street, Phys. Rev. **43**, 381 (1933).

[7] Johnson, Phys. Rev. **43**, 1059A (1933); J. Frank. Inst. (to be published) 1933; Phys. Rev. **43**, 834 (1933).

[8] Alvarez and Compton, Phys. Rev. **43**, 835 (1933).

* We are indebted to M. A. Tuve, A. G. McNish and W. E. Deming for a discussion of the statistical problem.

TABLE I. *The combined data for west-east difference.*

Angle from vertical	Total time T (min.)	Total counts C	Counting rate C/T	Number of data n	Probable error from residuals R	Probable error from number of counts R'	West–East difference
0°	3721	20,113	5.40	37	0.024	0.026	0
15° East	4418	22,109	5.00	33	0.028	0.023	0.05 ±0.034
West	5565	28,123	5.05	34	0.018	0.020	
30° East	4109	15,202	3.70	37	0.019	0.020	0.12 ±0.030
West	3755	14,367	3.82	37	0.022	0.022	
45° East	4520	10,851	2.40	35	0.016	0.016	0.06 ±0.024
West	5526	13,579	2.46	35	0.018	0.014	
60° East	5538	6330	1.143	26	0.014	0.010	0.012±0.016
West	5522	6380	1.155	28	0.010	0.010	
75° East	6815	2630	0.386	28	0.007	0.005	0.016±0.009
West	6550	2632	0.402	27	0.005	0.005	
90°	2896	294	0.102	12	0.004	0.004	0

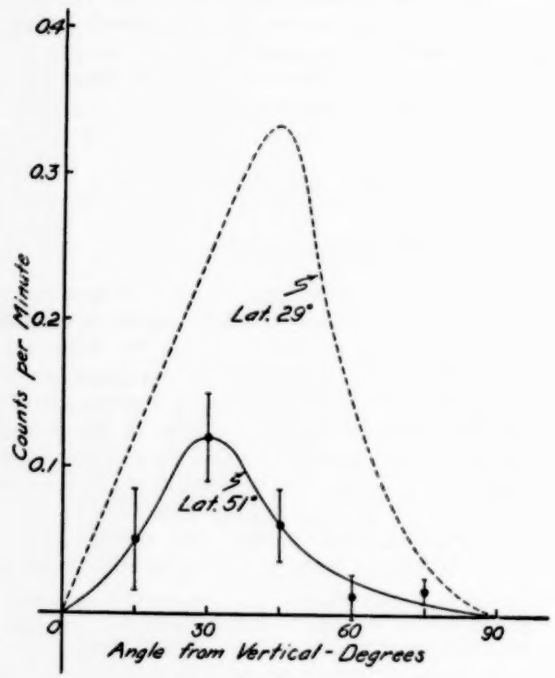

FIG. 1.

latitude 51° compared with 45° or 50° from the zenith at latitude 29°. The softer threshold rays at the higher latitude are thus able to penetrate the atmosphere only at angles closer to the zenith. The difference in the magnitudes of the effects at the two latitudes is perhaps also indicative of a difference in the rates of absorption of the two radiations though differences of this type could also be explained by the assignment of arbitrary energy distributions. In this connection it is also to be remarked that the range of energies involved in the asymmetry is shorter, according to the theory,[9] at the higher latitude, and this may partially account for the smaller observed effect. Differences in the two curves may also be accounted for by the fact that the data were obtained at two different altitudes. Some unpublished results at sea level in Vera Cruz, Mexico, however, show that by far the greater part of the changes in magnitude and distribution of the E–W differences are to be accounted for by the variation in latitude rather than by the difference in elevation.

These studies are being continued in Panama and Peru through the financial support of the Carnegie Institution of Washington and the Bartol Research Foundation.

THOMAS H. JOHNSON
E. C. STEVENSON

Bartol Research Foundation
of The Franklin Institute,
June 16, 1933.

[9] Lemaitre and Vallarta, Phys. Rev. **43**, 87 (1933).

Band Spectrum of NaK

Hitherto the only known visible band system of NaK has been the one in the neighborhood of the sodium D lines. There are, however, two visible systems of Na_2 and a visible and an infrared system of K_2, in each case involving transitions from a $^1\Sigma$ molecular ground level which dissociates into normal sodium, or potassium, atoms to excited molecular $^1\Sigma$ and $^1\Pi$ levels both of which dissociate into one normal atom and one in the resonance (^2P) state.

Theory indicates that there should be four systems of NaK bands in the visible and infrared, since, beside the ground level which dissociates into normal sodium and potassium atoms there should be a pair of levels, $^1\Sigma$ and $^1\Pi$, dissociating into normal sodium and excited potassium and a similar pair dissociating into normal potassium and excited sodium.

We have investigated the absorption and magnetic rotation spectra of NaK in the visible and photographic infrared, taking care to avoid the overlapping spectra of Na_2 or K_2 by working either with large proportions of sodium or of potassium in certain regions of the spectrum, and have found a new system in the green which appears in both magnetic rotation and absorption and is therefore presumably a $^1\Pi \leftarrow {}^1\Sigma$ transition. The yellow system also has a magnetic rotation spectrum and is another $^1\Pi \leftarrow {}^1\Sigma$ transition. The energy of dissociation of the upper state of the yellow system is only about 1000 cm^{-1} and has been deduced from the magnetic rotation spectrum with sufficient accuracy to make sure that the products of dissociation are normal sodium and excited potassium. We have also found two new systems in the infrared which appear clearly in absorption and which are presumably the two anticipated $^1\Sigma \leftarrow {}^1\Sigma$ systems.

TABLE I.

	T_e (cm^{-1})	ω_e	D (cm^{-1})	Dissociation products
ground state, $^1\Sigma$	0	123	4952	Na+K
$^1\Sigma$	11,751	82	6215	Na+K′
$^1\Sigma$	13,203	77	8714	Na′+K
$^1\Pi$	16,966	70	1000	Na+K′
$^1\Pi$	20,069	83	1848	Na′+K

Rough preliminary values of the constants of the five molecular levels are given in Table I.

F. W. LOOMIS
M. J. ARVIN

Department of Physics,
University of Illinois,
June 30, 1933.

Proceedings of the American Physical Society

MINUTES OF THE SALT LAKE CITY MEETING, JUNE 15, 1933

THE 185th meeting of the American Physical Society was held in affiliation with the Pacific Division of the American Association for the Advancement of Science in Room 313, Physical Science Building, University of Utah, Salt Lake City, Utah, on Friday, June 15, 1933, with Professor Orin Tugman presiding and twenty members of the American Physical Society in attendance.

The Society voted to hold the 188th meeting of the American Physical Society on the Pacific Coast on Friday, December 15, and, if necessary, Saturday, December 16, 1933, at Stanford University, California. The Physical Society was entertained at luncheon on Friday in the Union building at the University of Utah and an informal dinner, attended by some ten members, was held in the evening. The program of papers in abstract form follows.

LEONARD B. LOEB, *Local Secretary for the Pacific Coast*

ABSTRACTS

1. High Terms in the Spectra N^{v} and O^{v}. WILLOUGHBY M. CADY, *California Institute of Technology.*—Certain plates exposed a year ago in the vacuum spectrograph previously described (Phys. Rev. **43**, 322, 1933) have now been analyzed. The source was a condensed discharge through air at a pressure of about 0.5 mm Hg, taking place in a quartz tube 9 cm long and of 2 mm bore. About fifty discharges of the 0.33μF condenser at about 25,000 volts sufficed for a good exposure between 105 and 350A, showing known lines of N^{iv}, N^{v}, O^{iv}, O^{v}, and O^{vi}. New lines have been identified, which fix thirteen new levels in N^{v}, and thirty-six in O^{v}. Thus most of the bright lines on the plates have been identified; e.g., of the hundred lines with an estimated intensity of 3 or more, only about one quarter remain unassigned.

2. Hyperfine Structure and Nuclear Moment of Columbium. NORMAN S. GRACE (Commonwealth Fellow) and STANLEY S. BALLARD, *University of California at Berkeley. (Introduced by Leonard B. Loeb.)*—King (Astrophys. J. **73**, 13, 1931) observed a wide hyperfine structure in the arc spectrum of columbium. He found that many lines were broad enough to contain six components and some possibly eight. A very rich columbium I spectrum was excited in a Schüler tube cooled in liquid air and photographed with a glass spectrograph crossed with Fabry-Perot etalons. Although it has not yet been possible to completely resolve the lines possessing most complex structure we have found λλλ4059, 4675 and 5344 to possess at least eight components and λ4672 eight and probably more components. From intensities and intervals it is concluded that $I \geqslant 7/2$ for columbium.

3. Hyperfine Structure of Molybdenum. NORMAN S. GRACE (Commonwealth Fellow) and KENNETH R. MORE, *University of California at Berkeley.*—Mo I lines were excited in a liquid air cooled Schüler tube and photographed with a glass spectrograph and silvered Fabry-Perot etalons. λλλ5507, 5533, 5571 ($4d^5\,5s\,{}^5S_2 - 4d^5\,5p\,{}^5P_{123}$) and λλλ5792, 5858, 5888 ($4d^4\,5s^2\,{}^5D_{2,3} - 4d^5\,5p\,{}^5P_{1,2,3}$) with invar etalon separators, up to 20 mm showed no structure. With separators which were varied from 32 to 58 mm faint structure was observed in all of these lines. Aston reports for the isotopes of molybdenum, mass 92, 14.2 percent, 94, 10.2 percent, 95, 15.5 percent, 96, 17.8 percent, 97, 9.6 percent, 98, 23.0 percent, and 100, 9.8 percent. Thus one might expect hyperfine structure due to the isotopes of odd atomic weight by virtue of their mechanical and magnetic moments and also structure due to an isotope shift. The separations and intensities of the structure observed indicate that for at least one of the odd isotopes $I \geqslant \frac{1}{2}$, that the nuclear g-factors for both odd isotopes are small and that the isotope shift is extremely small. The very small magnitude of isotope shift observed in molybdenum in contrast with that observed in the spectroscopic homologue tungsten is of interest in connection with the theory of isotope shifts.

4. Hyperfine Structure and Nuclear Spin of Lanthanum. H. E. WHITE and O. E. ANDERSON, *University of California*

at Berkeley.—The arc spectrum of lanthanum was excited in a Schüler tube cooled in liquid air. Fabry and Perot etalons were used to investigate the hyperfine structure of line 6249.9A, which is the transition ${}^4G_{11/2}-{}^4F_{9/2}$. A 9 mm separator showed that this line had eight components. One of the authors, H. E. White (Phys. Rev. **34**, 1404 (1929)), from the work of Meggers and Burns suggested that the nuclear spin of lanthanum was at least 5/2. This present work indicates that the spin is 7/2.

5. Remarks on the "Lines" of Diffraction Gratings. HAROLD D. BABCOCK, *Mount Wilson Observatory.*—In most text books the elementary theory of the diffraction grating is given only for the case in which transparent or highly reflecting strips of an optical surface are separated by opaque, nonreflecting spaces of approximately the same width. Modern gratings ruled on metallic surfaces are distinctly different from this case in that the original polished surface of the metal is entirely destroyed and the burnished walls of the grooves formed by the ruling tool reflect the light largely in certain chosen directions. By means of photomicrographs and diagrams these types of gratings are illustrated. For a metal grating the effect is shown of varying the relation between the spacing of the grooves and their depth. The design of the shape of the groove to produce a desired concentration of diffracted light is described. Typical ruling diamonds are exhibited. Attention is called to Michelson's theory of the modern type of grating.

6. Measurement of the Townsend Coefficients for Ionization by Collision. FREDERICK H. SANDERS, *University of California at Berkeley. (Introduced by Leonard B. Loeb.)*—The photoelectric current between parallel plates in dry air was measured as a function of plate distance for constant field strength and pressure over plate distances ranging from 1 to 7 cm and at a pressure of 1 mm of mercury. The simple Townsend relation $i=i_0e^{\alpha d}$ was found to give excellent agreement for values of X/p from 40 to 110. The values of α/p plotted as a function of X/p lie on a smooth curve which does not fit either the equation $\alpha/p=Ce^{-CV_0p/X}$ suggested by Townsend nor the empirical relation $\alpha/p=Ae^{b(X/p)}$ found by the writer to hold for values of X/p from 20 to 36.5. Voltages and plate distances were measured to within 1/10 of 1 percent and pressures to 1/2 of 1 percent or better. For X/p's from 120 to 160 the current was found to increase with plate distance more rapidly than the simple exponential relation would indicate, as was observed by Townsend for plate distances less than 1 cm at much greater X/p's. The early appearance of this deviation may be ascribed to the greater sensitivity given by larger plate distances. Both of the relations suggested by Townsend:

$$i=i_0\frac{(\alpha-\beta)e^{(\alpha-\beta)d}}{\alpha-\beta e^{(\alpha-\beta)d}} \qquad (1)$$

which was derived on the assumption that each positive ion produces β new pairs of ions by collision in 1 cm of path, and

$$i=i_0\frac{e^{\alpha d}}{1-\gamma(e^{\alpha d}-1)} \qquad (2)$$

which assumes γ new electrons liberated by each positive ion which strikes the cathode, fit the experimental curves equally well. The values of β/p were found to increase steadily with X/p as found by Townsend for higher X/p's. The coefficient γ, which is approximately equal to β/α, was found to increase only very slightly over this small range of X/p's.

7. Uranium and Thorium Content of Rocks Determined from their Surface Radiation. ROBLEY D. EVANS, *National Research Fellow. University of California at Berkeley.*—Following the initial work of Graven (Akad. Wiss. Wien, 2A, **139**, 181 (1930), *ibid.* **141**, 515 (1932)), an attempt was made to measure the sum of the uranium and thorium content of rocks by means of alpha- and beta-rays emitted from the surface of the rocks. These were detected with a Workman-DeVore quartz fiber electroscope having two 75 cm² windows of 0.8μ aluminum, hence a stopping power of only *ca.* 1.3 mm of air. That *ca.* 90 percent of the ionization is due to alpha-rays, *ca.* 10 percent to beta-rays, and none to gamma-rays was demonstrated by using aluminum and lead screens with the ionization chamber, as well as by oscilloscope observations employing a sensitive linear amplifier. The technique becomes quantitative by employing smooth semi-polished surfaces of rocks, in which a definite amount of surface is exposed. Absorption measurements in both pure and poisoned gypsum were made using artificial rocks composed of gypsum poisoned with minute quantities of thorium and uranium and their decay products. These measurements confirm the experiments of Graven for the uranium series but definitely disagree with his thorium measurements. The existence of intense secondaries from gypsum under the action of feeble γ-radiation, and the dependence of the method on γ-radiation, as reported by Graven, were not confirmed. Although a slightly different absorption ratio for the Th and U series in gypsum was observed, the difference was *not sufficiently large* to provide a practical basis for evaluating both the thorium and uranium content of ordinary rocks. The unscreened radiation from rock surfaces is, however, capable of indicating the sum of the uranium and thorium content of a specimen, and if either can be measured by an independent experiment, Evans, R. S. I. **4**, 223 (1933), then the other may be obtained.

8. The Heat of Dissociation of Bi_2 Determined by the Method of Molecular Beams. CHENG CHUAN KO, *University of California at Berkeley. (Introduced by Leonard B. Loeb.)*—With the velocity analyzer of Zartman with improved technique the combined velocity spectrum of Bi atoms and Bi_2 molecules was obtained at 827°, 851°, 875°, 899°, 922°, 947°C. From the spectral distribution curves the relative abundance of Bi atoms and Bi_2 molecules in the beams at the above temperatures could be determined to 1 percent. The vapor pressure curve of Bi was obtained experimentally by the method of effusion and the values so obtained were combined with the degree of dissociation of the vapor as computed from the beams to give the heat of dissociation. The heat of dissociation was computed from the data, assuming the pressure to be

given by the temperature of the crucible T_c. In calculating the heat of dissociation, the equilibrium temperature was taken as that of the slit chamber T_s which was 24° above T_c. The results of these calculations plotted with $\log_{10} K_p$ as ordinates against $1/T_s$ give a straight line whose slope yields the value of the heat of dissociation as 77,100±1200 calories. The curves for the distribution of velocities observed and computed on the assumption of a given ratio of Bi atoms to Bi_2 molecules in the beam were compared to test the law of distribution of velocities. On the high velocity side agreement was obtained within the limits of experimental accuracy. On the low velocity side deviations were noted of such a sort that the observed curves below a velocity of $\alpha/2$ (i.e., ½ the most probable) gave *more* molecules than the theory demanded. Other deviations were observed on some of the runs taken with a fourth slit in which a *deficiency* of molecules was observed between velocities of 0.75α and $\alpha/2$. This deviation was probably due to a warping of the image slit carriage due to heat. The nature of the variation at velocities less than $\alpha/2$ indicated the presence of molecules of greater mass than Bi_2 in the beam and at the lower temperatures a distinct peak corresponding to Bi_3 molecules was observed which were present to less than 2 percent.

9. Charging Devices for Portable Ionization Electroscopes. E. J. WORKMAN,* *Reed College.*—The increasing use of portable ionization electroscopes for radiation measurement has created a demand for lighter and more compact sources of potential for charging than is obtainable by the use of commercial dry batteries. One method of meeting this need depends upon the use of a small variable air condenser and a dry battery of a few volts. A well-insulated (hard rubber or better) variable radio condenser of approximately 900 cm capacity is charged to a potential of 22 volts by a small C-battery. A turn of the dial toward smaller capacity disconnects the battery and connects the condenser to the deflecting element of the electroscope when the potential has been raised the desired amount. All switching is controlled by a mechanism on the dial shaft and with a given arrangement of connections the electroscope can repeatedly and accurately be charged to the desired potential. In cases where pocket size equipment is desirable a 1.4 volt flash light battery may be used with a small, say 4 cm in diameter, parallel plate condenser. A thin sheet of mica serves for the dielectric at the position of maximum capacity and the separation of the plates and switching action is accomplished by pressing the charging "button" of the electroscope into contact with the charging device. Crude apparatus of this type has been found satisfactory for charging a small deflecting element to potentials around 300 volts, but is less reliable because of the "creeping" action on the dielectric.

10. The Study of a Powerful Source of Positive Alkali Ions. PAUL KECK and LEONARD B. LOEB, *University of California at Berkeley.*—A positive alkali ion source was developed in which an atomic beam of alkali atoms was projected against a platinum strip filament at 1000°C in a high vacuum. By accelerating the resulting positive ions in an electrical field positive ion currents of the order of 2×10^{-4} amperes/cm² could be obtained with the source of potassium at 330°C and a potential of 340 volts. Over 60 percent of the atoms in this beam had an energy distribution of less than 25 volts. This device can be further developed and could be used for the study of light emission by positive ion impact at low voltages, for an effective separation of the Li isotopes when coupled with a positive-ray analyzer at the rate of 0.13 mg Li per day, and as a 3 electrode tube for the production of electrical oscillations.

11. Azimuthal Investigation of Cosmic Radiation. S. A. KORFF, *National Research Fellow, Mt. Wilson Observatory.*—A study is being made of the distribution of cosmic radiation east and west of the magnetic meridian, employing Gieger-Müller counters connected to record coincidental discharges. Preliminary results indicate that at the Mt. Wilson laboratories, Pasadena (elev. 885 ft.), counting rates at equal altitude angles east and west are equal within the experimental errors of about 4 percent. This result is in agreement with the observations of Millikan and Neher, and with the calculations of Lemaitre and Epstein. The experiments are being continued at higher elevations.

12. The *K* Absorption Discontinuities of the Elements Zirconium to Iodine. P. A. ROSS, *Stanford University.*—A study of the *K* discontinuity has been made with a double crystal spectrometer. All of the elements studied except cadmium show faint fine structure on the high frequency side of the discontinuity, the fine structure appearing as narrow bands of slightly decreased absorption lying within a range of from 20 volts to 120 volts of the main absorption edge. The width of the discontinuity in volts has been measured and shows a somewhat erratic increase with increasing atomic number. Defining the wave-length of the discontinuity as that corresponding to the point of inflection of the main absorption curve, values of the wave-length have been obtained to an estimated accuracy of ±0.02 x.u.

Element	$\theta\pm0.5''$ (calcite at 18°)	$\lambda\pm0.02$ (x.u.)	Width (volts)
Zr	6° 30′ 56.5″	687.43	12.9
Cb	6° 10′ 32.6″	651.71	18.0
Mo	5° 51′ 35.7″	618.51	15.2
Ru	5° 17′ 51.8″	559.35	19.3
Rh	5° 2′ 44.7″	532.82	20.0
Pd	4° 48′ 38.7″	508.06	22.4
Ag	4° 35′ 26.7″	484.88	25.0
Cd	4° 23′ 6.3″	463.07	25.1
Sn	4° 0′ 40.2″	423.76	30.2
Sb	3° 50′ 27.2″	405.81	30.0
Te	3° 40′ 51.2″	388.93	34.9
I	3° 31′ 49.2″	373.04	38.2

13. Probabilities of *L* Ionizations of Au by Cathode Rays. D. L. WEBSTER, L. T. POCKMAN AND PAUL KIRKPATRICK, *Stanford University.*—Probabilities of ionization of L_{22} and L_{21} electrons were measured in arbitrary units as functions

* Read by title.

of cathode-ray energy by intensities of the $L\alpha$ and β_1 lines from gold leaf. Corrections for cathode-ray diffusion are unreliable below 80 or 90 kv. From there to 180 the probabilities follow Bethe's formula of proportionality to $U^{-1} \ln (4U/B)$, where $U = V/$(minimum ionizing potential V_0), but with $B = 4.4$ and 6.5 respectively, values probably too high for his theory. These values were found after deducting effects of L ionization by $K\alpha$ transitions, estimated by assuming an ionization probability $V_0^{-2} f(U)$ with $f(U)$ the same for all electrons. This deduction is only 1.5 percent at 180 kv for $L\alpha$ and 1.9 percent for $L\beta$; and empirically, the change of slope of the L intensity graphs at V_K is too small to detect with present technique.

14. Failure to Detect Radioactivity in Beryllium. ROBLEY D. EVANS, *National Research Fellow*, AND M. C. HENDERSON, *University of California, Berkeley.*—We have attempted to confirm the presence of radioactivity in beryllium, as observed in the ionization-chamber-electrometer measurements of Langer and Raitt (Phys. Rev. **43**, 585 (1933)), by using a linear amplifier that will detect individual alpha-particles; but we have obtained negative results. In the present experiments an ionization chamber was used resembling that used by Wynn-Williams and others, 20 mm in diameter and 4.5 mm deep, with only a coarse wire-grid as first electrode. The output of the amplifier operated a loudspeaker, an oscilloscope, and a Thyratron counter. The apparatus was standardized against polonium alpha-particles. A flat boss 20 mm in diameter was ground on a face of a lenticular block of beryllium, and this fresh beryllium surface was mounted 1 mm from the entrance to the ionization chamber. Based on the beryllium decay constant and alpha-particle range given by Raitt and Langer, we expected about 2.9 alpha-particles per minute. Within a probable uncertainty of 0.1 counts per minute, no alpha-particles were observed. The present experiments are therefore interpreted as suggesting that beryllium is stable.

15. Analysis of the Action of Hydrogen Peroxide on Photographic Emulsions. MERTON W. JONES AND JULIAN M. BLAIR.*—Data published by Sheppard and Wightman for the production of the latent photographic image by hydrogen peroxide are analyzed in terms of the Blair-Leighton equation. It is found that this equation fits the experimental data well, except for fluctuations observed by Sheppard and Wightman at high densities. Experimental data are presented which follow values indicated by the equation, but do not confirm the existence of such variations at high density. Neither do they confirm the previously reported evidence of solarization under certain conditions of treatment with hydrogen peroxide. There is apparently no correlation between the sensitivity of an emulsion to light and its sensitivity to hydrogen peroxide. Two different emulsions of the same brand of plates were found to be practically identical with regards to their sensitivity to light but differed more in their sensitivity to hydrogen peroxide than did a slow process emulsion and a fast process emulsion.

16. The Intermittency Effect in Photographic Exposure. JULIAN M. BLAIR AND MALCOLM C. HYLAN,* *University of Colorado.* (*Introduced by L. B. Loeb.*)—It has long been known that intermittent exposures produce different effects upon a photographic emulsion from equal amounts of light in a continuous exposure. Earlier investigators have not agreed as to the cause of this effect. The results of these investigators are discussed. An explanation of the varied aspects of this phenomenon is offered on the basis of the Blair-Leighton equation, combined with a theory of photochemical lag. Certain predictions are made concerning the effects of intermittency upon exposures to radiations of different wave-lengths. Conditions under which abnormal intermittency effects can be obtained are also described. Experiments verifying these predictions are described.

17. Photographic Studies of the Planets in Light of Different Wave-Lengths. W. H. WRIGHT.

18. Spectra of Mars, Venus, and Jupiter under High Dispersion. T. DUNHAM.

19. Molecular Spectra in the Photographic Infrared. D. M. DENNISON AND A. ADEL.

20. Radioactivity and the Age of Meteorites. R. D. EVANS.

---

* Read by title.

AUTHOR INDEX TO ABSTRACTS OF THE SALT LAKE CITY MEETING

Adel, A.—see Dennison
Anderson, O. E.—see White

Babcock, Harold D.—No. 5
Ballard, Stanley S.—see Grace
Blair, Julian M.—see Jones
—— **and Malcolm C. Hylan**—No. 16

Cady, Willoughby M.—No. 1

Dennison, D. M. and A. Adel—No. 19
Dunham, T.—No. 18

Evans, Robley D.—Nos. 7 and 20
—— **and M. C. Henderson**—No. 14

Grace, Norman S. and Stanley S. Ballard—No. 2
—— **and Kenneth R. More**—No. 3

Henderson, M. C.—see Evans
Hylan, Malcolm C.—see Blair

Jones, Merton W. and Julian M. Blair—No. 15

Keck, Paul and Leonard B. Loeb—No. 10
Kirkpatrick, Paul—see Webster
Ko, Cheng Chuan—No. 8
Korff, S. A.—No. 11

Loeb, Leonard B.—see Keck

More, Kenneth R.—see Grace

Pockman, L. T.—see Webster

Ross, P. A.—No. 12

Sanders, Frederick H.—No. 6

Webster, D. L., L. T. Pockman and Paul Kirkpatrick—No. 13
White, H. E. and O. E. Anderson—No. 4
Workman, E. J.—No. 9
Wright, W. H.—No. 17